The Effects of Ground Motions Characteristics and Higher Modes on the Seismic Response of Steel Strongback Braced Frame Buildings

Shuaikang Wang

A Thesis

in

The Department

of

Building, Civil and Environmental Engineering

Presented in Partial Fulfilment of the Requirements

for the Degree of Master of Applied Science (Civil Engineering) at

Concordia University

Montreal, Quebec, Canada

September 2024

CONCORDIA UNIVERSITY

School of Graduate Studies

This is to certify that the thesis prepared

By: Shuaikang Wang

Entitled: The Effects of Ground Motions Characteristics and Higher Modes on the Seismic Response of Steel Strongback Braced Frame Buildings

and submitted in partial fulfillment of the requirements for the degree of

Master of Applied Science (Civil Engineering)

complies with the regulations of the University and meets the accepted standards with respect to originality and quality.

Signed by the final examining committee:

Dr. A. Bhowmick Chair

Dr. G. Hafeez Examiner

Dr. A. Bhowmick Examiner

Dr. L.Tirca Thesis Supervisor

Approved by Dr. Po-Han Chen, Graduate Program Director

Sep. 13, 2024 Dr. M. Debbabi, Dean of Faculty

ABSTRACT

The Effects of Ground Motions Characteristics and Higher Modes on the Seismic Response of Steel Strongback Braced Frame Buildings

Shuaikang Wang

To mitigate the weak-storey response that characterize traditional steel braced frames under seismic excitations, researchers proposed the Strongback Braced Frame (SBF) system, which is composed of a primary ductile system and an elastic vertical truss (strongback, SB). Although this system is not new, a comprehensive design method for sizing the SB truss members is lacking. It is worth mentioning that higher-mode forces are not limited by the yield mechanism of ductile system and they lead to large inertial effects relative to the first-mode response. Current studies conducted on SBF are limited for low-rise buildings where the strongback truss is integrated into the half side of ductile braced frame which leads to large ductile brace sizes. Hence, installing the SB truss exterior to the ductile system is beneficial.

In this research work, the SBF is derived from Moderately Ductile Concentrically Braced Frame (MD-CBF) with split-X braces and two SB configurations are considered: adjacent exterior and reversed exterior.

The main objectives are: i) to simplify the design method for SBF to be appealing for practitioners, ii) to analyse the effects of ground motions characteristics and higher modes on the nonlinear seismic response of low-rise buildings braced by Strongback Braced Frame (SBF) with exterior SB, and iii) to discuss the seismic performance of SBF against that of traditional MD-CBF.

The case study is a 4-storey SBF office building located on Site Class C in Victoria, B.C. Two sets of ground motions were considered in analysis: the short-duration crustal ground motions, and

long-duration subduction ground motions characterised by Trifunac duration > 60 s. Detailed numerical models were developed in OpenSees and the nonlinear seismic responses of buildings were expressed in terms of interstorey drift (ISD), residual interstorey drift (RISD), floor acceleration (FA) and storey shear. To identify the types of failure mechanism, the incremental dynamic analysis (IDA) was employed and the IDA curves were developed considering both sets of ground motions. The collapse margin safety was assessed and the performance of SBF building was compared against that of the benchmark 4-storey MD-CBF building.

The SBF system is found effective in mitigating the weak-storey response, distributes ISDs uniformly along the building height, exhibits reduced residual drift, and provides about 50% larger safety margin compared to traditional MD-CBF systems. In addition, the SB truss is able to respond in the elastic range while engaging all ductile braces to dissipate the input energy. Although one or even two ductile braces experienced fracture caused by low-cycle fatigue, the SB is able to prevent the occurrence of dynamic instability. Moreover, the subduction zone records that are reach in high frequency content, excite the higher modes and in consequence amplify the upper floors responses. Thus, the type of failure mechanism of SBF is strongly influenced by the mean period of ground motions; hence, the records with short mean period trigger amplified demand at upper floors, while those with longer mean period trigger damage at lower floors. It was also found that the SBF buildings show sufficient collapse margin safety and the SB location slightly influences the seismic response of SBF. However, the 4-storey MD-CBF building showed a borderline pass of margin safety criteria and is not recommended in subduction zone prone regions.

Future research is required to investigate the higher modes effect on building height, as well as the impact of differed types of ductile braces on the global response of steel SBF buildings.

ACKNOWLEDGEMENTS

I would like to express my sincere gratitude to my supervisor, Dr. Lucia Tirca, for her unwavering support and guidance throughout this research. Her patience, enthusiasm, and expert knowledge were instrumental in the completion of this dissertation.

My appreciation extends to Dr. Anjan Bhowmick and Dr. Hafeez for serving as my committee members and providing insightful comments and questions that enhanced the quality of this work.

I am grateful to Concordia University for providing a supportive academic environment and enlightening lectures from its exceptional faculty. The funding received from NSERC is also gratefully acknowledged.

I wish to express my thankfulness to my colleagues and friends: Lizhu Chen, Yudong Wang, and Anastasia Athanasiou, for their valuable assistance during my research.

Finally, I want to convey my deepest appreciation to my parents, whose endless love and support have been a constant source of encouragement throughout my academic journey.

Table of Contents

Table of Figures

List of Tables

CHAPTER 1. INTRODUCTION

1.1 Background and Motivation

Steel Seismic Force Resisting Systems (SFRSs) are designed to resist the earthquake loads. Among them, the Concentrically Braced Frames (CBFs) have been widely used due to their ability to withstand both wind and seismic loads. CBFs dissipate the input energy through braces yielding in tension and buckling in compression. The National Building Code of Canada (NBC) defines ductility and overstrength force-reduction factors, R_d and R_o, respectively, while the CSA S16 steel design standard outlines design rules, including the capacity design principle for sizing the CBF's beams, columns, and their connections.

However, CBFs have several drawbacks: yield at low earthquake demand, possess low redundancy, exhibit significant residual interstorey drift under strong earthquakes which leads to challenges in ensuring building safety and post-earthquake repairability, and are prone to weak-storey response. Thus, the compression strength of braces decreases after buckling and the system is not able to redistribute the internal forces along the building height, which leads to damage concentration within one or a few floors. McCormick et al. (2008) proposed a 0.5% h_s residual interstorey drift threshold for building repairability, highlighting the importance of minimizing structural damage.

To overpass the CBF's shortcomings, researchers proposed various solutions, as well as innovative SFRSs. Firstly, they investigated the beneficial effect of continuous columns including gravity columns and that of dual CBF-MRF or BRBF-MRF system, where the BRBF and MRF are the Buckling Restrained Braced Frame and Moment Resisting Frame, respectively. Among the innovative SFRSs are the Zipper Braced Frame (ZBF), Tied Eccentrically Braced Frame (TEBF) for low-rise and middle-rise buildings and the Modular TEBF (M-TEBF) for taller buildings, as well as the Rocking Braced Frame (RBF) with and without controlled rocking, the Self-centering Braced Frame (SCBF) and others. While each of these advancements offers unique benefits, they also come with their own set of drawbacks, such as susceptibility to dynamic instability (e.g. ZBF) or the need for specialized construction and maintenance (e.g. RBF, SCBF).

In light of these challenges, a promising alternative is the Strongback Braced Frame (SBFs), which is a combination of a traditional braced frame system (e.g. CBF, BRBF or other) with a stiff elastic truss. The steel SBF offers a cost-efficient and straightforward solution for buildings in seismic regions. The elastic truss drives the building into the first mode response, ensures more uniform drift distribution, and prevents the formation of weak-storey response.

The strongback system (elastic truss) could be positioned in various configurations such as interior, adjacent exterior, or reversed exterior with respect to the ductile braced frame system. Steel SBFs offer a promising solution to address the challenges faced by traditional CBFs or BRBFs and provide a valuable contribution to the advancement of seismic-resistant structural systems.

1.2 Design Challenges and Research Gaps

Designing the steel SBF is challenging because sizing the members of elastic truss (strongback) is not straightforward. The traditional force-based design method, effective for CBFs or BRBFs, prove inadequate due to the significant contribution of higher modes, especially at upper floors. The elastic truss, which chord is a continuous column, responds to both inelastic first mode and elastic higher modes during earthquakes, resulting in a bending response similar to shear walls or rocking-braced frames (Steele and Wiebe, 2016).

Over the past two decades, researchers have explored various approaches to address these design challenges:

1. Empirical approaches: Tremblay (2003), Tremblay and Poncet (2007), and Merzouq and Tremblay (2006) found that the demand induced in the elastic braces of upper stories is higher than anticipated due to the higher modes effect. They sized the elastic braces of the strongback system based on an empirical approach consisting on demand amplification.

2. System overstrength factor method: Lai and Mahin (2015) employed a system overstrength factor to design the strongback system, but they observed that this strategy underestimated the demand in the upper storeys of the strongback.

3. Dynamic capacity design method: Tremblay et al. (2014) and Simpson (2018, 2020) proposed a dynamic capacity design method based on Performance-Based Design (PBD) methodology, which involves iterative design using nonlinear dynamic analysis. This approach yields adequate sections for the elastic truss members by considering the higher mode effect. However, it requires extensive expertise in numerical modelling and involves computationally intensive nonlinear analyses, leading to design challenges and computational expenses.

While these methods have made significant advancement, they each have limitations, such as underestimating demands in upper storeys or requiring extensive expertise and computational resources. Thus, there is a need for a reliable design method for SBFs, as well as the development of case studies located in various seismic regions in order to prove the system's efficiency.

1.3 Research Objectives

This thesis aims to address the identified research gaps through the following objectives:

1. To simplify the design method for SBF to be appealing for practitioners.

2. To analyse the effects of ground motions characteristics and higher modes on the nonlinear seismic response of low-rise buildings braced by Strongback Braced Frame (SBF) with exterior SB.
3. To discuss the seismic performance of SBF against that of traditional MD-CBF.

1.4 Methodology

To achieve these objectives, the following methodology was applied to the case study consisting of a 4-storey office building located in Victoria, B.C.:

1. Design the benchmark 4-storey MD-CBF office building in Victoria, B.C. using the building code (NBC 2015) and steel design standard (CSA S16-2014). Develop nonlinear numerical models using the OpenSees software.
2. Select and scale ground motions suitable for buildings located on Site Class C in Victoria, B.C. The first set comprises seven crustal ground motions from magnitude 7 Californian earthquake records and the second set consists of seven subduction ground motions recorded during the magnitude 9 Tohoku earthquake in Japan (March 11, 2011).
3. Revamp the existing design methodology proposed for SBF by Simpson (2018). To optimize the location of vertical truss (strongback) several case studies are considered. Conduct nonlinear analyses using OpenSees. The selected engineering demand parameters are the interstorey drift, residual interstorey drift, and floor acceleration.
4. Conduct incremental dynamic analysis (IDA) and plot the IDA curves for each ground motion. Identify the failure modes of SBF buildings under crustal and subduction records.
5. Assess the collapse safety of SBF buildings with external strongback against the benchmark MD-CBF building using the procedure outlined in FEMA P695 (2009).

1.5 Thesis Organisation

The thesis is structured into six chapters:

- Chapter 1: This chapter presents the introduction and provides an overview of thesis objectives and the methodology employed.
- Chapter 2: Literature review is conducted on traditional steel braced frames and their drawbacks when subjected to earthquake loads. Then, prior research on innovative structural systems including the Strongback Braced Frame that were developed for weak-storey response mitigation is presented. Numerical models developed in OpenSees environment and techniques aim to capture members failure are also presented.
- Chapter 3: This chapter presents a case study of a 4-storey MD-CBF office building located on Site Class C in Victoria, B.C. This building's design is based on the NBC 2015 and CSA S16 (2014) standard requirements. This chapter covers the selection and scaling of crustal and subduction ground motions. The seismic performance of this benchmark building, designed to withstand the code 2% probability of exceedance in a 50-year earthquake, is assessed through nonlinear time history analysis. The numerical model for the MD-CBF is developed using OpenSees.
- Chapter 4: This chapter outlines the design procedure for a 4-storey SBF system featuring buckling braces for energy dissipation and an external strongback system. Both adjacent external and reversed external strongback system are considered. The chapter reviews existing methods for evaluating the impact of higher modes on the SB system and reworks the existing design methodology. Nonlinear responses of 4-storey SBF buildings are carried out using OpenSees.

- Chapter 5: This chapter presents the outcomes obtained from incremental dynamic analysis, considering both crustal and subduction ground motion sets. A comparative analysis is conducted on the collapse safety of SBF building with external strongback against the benchmark MD-CBF building. The assessment of collapse safety is based on the FEMA P695 (2009) procedure.
- Chapter 6: This chapter presents conclusions and provides insight into potential avenues for future research.

Through this comprehensive study, the thesis aims to contribute to the advancement of seismic-resistant structural systems, particularly the Strongback Braced Frame. By analyzing the seismic responses of different SBF buildings and comparing them with the traditional MD-CBF building, this research seeks to demonstrate the efficiency of the revamped design methodology and the benefit of selecting SBFs to brace buildings in seismic regions particularly in subduction zone prone regions.

CHAPTER 2. LITERATURE REVIEW

2.1 Introduction

The aim of this chapter is to explore existing research related to seismic force resisting systems (SFRSs) designed to mitigate the weak-storey response of steel buildings. This chapter is divided in three parts: (i) The drawback of traditional seismic force resisting systems (SFRSs), (ii) Past studies related to weak-storey mitigation, and (iii) Research pertaining to strongback-braced frames (SBFs). The presentation highlights the energy dissipation mechanism of selected steel SFRSs and the evolution of the strongback concept.

2.2 Drawbacks of Traditional Steel SFRSs

Concentrically braced frame (CBF) system has gained popularity for low-rise and medium-rise buildings in seismic regions due to its simplicity in design and fabrication, cost-effectiveness, and ability to provide sufficient strength and stiffness (Tremblay et al, 1995). The CBF braces buckle at their mid-span length under lower seismic demand (Popov and Black, 1981). Typically, braces are made of hollow structural sections (HSS) and they dissipate the input energy through tension yielding and inelastic bending of plastic hinges formed at their mid-span length under compressive loads. To prevent local buckling and premature failure at plastic hinge location, it is recommended that braces be Class 1 as required in CSA S16:19. Proper selection of brace members contributes to ductile and stable behavior of CBFs under severe ground shaking (Khatib et al., 1988, Tremblay and Robert, 2001). However, the CBF is prone to damage concentration within one or a few floors, which leads to the formation of storey mechanism under strong earthquake shaking. Initially, braces contribute to the primary lateral stiffness, but once buckling occurs, the inelastic response of braces becomes the governing factor for the overall nonlinear response of CBFs. However, during intense earthquake shaking, the significant reduction in brace stiffness following buckling results in non-uniform force redistribution across the building height. This phenomenon leads to premature strength loss and the concentration of deformation in specific storeys, exacerbating the structural response. Example of damage concentration in CBFs with chevron bracing scheme and the formation of two-storey mechanism is illustrated in Fig. 2.1 (Tremblay and Robert, 2001).

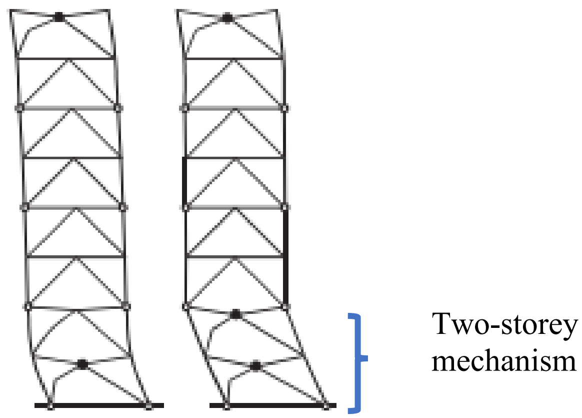

Fig. 2.1. The propagation of storey mechanism formation (Tremblay and Robert, 2001)

Steel eccentrically braced frames (EBFs) are also prone to damage concentration due to large rotation demand of shear link (Chen et al., 2019b) as illustrated in Fig. 2.2a. The traditional steel Moment Resisting Frame (MRF) is also prone to storey mechanism formation (Fig. 2.2b).

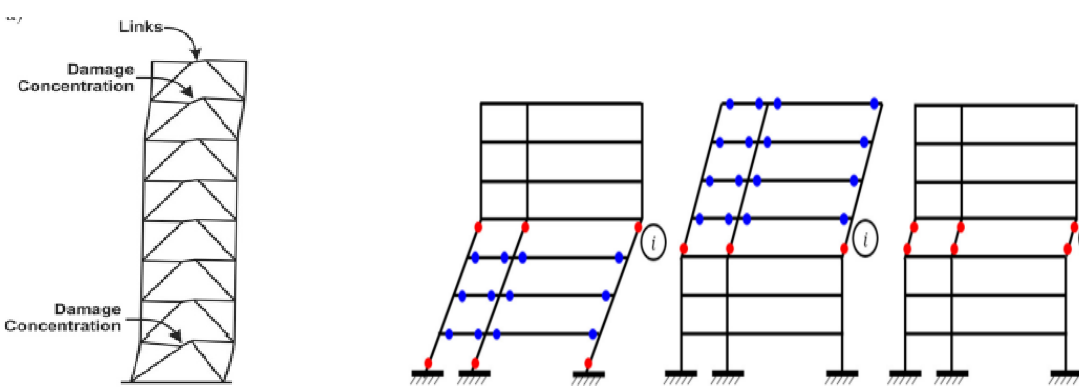

(a) (b)

Fig. 2.2. Damage concentration: a) EBF (Chen et al., 2019b) and b) MRF (Sepahvand et al., 2019)

2.3 Past Studies on Mitigating Storey Mechanisms

Researchers have conducted extensive research to mitigate the formation of storey mechanism of traditional steel SFRSs. Several alternative innovative systems aimed at mitigating such behavior are presented below.

2.3.1 Continuous Column System

Unlike traditional discrete column systems, continuous column systems provide enhanced load transfer and resistance to lateral forces. According to MacRae et al. (2004), in CBF buildings, a significant number of gravity load-resisting columns are typically connected with pin joints at each floor or every two floors. Modifying the column splices and ensuring continuity among gravity columns and CBF columns could be an effective strategy to mitigate the weak-storey response. This approach aims to minimize the occurrence of storey mechanisms by promoting a continuous load transfer path throughout the structure.

However, the continuous column system introduces additional complexities in terms of design, construction, and maintenance. The integration of continuous columns throughout the building requires careful consideration of connections, reinforcement detailing, and construction sequencing. These complexities may increase the construction costs. For example, the sizing of continuous columns in both multi-tiered and conventional systems becomes economically burdensome (Ji et al., 2009). In addition, relying solely on the implementation of continuous columns is inadequate for enhancing building safety in regions prone to high seismic activity (Millichamp, 2021).

2.3.2 Dual System

Several researchers studied the seismic response of Dual Braced Frame system (Giugliano et al., 2010; Bosco et al., 2012; Longo et al., 2014, 2016; etc.).

In earlier studies, there was a notable inclination towards the integration of either CBF or EBF with a MRF to create a dual system. This approach aimed to enhance the structural redundancy of the combined system and mitigate the risk of structural collapse (Whittaker et al., 1990). By incorporating both braced frames and moment frames, the dual system exhibited increased resistance to seismic forces and improved structural performance. The combination of these two systems enhances the overall robustness and redundancy, while gaining recognition for its ability to effectively distribute loads and dissipate energy during seismic events.

Kiggins and Uang (2006) explored the integration of Buckling-Restrained Braced Frames (BRBF) and Moment Resisting Frames (MRF) to form a dual system. Their findings revealed that the dual BRB-MRF system exhibited a slight reduction in ductility demand and a notable decrease in peak interstorey drift, ranging from 10% to 12%. This demonstrated the potential of the dual system to enhance the overall seismic performance of the structure. Further research by Xie (2008) focused on the dual BRB-MRF system and determined that by employing a backup MRF with 20% stiffness, significant reductions in maximum interstorey drift were achieved. These studies underscore the effectiveness of the dual BRB-MRF system in mitigating structural deformation and improving seismic resilience.

Wang (2018) used a dual system that comprises MD-CBFs and backup MRFs, to brace the 8-storey office building located on Site Class C in Vancouver, B.C. Nonlinear time history analysis and incremental dynamic analysis were employed to compare the performance of the Dual system with that of the standalone MD-CBF and MD-MRF systems. The findings demonstrated that the Dual braced frame system exhibited enhanced seismic resistance capabilities and facilitated more uniform distribution of damage throughout the building height. Notably, in Wang's (2018) study, the backup MRFs were positioned at the building's perimeter and were proportioned to carry an additional 25% of base shear, while the MD-CBFs were sizes for 100 % base shear. The purpose of adding the backup MD-MRF was to provide the elastic frame action until the beams of MD-MRF start yielding.

Although dual systems have been provided in the building code, they rely solely on the elastic frame action to distribute inelastic demands. However, after the MRF beams experienced hinging, the system is inefficient in mitigating the storey mechanism (Tremblay, 2003). Thus, when both the braced frame and MRF yield, the re-centering tendency significantly diminishes. This limitation highlights the need for alternative strategies to effectively address the challenges posed by storey mechanisms and potential dynamic instability.

2.3.3 Zipper Braced Frame

Khatib et al. (1988) introduced the Zipper braced frame system as a solution to prevent weak storey mechanisms in traditional chevron braced frames (CBF). The Zipper system incorporates vertical tie members at each floor, intersecting with the braces and beams, as illustrated in Fig. 2.3. Tie members, known as zipper columns, counteract the vertical unbalance caused by brace buckling. The goal is to sequentially buckle multiple braces and dissipate the input energy. Tension braces reach their yield strength, while the braced bay columns remain protected from inelastic deformation using the capacity design method. Under severe lateral loads, the vertical zipper columns utilize beam stiffness and remaining braces to resist unbalanced vertical forces after half-side brace buckled. This results in progressive brace buckling sequence started from the first storey to the top or reversed, while forming plastic hinges at mid-span beams.

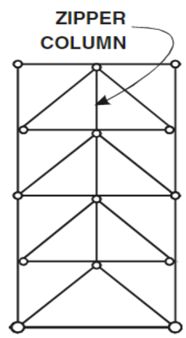

Fig. 2.3. Zipper braced frame configuration, (Tremblay and Tirca, 2003)

The Zipper braced frame (ZBF) has gained popularity, and several studies have focused on ZBF buildings (Yang et al. 2008 and 2010; Tirca and Chen, 2012; Rahimi et al., 2016; Yu et al., 2016; Wijesundara et al., 2018).

Khatib et al. (1988) suggested a design approach for the tension force in the zipper column, considering the unbalanced vertical forces transmitted from the stories above and below. Tremblay and Tirca (2003, 2004) proposed a design method for predicting the forces in zipper columns based on different brace buckling sequences. Tirca and Chen (2012) further refined this method by considering six lateral load distribution patterns. Yang et al. (2008a) proposed a design procedure that combined a partial-height zipper mechanism with a hat truss system in order to prevent the dynamic instability. Razavi and Sheidaii (2012) proposed using pre-stressed cables instead of zipper columns for transferring unbalanced forces to upper levels. Experimental results demonstrated the strength and ductile behavior of tested ZBFs. However, building codes do not include explicit provisions for the design of ZBFs. In general, after half side braces reached yielding almost simultaneously, the ZBF is prone to dynamic instability.

2.3.4 Tied Eccentrically Braced Frame

In Eccentrically Braced Frames (EBFs), deformations of beam links may vary unevenly with building height (Whittaker et al., 1990). This drawback can be mitigated by appropriately adjusting the sizing of beam links based on their height-wise distribution demands. However, as the height of EBFs increases, the influence of higher modes on the overall response tends to amplify shears in upper stories while diminishing them in middle and lower stories. It was highlighted that incorporating second and third mode responses when determining static demands is essential to prevent uneven deformations of links with building height (Popov et al., 1992).

To address the abobe issue, Martini et al. (1990) proposed an innovative solution and the system was called the Tied Eccentrically Braced Frame (TEBF). In this concept, beam links are enclosed between two "super" columns, which are hinged at the base and interact with the beam link similarly to a coupled shear wall as depicted in Fig. 2.4(a). To offset the added cost of the TEBF, the study proposed reducing the strength of beam links while enhancing the overstrength of the super columns. The focus was on ensuring the predictability of TEBFs and the supplementary stiffness provided by columns, braces, and ties within the super columns. Further, the TEBF was studied by Rossi (2007), Bosco and Rossi (2009), Tremblay et al (2014) and Chen et al. (2019a and 2019b). To reduce the development of base shear, Tremblay et al. (2014) proposed for tall building the modular concept of TEBF labeled simply TBF, while the modular TBF was called M-TBF.

Thus, the two vertical elastic trusses formed by column, tie and braces, were segmented into modules to mitigate the large shear demands that arise in ties and increase when building height increases. Beam links were designed based on the average storey shear force in a module. This modular setup of M-TBF (Fig. 2.4b) led to reduced tie demands but increased drift demands between modules. Additional energy dissipation devices, including Buckling Restrained Braces (BRBs), friction dampers, and self-centering braces, can be utilized to mitigate these drift effects, as illustrated in Fig. 2.4c.

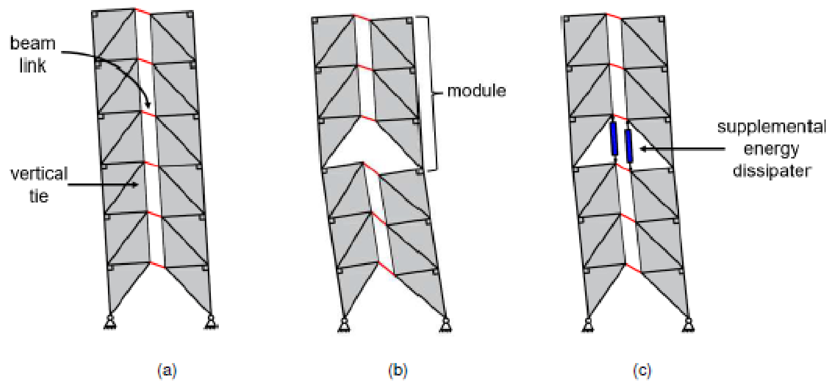

Fig. 2.4. Tied Braced Frames and Modular Tied Braced Frames (Tremblay et al., 2014)

2.3.5 Rocking braced frames and Self-centering system

To mitigate the storey mechanism, researchers have also proposed the Rocking Braced Frame (RBF) with and without controlled rocking and Self-centering Braced Frame and Self-centering Moment Resisting Frame. A detailed review on RBFs was released by Froozanfar et al. (2024) and a dual rocking braced frame is presented in Fig. 2.5. Details on Self-centering systems are presented in Hajjar et al. (2013).

Takeuchi et al. (2015) noted that applications of self-centering systems to real buildings are not yet popular due to the need for large self-centering posttensioned (PT) strands and special solutions at the uplift column bases. To eliminate these drawbacks, Takeuchi et al. (2015) investigated a non-uplifting spine frame system without PT strands whose self-centering function is achieved by envelope elastic-moment frames. The proposed system illustrated in Fig. 2.6c was tested by applying it to an actual building structure under construction, and its performance was compared with a conventional BRBF (Fig. 2.6a) and controlled rocking frame with PT strands (Fig. 2.6b). In summary, the NL spine frame showed very good performance in preventing damage concentration in weak stories, as well as sufficient self-centering capacity under strong earthquakes even without the PT strands. In 2014 this system was employed in the design of a real building.

Fig. 2.5. A dual rocking steel braced frame system and its different components (Froozanfar et

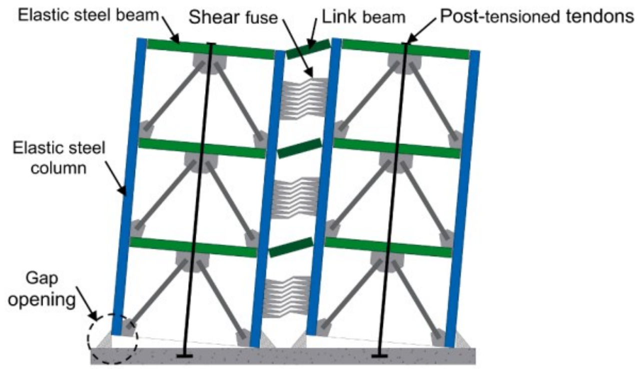

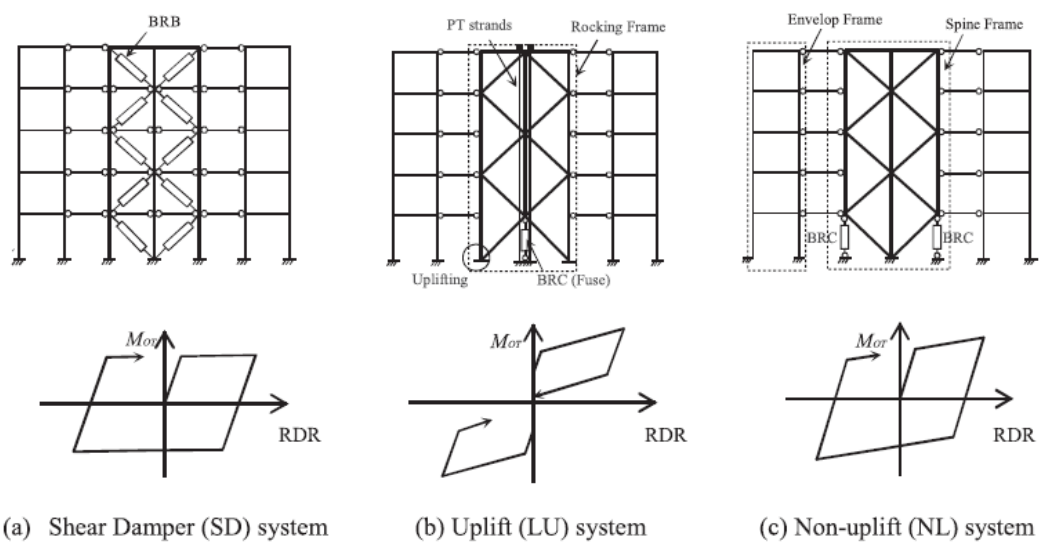

al., 2024).

Fig. 2.6. Configurations and hysteretic curves of three SBRSs

2.4 Evolution of Strongback Braced Frame

2.4.1 Early Conceptualization of Strongback Braced Frames

The concept of strongback system, referred as elastic truss system, was firstly proposed by Khatib et al. (1988). Then, Tremblay (2003) proposed a dual buckling-restrained braced frame system, consisted of two vertical steel trusses, where one was designed to exhibit inelastic behavior for energy dissipation and the other designed to maintain its elastic response. The research acknowledged the potential of incorporating a strongback to mitigate dynamic instabilities in braced frames. However, specific design requirements for the elastic truss were not provided, and it was emphasized that nonlinear dynamic analysis was necessary to assess the demands on the strongback members.

In a subsequent study, Tremblay and Poncet (2007) investigated 12-storey and 16-storey buildings braced by inverted-V or "chevron" system for energy dissipation and elastic trusses for dynamic stability. Buckling-restrained braces were employed to dissipate the input energy. The brace and tie sizes of elastic truss were kept consistent across all stories. The size of the strongback braces was determined as two times the force resulting from the yielding of the first-storey buckling-restrained brace (BRB). The design of the tie was based on the unbalanced load derived from the adjusted compression capacity of the BRBs and the yield capacity of the adjacent strongback brace. Adding the elastic truss to the BRBF, demonstrated improved performance compared to traditional BRBF. However, the study acknowledged that the design approach used for BRBFs with elastic trusses was not optimal and called for more refined design guidelines to be developed.

Merzouq and Tremblay (2006) expanded the study conducted by Tremblay and Poncet (2007). They investigated two-bay elastic truss systems in buildings ranging from 8 to 24 stories, as shown in Fig. 2.7. These buildings were designed for a specific location and subjected to near-fault and simulated subduction ground motions. The design of the elastic truss included braces and ties were done in groups of four successive stories. From the study was observed that yielding of BRBs occurred in batches of stories between 1/5 and 1/4 of the frame height, while peak demands in the elastic braces followed a similar pattern with a lag behind the BRBs. Higher-mode effects were found to increase the demand on elastic braces in the upper stories of the frame.

Based on these observations, empirical guidelines for the design of the elastic truss members were proposed. The demand in the elastic braces was calculated by empirically amplifying the demand triggered in the inelastic braces by using a factor dependent on the building height. The demand in ties was determined by accumulating the unbalanced demand from the inelastic and elastic brace forces, summed from both the top and bottom of the structure. The minimum envelope of these cumulative unbalanced demands represented the peak tie demand. Then, empirical correction factors, considering the frame height, were applied to account for the response amplification in the upper stories and the variation in brace forces between consecutive stories. It was observed that the tie demand was highest when the brace demand changed sign in consecutive stories.

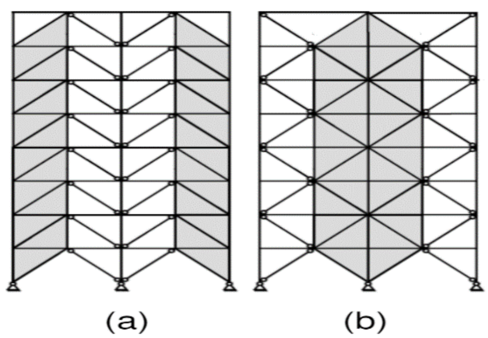

Fig. 2.7. Schematic of braced frames with strongback systems: (a) and (b) two-bay braced frame with elastic truss systems (Merzouq and Tremblay, 2006)

The comparison between the elastic truss system and conventional BRBF revealed that the elastic truss system exhibited more uniform deformation distributions with building height and had greater reserve capacity. However, it was noted that the duration of subduction events could be crucial for the performance of elastic truss systems, potentially leading to the formation of a complete collapse mechanism and global instability. Additionally, accelerations were found to be uniform but higher than those observed in a BRBF.

Further research on Strongback Braced Frame (SBF) was carried out by Lai and Mahin (2015). They evaluated different bracing configurations through static pushover and nonlinear dynamic analyses. To reduce damage concentration in steel-braced frames during severe seismic excitations, the SBF combines aspects of a traditional concentrically braced frame (CBF) with that of an elastic truss. A comparative response between a CBF and SBF is shown in Fig. 2.8.

The study released by Lai and Mahin (2015) demonstrated the effectiveness and economic feasibility of installing SBF buildings in seismically active regions. The SBF is able to reduce deformation concentration and outperform traditional braced frames. Additionally, the study explored the impact of gravity columns on structural response and provides recommendations for further design optimization and investigation into member sizes and yielding in the SBS.

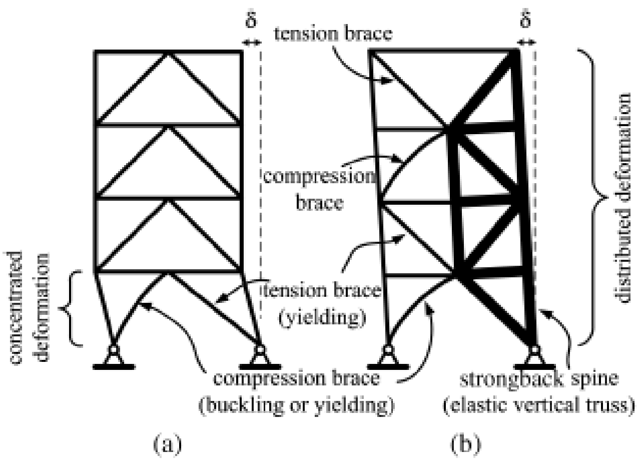

Fig. 2.8. Comparison of braced frame drift: a) CBF and b) SBF (Lai and Mahin, 2015)

The building selected as case study is a 4-storey office building located in downtown Berkeley, California. The building has a square plan and is braced by four braced frames in each orthogonal direction. The design followed the ASCE 7-5 and AISC seismic provisions (AISC 2005). In this study, a total of six different configurations of seismic force-resisting systems were selected as shown in Fig. 2.9. The analysis included two typical bracing configurations, one is a typical CBF with chevron-bracing configuration (Model V6 shown in Fig. 2.9a) used as a benchmark, and another one is a double-storey split-X bracing configuration (Model X6 shown in Fig. 2.9b). A geometrically transformed model, Model X6-3, shown in Fig. 2.9c, maintained the same basic structure as Model X6 but shifted the intersection of the braces from the beam's midpoint to the one-third point. This adjustment allows for better distribution of load among different components in the structure. Since the vertical elastic truss section of the bay is narrower than half the bay width, the inelastic elements become longer, providing longer brace's length over which they can yield. By reducing the inclination of these inelastic braces, they can be smaller while still effectively resisting the same lateral load on the structure. Additionally, when the frame experiences significant lateral displacements, the increased length of the beam in the inelastic portion of the bay helps reducing shear forces and minimizing plastic hinge rotations at the beam ends. To ensure symmetry in the lateral force-resisting system, the shifted brace points aligned along the centerline of the elevation. The prototype office building had four braced bays in each direction, with two at each perimeter face. If one bay had a left-inclined yielding/buckling brace, the corresponding bay had its brace inclined to the right. By incorporating vertical tie columns along the height of the braced bay, the vertical spine (elastic truss) is formed and the traditional X6-3 braced frame system is transposed into the SBF labelled SB6-3 (Fig. 2.9d).

The members within the vertical elastic truss were intentionally designed to remain primarily elastic when subjected to seismic loads scaled at design level. The design approach employed here relies on the system's code-specified over-strength factor, which is set at 2.0 in this specific case. Stress checks for individual members were conducted using SAP2000 (CSI 2009), considering the load combinations specified in ASCE 7-05. Within the vertical spine, stress ratios were carefully controlled to be less than 0.5, which is the reciprocal of the system overstrength factor for special

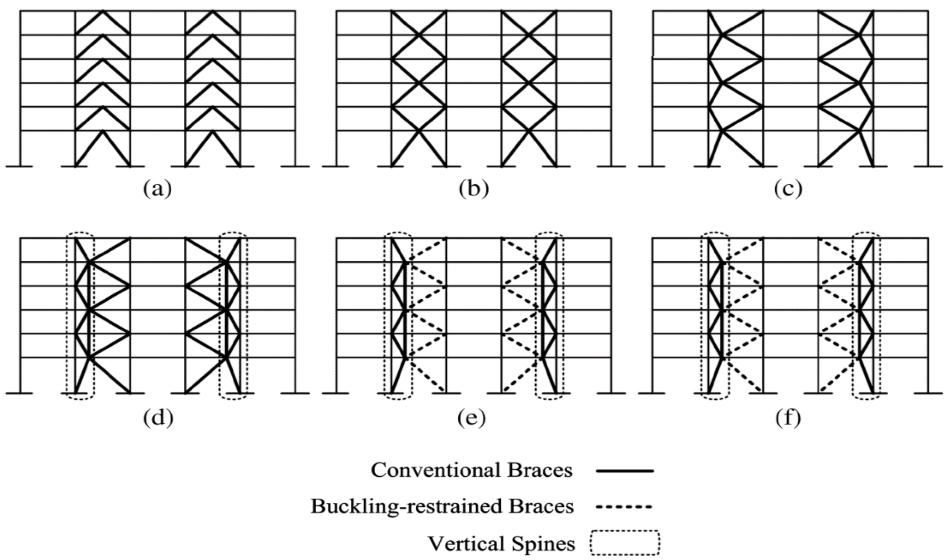

Fig. 2.9. Elevation views of six different bracing configurations: (a) V6; (b) X6; (c) X6-3; (d) SB6-3; (e) SB6-3B; (f) SB6-3 L (Lai and Mahin, 2015)

CBFs. All tie columns were sized based on the maximum anticipated tension and compression forces that could arise from brace capacity forces. The first design intent was to preserve the vertical spine in the elastic range. However, during severe ground shaking, certain members of the elastic truss experienced inelastic response. Thus, a more elaborated design method is required, while keeping the cost manageable.

It is noted that conventional buckling braces were used in Models V6, X6, X6-3, and SB6-3 illustrated in Fig. 2.9a-d. Due to the non-symmetric hysteresis response caused by the significant compression strength degradation of conventional buckling braces, BRBs were employed outside the vertical spine, as illustrated in Fig. 2.9e. Model SB6-3L shown in Fig. 2.9f is similar to Model SB6-3B, except it uses low yield-strength steel, LYS (with a yield strength of 103.4 MPa) for the steel cores of BRBs. Lateral displacements in frames with BRBs tend to be larger than those in conventional braced frames due to the reduced steel area in the braces, resulting in a more flexible system. The use of LYS steel aims to increase stiffness and reduce displacement without significantly increasing strength. The design strategy for the vertical spines in Models SB6-3B and SB6-3L was the same as for Model SB6-3. From analysis, the first and second vibration mode of each building model is provided in Table 2.1. As shown, the 1st mode period of X6-3 model is 0.7 s and that of derived SBF (see model SB6-3) is 0.67 s; hence, a small increase in stiffness occurred when the strongback system was considered.

Table 2.1 The first and second vibration mode of each building model (Lai and Mahin, 2015)

Model name	First mode (s)	Second mode (s)
V6	0.69	0.25
X6	0.70	0.24
X6-3	0.70	0.25
SB6-3	0.67	0.24
SB6-3B	0.77	0.29
SB6-3 L	0.57	0.20

The Nonlinear Dynamic Response History Analysis (NDRHA) was considered using OpenSees. The fault-normal and fault-parallel components of ground motions were used in analyses. The distribution of storey drift and residual storey drift over the building height for all building models is plotted in Fig. 2.10. The storey drift ratios varied among the models, with Model V6 forming a soft-storey mechanism at the bottom floor and Model X6 exhibiting a soft two-storey mechanism.

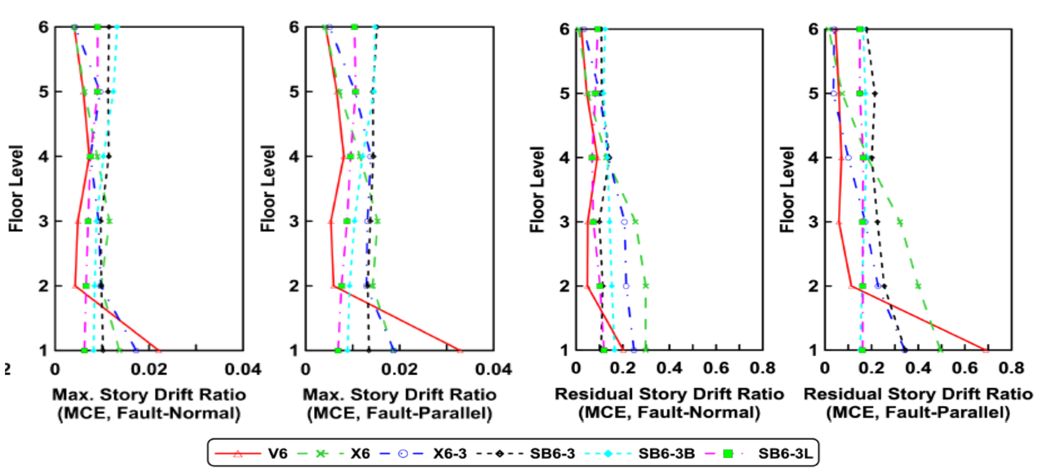

Fig. 2.10. Mean storey drift and residual storey drift for each building model (gravity columns included) under MCE level ground motions (Lai and Mahin, 2015)

Models SB6-3, SB6-3B, and SB6-3L showed slightly larger storey drift ratios in upper stories compared to lower stories, while Model SB6-3 had a more uniform distribution of storey drift.

All residual storey drift were less than 0.5% for all cases but one V6 that reached 0.7% at 1st floor. Moreover, under fault-parallel ground motions, both drift and residual drift were larger than under fault-normal ground motions. The time-history series of each floor drift is plotted in Fig. 2.11 under MCE level ground motions. From analyses also resulted that the peak base shear forces ranged between 4,600 and 7,100 kN, with the order following the fundamental periods of the models. Models with lower fundamental periods experienced higher peak shear forces.

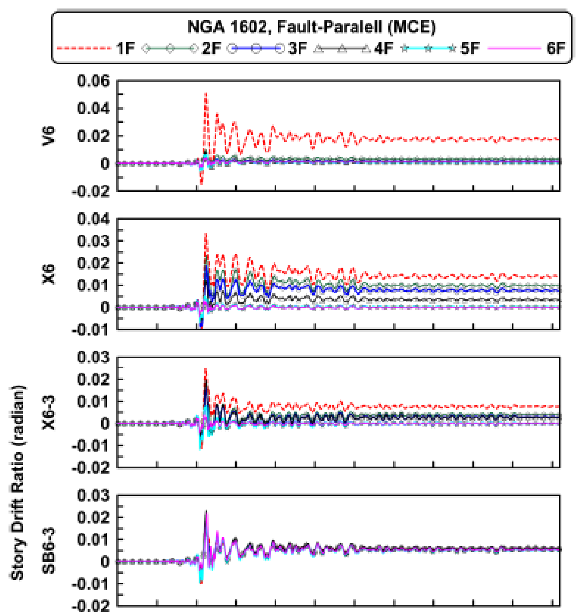

Fig. 2.11. Storey drift histories of V6, X5, X6-3 and SB6-3 models under scaled NGA 1602 fault-parallel component ground motion scaled at MCE level (Lai and Mahin, 2015)

The hysteresis of all 12 braces of models V6, X5, X6-3 and SB6-3 under scaled NGA 1602 fault-parallel component ground motion scaled at MCE level are plotted in Fig. 2.12. The hysteresis of ties of SB6-3 model is also plotted. From Fig. 2.12 resulted that large demand occurred at the bottom floor of V6 model (Fig. 2.9a), the damage is more uniformly distributed in X6 and X6-3 models (Figs. 2.9b-c), and braces of elastic truss of SB6-3B model (Fig. 2.9d) performed elastically as anticipated but the tie-column at upper floors exhibited light nonlinearity as shown in Fig. 2.12e. In addition, it was found that gravity columns improved the response of non-strongback braced

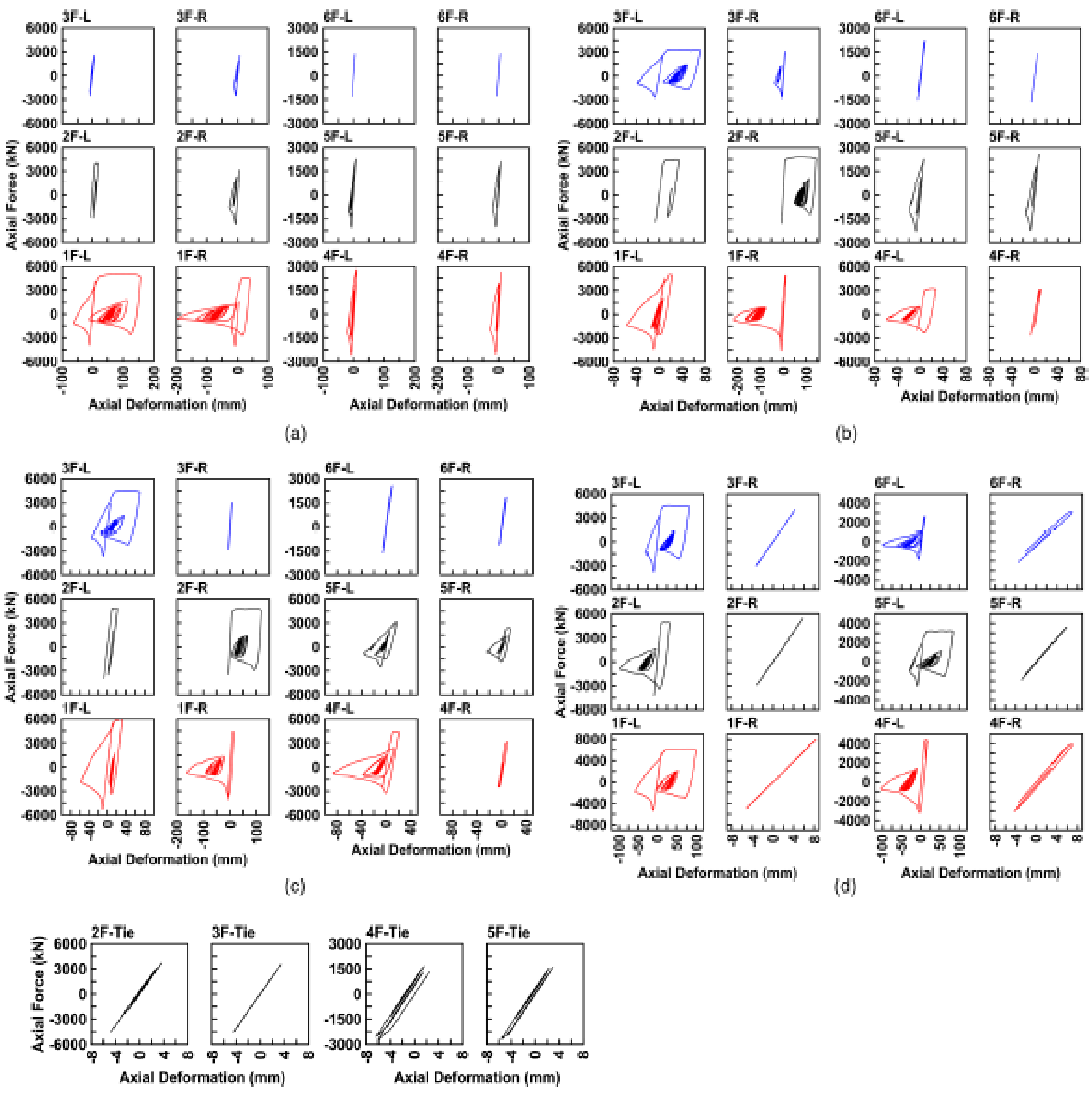

Fig. 2.12. Brace and tie hysteretic responses of four models under scaled NGA 1602 fault-parallel component ground motion scaled at MCE level: a) V6, b) X6, c) X6-3 and d)-e) SB6-3B (Lai and Mahin, 2015)

frame but not that of SBF. To conclude, the SBF effectively mitigates the soft-storey mechanism, and the simplified design strategy leads to the achievement of a uniform distribution of storey drift. Considering BRBs in SBFs may decrease the drift along the building height but could increase the residual drift in upper floors. However, the simplified design strategy does not adequately size members near the top of the strongback systems; hence, further investigation is needed.

2.4.2 Experimental Tests

Simpson and Mahin (2018b) conducted full-scale quasi-static experiments in the laboratory environment to evaluate the performance of a retrofit braced frame using the strongback system. This retrofit was designed as an enhancement for two vintage CBFs, representative of construction practices from the 1970s and 1980s. The outcomes of these experiments demonstrated the strongback's capability to effectively mitigate the weak-storey behavior, thereby promoting more uniform drift demands across the structure height. The schematic illustration depicting the inelastic behavior of the two vintage braced frame and the SBF as retrofit design that were tested are presented in Fig. 2.13. Throughout the experimental tests, several practical detailing issues came to light. The geometry of the strongback and its corresponding kinematic relationships were identified as factors that could impose considerable demands on the inelastic components of the system. However, strategies such as adopting an offset bracing configuration, as proposed by Lai and Mahin (2015), showed promises in alleviating the inelastic demand. In the offset configuration, the intersection point of braces deviates from the centerline of the bay. Further analysis conducted by Simpson and Mahin through numerical simulations revealed that this approach allowed the strongback frame to accommodate larger displacement while experiencing reduced deformation demands compared to configurations lacking offsets.

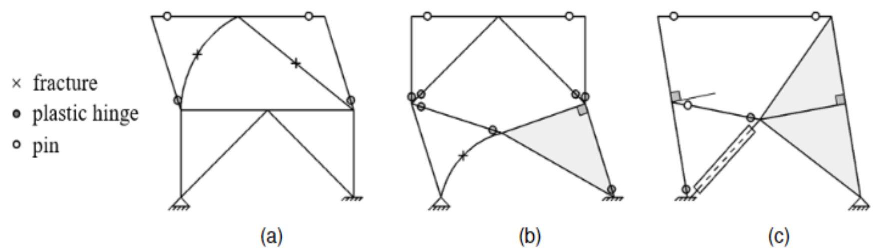

Fig. 2.13. Schematic of damage observed in experiments (Simpson and Mahin, 2018b)

2.4.3 Principle of Strongback Braced Frame Design

Simpson (2020) proposed a design approach that includes higher-mode force demands triggered in the Strongback Braced Frames (SBFs). Then, accounted on these forces, members of strongback (elastic truss) were sized to satisfy elastic response and ensure structural integrity under seismic loading conditions. It was noted that the significant source of uncertainty in the design process is related to the uncertainty in force demands in the elastic truss caused by higher modes effect. The magnitude of higher-mode response depends on: (a) ground shaking intensity, (b) mass participation in higher modes, and (c) mass distribution on a story-by-story basis. The forces in the elastic truss exhibit varying patterns due to inertial forces changing with time, influenced by multiple modes of vibration and nonlinear responses triggered by yielding of ductile braces. The higher-mode effect is influenced by the interaction of higher modes during ground shaking, redistributions of forces upon ductile braces yielding, and the dependence of structural response on earthquake excitation. Large variabilities are associated with forces in members designed to remain elastic, leading to different load patterns and demand distributions. Thus, higher-mode force demands need to be considered in the design of the strongback to meet realistic strength and stiffness criteria. However, the calculation of higher-mode demands in term of storey shear contribution is not straightforward and a methodology is presented by Simpson (2020).

Simpson (2020) noted that nonlinear dynamic analyses can directly simulate the dynamic behaviour of SBF at any time step of ground motion shaking. This type of analysis addresses capacity design limitations in SBFs and is able to incorporate higher-mode force demands used to size the elastic truss members to respond elastically. However, this method requires several iterations because the initial estimation of forces in strongback members and respectively their size does not account on higher modes. Hence, the stiffness of strongback members is updated in order to provide an elastic response. However, using the iteration process the uncertainty is high due to the record-to-record variability. Additionally, the design iterations involve minimizing the weight of members in the elastic truss until the design meets acceptance criteria, resulting in an SBF design that considers non-negligible higher-mode contributions.

The **acceptance criteria,** used for SBF design iterations, ensures that the SBF exhibits less than a 10% probability of failure at the Maximum Considered Earthquake (MCE) level as per FEMA P-695 (2009) procedure. Herein, the failure includes limit states associated with both collapse and inelastic response in the elastic truss. The FEMA P-695 (2009) procedure assumes a lognormal distribution of spectral intensity at failure with median intensity $\hat{\mu}(T)$ and total uncertainty β_{total}, where $\beta_{total} = (\beta^2_R + \beta^2_D + \beta^2_T + \beta^2_M)^{0.5} = 0.525$. In the provided example, the following values were considered: $\beta_R = 0.4$ (record-to-record variation), $\beta_D=0.2$ design criteria, $\beta_T=0.2$ the quality of test data and $\beta_M=0.2$ numerical modelling. For values of uncertainties provided, the quality rating was considered "good" and the collapse safety criteria is expressed by Eq. (2.1) below

$$ACMR \geq ACMR_{10\%} \qquad (2.1)$$

where ACMR is the adjusted collapse margin ratio (ACMR = SF X CMR) and $ACMR_{10\%}$ is the acceptable collapse probability taken as 10%. The CMR is the ration between the median spectral acceleration intensity at failure and S(T1) at design level, while SF is the spectral shape coming from tables in function of building period and ductility. The $ACMR_{10\%}$ is selected from FEMA P-695 tables in function of β_{total} and its value increases as β_{total} increases. For example, for β_{total} =0.3, $ACMR_{10\%}$ = 1.42 and for β_{total} =0.525 is 1.92. In addition, for a building with a first mode period of 1.3 s and period-based ductility μ_T =5, from tables it results SF=1.41. Hence, for CMR =X, where X resulted from incremental dynamic analyses, it results ACMR = 1.41X.

Thus, to satisfy the collapse safety criteria, 1.41X = 1.92 and X =1.36. Based on this simple calculation, Simpson (2020) concluded that the SBF design is considered acceptable if the fragility curve associated with a trial design has a median failure intensity greater than or equal to 1.36 times the spectral pseudo acceleration at the fundamental period, S_a(T1) as shown in Fig. 2.14.

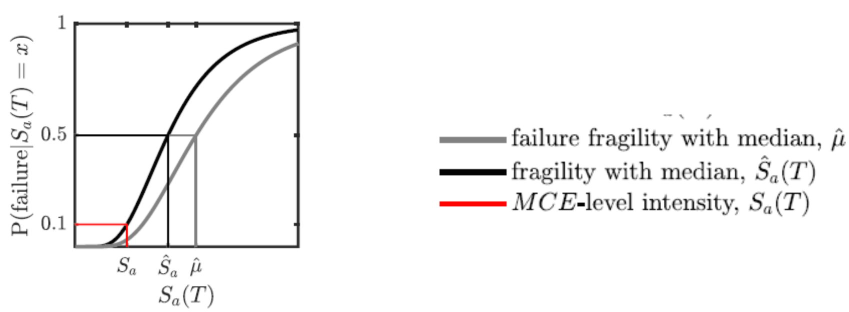

Fig. 2.14. Failure fragility

A 4-storey SBF office building located in downtown Berkeley and presented in Fig. 2.15 was selected as the archetype design. The nonlinear braces are buckling restrained braces and the shaded truss is the strongback system designed to perform elastically. The BRB braces were designed according with ASCE/SEI 7-16 and the capacity design was considered for the beams and columns that are not part of elastic truss. The elastic truss was designed using an iterative scheme employing nonlinear dynamic analyses and FEMA P-695 (2009) requirements.

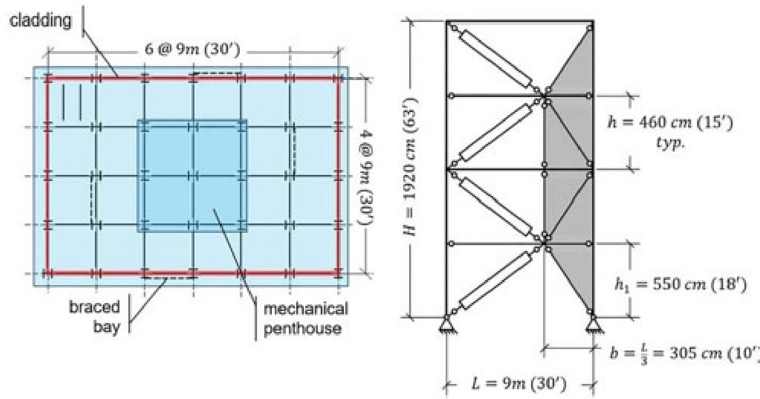

Fig. 2.15. Case study

Herein, the same BRB size was used for all nonlinear braces and the model was labelled SBF-u. This option of BRBs selection is based on the assumption that similar deformations are expected in each storey due to the building's geometry and plastic mechanism. This decision was based on the observation that using the same BRB in every storey results in a larger base shear strength during the formation of a complete mechanism. For comparison purposes, the same design process for SBF was used, but BRBs were designed based on demand-to-capacity ratios under the first-mode equivalent lateral force distribution and the system was labelled SBF-d (see Fig. 2.16a). The SBF-u and SBF-d configurations were used to investigate the impact of different distributions of buckling restrained brace (BRB) sizes on the seismic behavior of SBF.

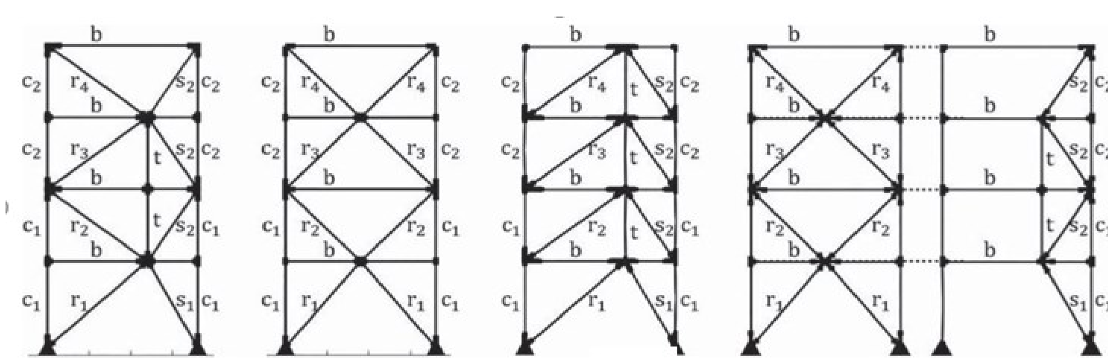

a) b) c) d)

Fig. 2.16. Archetype designs: a) SBF-u and SBF-d; b) BRBF in configurations BRBF-u and BRBF-d; c) SBF-v, and d) SBF-s (Simpson 2020)

The seismic response of SBF system is presented against that of traditional BRBF, where two models were considered for BRB distributions, and the system was labelled BRBF-d and BRBF-u (Fig. 2.16b). The beam links were capacity designed based on the resulting shear developed from the plastic moments at the ends of the beam link length, because the moment behavior in the beam links is similar to the flexural yielding behavior at the ends of a long link in an eccentrically braced frame. To analyse the effect of elastic truss configuration, an inverted V bracing configurations (SBF-v) is also investigated (Fig. 2.16c), as well as the case when the strongback is separated from the nonlinear braces (SBF-s) presented in Fig. 2.16d.

The seismic response of configurations presented in Fig. 2.16 are provided in Fig, 2.17 in terms of median of peak storey drift, median of peak absolute floor acceleration and median of peak storey shear under MCE level earthquake demand. The comparison of BRBF and SBF behavior revealed that the BRBFs exhibited a storey drift profile indicative of a first-storey mechanism, with larger first-storey drifts in BRBF-u compared to SBF configurations. In contrast, the SBF drift response was less dependent on the proportioning of the BRBs and was mitigated by the inclusion of the strongback, resulting in smaller overall peak storey drift demands. However, the SBFs showed larger storey shears and absolute floor accelerations compared to the BRBFs.

The shear forces in the SBFs exhibited a greater sensitivity to ground motion characteristics. In term of storey drifts, both BRBFs and SBFs showed similar sensitivity of drift response to ground motions. Additionally, force demands in the SBF, particularly in the elastic truss, were significant compared to those triggered in the BRBF, with yielding occurring in all nonlinear braces of the SBF but only in the bottom story braces of the BRBF. The explanation of high magnitude of axial forces triggered in the elastic truss is due to their elastic nature and the higher-mode inertial forces which are not limited by the nonlinear response.

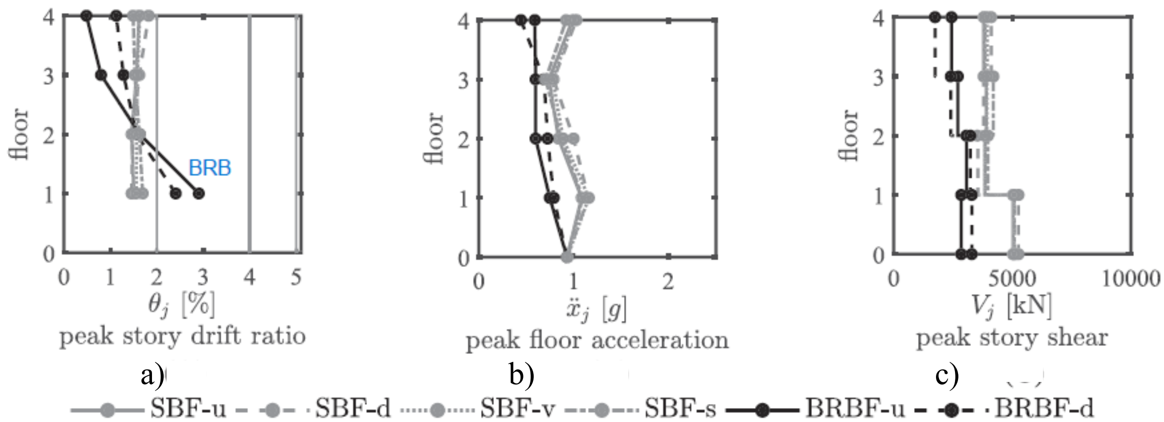

Fig. 2.17. Comparison of SBFs against BRBFs at MCE code-level demand: a) median of peak storey drift, b) median of peak absolute floor acceleration and c) median of peak storey shear

To gain insight into the conditions influencing the higher-mode response, equivalent static forces using the mode shapes were compared with the nonlinear dynamic results. Discussions focus on SBF-u configuration. The comparison results show that: i) the strongback (elastic truss) remained elastic under the additional forces generated by the higher modes and forces triggered in the elastic truss are governed by bending-like demand caused by higher-mode contributions that depend on the intensity of ground motion and its frequency content; ii) the peak force demands in the nonlinear braces aligned with the first-mode equivalent static forces estimated from a plastic analysis, while the elastic second-mode and third-mode equivalent static forces aligned with the forces in the elastic braces and tie; iii) forces in the elastic truss are amplified with respect to the first mode under higher-mode (bending) contributions, resulting in significant higher-mode force contributions to the total storey shear response and a different distribution of storey shear demands over the building height; iv) the higher-mode force demands could be significant in the first and upper stories due to the flexural strength of the elastic truss; v) the higher-mode forces are not limited by the yield mechanism, leading to large inertial effects relative to the first-mode response;

and vi) the distribution of story shear over the building height is also influenced by the higher-mode profile, resulting in amplified storey shears in some stories and negligible effects in others.

To conclude, the case studied employing the SBF that are provided in the literature are limited to low-rise and middle-rise buildings and some potential configurations as have been also indicated in Simpson (2018). Further research is necessary to explore a broader range of SBF designs and configurations.

2.5 Modeling of steel braced frame buildings using OpenSees

Open System for Earthquake Engineering Simulation (OpenSees) is a collection of modules that facilitate the implementation of models and simulation procedures for structural and geotechnical earthquake engineering. The software framework was created by McKenna et al. (2004) at the University of California at Berkeley. The open-source approach has resulted in collaboration among a substantial community of developers and users within and outside of the Pacific Earthquake Engineering Research Center (PEER). The software is open-source and written in C++ with several Fortran numerical libraries. It allows users to create programs and applications with scripts in Tcl language. OpenSees has been widely adopted by researchers for nonlinear analysis of structures due to its flexibility in material calibration and nonlinear dynamic simulations.

Uriz (2005) was the first to develop a brace fracture model within the OpenSees framework. This model utilized a low-cycle fatigue approach with constant plastic strain amplitude, employing an accumulative strain to predict damage in accordance with Miner's rule (ASTM 2003). Hollow structural section (HSS) braces were assigned fatigue material properties to simulate strength deterioration and eventual brace fracture in concentrically braced frames (CBF). The fatigue ductility coefficient (ε_0) and the fatigue ductility exponent (m) are required as input parameters for defining fatigue material in OpenSees. Based on the accumulated strain approach and experimental tests conducted by Yang and Mahin (2005), Uriz proposed the following fatigue material parameter values for HSS brace members: $\varepsilon_0 = 0.095$ and $m = -0.5$. Subsequent studies estimated different ε_0 and m values from experimental tests. For instance, Santagati et al. (2012) proposed $\varepsilon_0 = 0.07$ and m = -0.45, while Salawdeh and Goggins (2013) estimated $\varepsilon_0 = 0.19$ and $m = -0.5$. As a result, the largest recommended ε_0 value is 0.19, which is more than double that the smallest value (0.07) proposed by previous researchers.

To simulate the inelastic response of braces in OpenSees, nonlinear force-based beam-column elements with distributed plasticity are used. The parental steel material is modeled with the Giuffre-Menegotto-Pinto material (*Steel02*) as defined by Aguero et al. (2006). The brace member is divided into n_e number of nonlinear beam-column elements with fiber cross-section formulation and distributed plasticity, as shown in Fig. 2.18a. The model employs the corotational geometric transformation approach and considers a sinusoidal pattern deformation at the onset of buckling, as well as the Gauss-Lobatto integration rule for distributed plasticity. Hsiao et al. (2013) recommended that a minimum of 16 nonlinear beam-column elements with distributed plasticity are sufficient to simulate the hysteretic behavior of HSS brace upon failure.

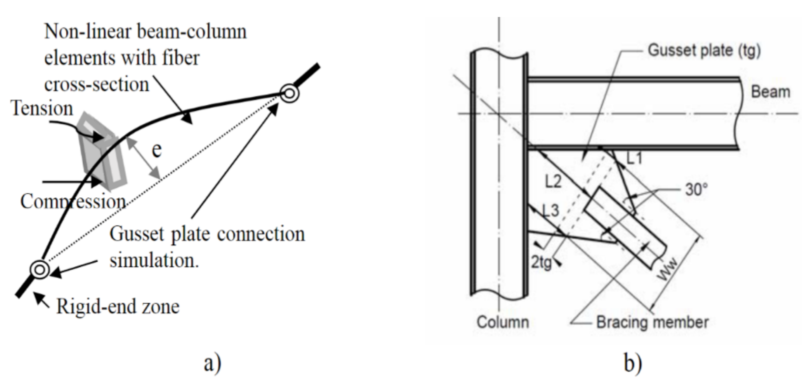

Fig. 2.18. Model of brace and brace end connection: a) OpenSees model; b) geometry of gusset plate connecting the HSS brace to frame. (Tirca et al., 2015)

Lignos and Karamachi (2013) introduced an empirical formula for HSS braces to enhance the precision of fatigue material, as demonstrated in Eq. (2.2), which relies on regression analysis to predict the material parameter value $\varepsilon_{0,pred}$.

$$\varepsilon_{0,pred} = 0.291(\frac{kL}{r})^{-0.484}(\frac{w}{t})^{-0.613}(\frac{E}{F_y})^{0.3} \quad (2.2)$$

In Eq. (2.2), strain ε_0 is calculated based on the slenderness ratio (kL/r), width-to-thickness ratio (w/t), and properties of brace steel material, such as yield strength (F_y) and Young's modulus (E). The fatigue ductility exponent m was assumed to be -0.3. This prediction was validated for HSS braces with slenderness ratios between 27 and 85, primarily for stocky braces. The low-cycle fatigue parameters were calibrated against various experimental test results, concluding that the predicted and calibrated ε_0 values corresponded well, with ε_0 values ranging from 0.05 to 0.10 and an average of 0.064.

Tirca and Chen (2014) validated the numerical model of HSS brace developed in the OpenSees framework using 14 HSS brace specimens with slenderness ratios between 52.4 and 143.5 to cover a wide range of brace slenderness ratios. The test results considered were primarily from Tremblay (2002) and Shaback and Brown (2003). The selected experimental tests were those where braces buckled out-of-plane and reached fracture failure. Using regression analysis, the predicted failure strain value for square HSS braces with slenderness ratios between 50 and 150 is given in Eq. (2.3).

$$\varepsilon_{0,pred} = 0.006(\frac{kL}{r})^{0.859}(\frac{b_0}{t})^{-0.6}(\frac{E}{F_y})^{0.1} \quad (2.3)$$

In this equation, according to the CSA S16 standard, $b_0 = b - 4t$, where b is the effective width and t is the thickness of the HSS brace. It is important to note that the slope of the Coffin-Manson curve is assumed to be m = -0.5, consistent with the value proposed by Uriz and Mahin (2008).

Studies have indicated that the gusset plate connection plays a crucial role in the stiffness, resistance, and inelastic deformation capacity of braces. To model the behavior of the gusset plate connection, two rotational and one torsional springs are introduced in the zero-length element that connects the brace ends to a rigid link, as illustrated in Fig. 2.18b. To represent the flexural stiffness of the gusset plate in the out-of-plane direction, the recommended equation proposed by Hsiao et al. (2012) involves parameters such as Young's modulus of steel (E), Whitmore width (W_w) defined by a 30º projection angle, average length (L_{avg}) computed from L_1, L_2, and L_3 as shown in Fig. 2.18b, and the thickness of the gusset plate (t_g):

$$K_{gusset} = \frac{E}{L_{ave}}\left(\frac{W_w {t_g}^3}{12}\right) \tag{2.4}$$

Another rotational spring is added in the same zero-length element to mimic the in-plane flexural stiffness of the gusset plate, which should exceed the stiffness of the brace. Additionally, when out-of-plane buckling is anticipated, a third spring representing the torsional restraint of the gusset is included and calculated using the shear modulus of steel (G) and the torsional constant of the Whitmore cross-section (J):

$$K_{torsional} = \frac{GJ}{L_{ave}} \tag{2.5}$$

The flexural springs are modeled using the Giuffre-Menegotto-Pinto steel material, while the torsional spring employs an elastic uniaxial material, as proposed by Tirca and Chen (2014).

In addition to defining the brace fracture model and formulating the gusset plate behavior, the model for braces with end gusset plates depends on several parameters: the initial out-of-straightness (e) or initial imperfection, the number of integration points per element (n_i), the fiber discretization technique, and the number of fibers within the cross-section (n_f). Tirca and Chen (2014) conducted an investigation on these parameters and made the following conclusions:

1. The initial out-of-straightness of $\frac{1}{500}l_b$ proposed by Ziemian (2010) provides a good fit for the response, where l_b is the effective length of the brace.
2. Although the sensitivity to the number of integration points is low, a minimum of three integration points per element (n_i) are recommended (Uriz & Mahin, 2008; Tremblay, 2008)
3. Three different fiber discretization techniques have been used by researchers, as shown in Fig. 2.19. Among them, the technique illustrated in Fig. 2.19c is recommended due to its ability to avoid convergence issues.
4. The number of fibers used to discretize the brace section has an impact on the hysteresis response. Finer meshing improves convergence but increases computation time. Uriz and Mahin (2008) concluded that mesh refinement is important for determining inelastic deformations at critical brace sections but does not significantly affect the overall response.

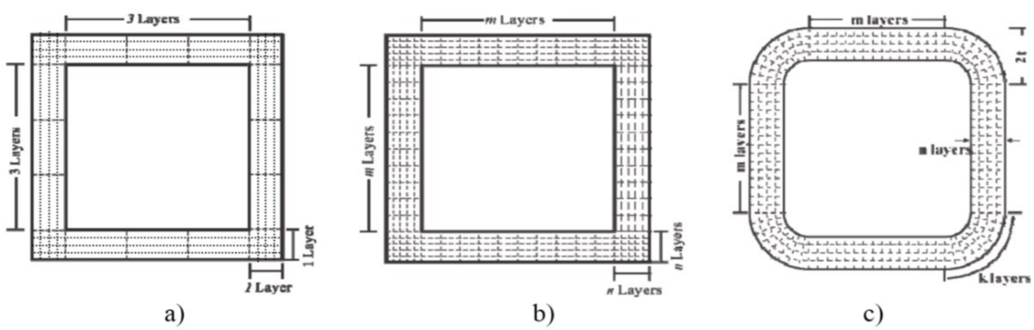

Fig. 2.19. Fiber discretization techniques developed for the HSS brace cross-section: a) Type A, 4n(1+m) fibers; b) Type B, 4n (n + m) fibers; c) Type C, 4n (k + m) fibers (Tirca & Chen, 2014).

2.6 Applications of Incremental Dynamic Analysis

Incremental Dynamic Analysis (IDA) is a computational method in earthquake engineering that provides a comprehensive evaluation of the behavior of structures under seismic loads. IDA was first proposed by Bertero (1977) and later gained widespread use in seismic capacity analysis and overall collapse performance evaluation of frames after a research study by Vamvatsikos and Cornell (2002). IDA involves multiple nonlinear dynamic analyses conducted on a numerical building model under a suite of ground motion records, each scaled to incremented levels of seismic intensity. The scaling levels are appropriately selected to force the structure through the entire range of behavior, from elastic to inelastic and finally to global dynamic instability, where the structure essentially experiences collapse (Vamvatsikos and Cornell, 2002).

Vamvatsikos and Cornell (2002) methodology involves constructing the Incremental Dynamic Analysis (IDA) curve under a given ground motion by connecting points determined by two measurements: the Intensity Measure (IM) and the Damage Measure (DM). For this purpose, a suitable Monotonic Scalable Ground Motion Intensity Measure, such as Peak Ground Acceleration (PGA), Peak Ground Velocity (PGV), or the 5% damped Spectral Acceleration at the structure's first-mode period ($S_a(T_1,5\%)$), is typically chosen. The Damage Measure (DM) characterizes the structure's response under specified earthquake loading conditions. Common examples of DM include maximum base shear, node rotations, peak storey ductility, and floor peak interstorey drift. As highlighted by Vamvatsikos and Cornell (2002), that a single IDA curve can exhibit diverse behaviors, such as "softening," "hardening," and "weaving," depending on the particular ground motion record. The term "softening" refers to a decrease in the slope of the curve as the Intensity Measure (IM) increases, while "hardening" indicates the opposite trend. A twisting pattern characterized by alternating segments of softening and hardening is called "weaving". Figure 2.20 showcases the IDA curves of a 5-storey steel braced frame, where the IDA curves show "weaving". The waving behavior suggests that the structure may undergo periods of both acceleration and deceleration in the rate of Damage Measure (DM) accumulation, depending on the IM. At times, the deceleration can be significant enough to momentarily halt or even reverse the DM accumulation, causing the IDA curve to shift to lower DM values at higher IMs. An interesting phenomenon observed in the waving curve is the occurrence of "period elongation," where simple

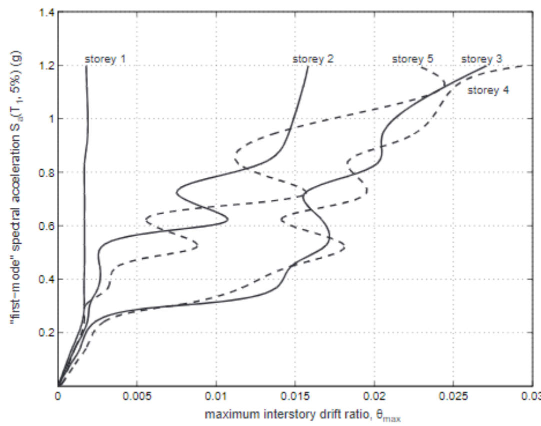

Fig. 2.20. IDA curves of peak interstorey drifts for each floor of a T1=1.8 sec typical 5-storey steel braced frame. (Vamvatsikos and Cornell, 2002)

oscillators that yield in earlier cycles may exhibit reduced responsiveness in subsequent cycles that previously yielded higher DM values. This behavior can be attributed to hardening which occurs when a system is pushed to the point of global collapse at a certain IM, only to re-merge as non-collapsing at a higher intensity level, displaying a high response while still remaining intact.

In performance-based earthquake engineering (PBEE), the definition of performance levels or limit-states plays a crucial role in assessing the structural response. These limit-states can be obtained from the Intensity-Damage-Acceleration (IDA) curves. Vamvatsikos and Cornell (2002) proposed three rules for analyzing IDA curves: the DM-based rule, the IM-based rule, and composite rules. The DM-based rule considers the Damage Measure (DM) as an indicator of damage. When the DM (e.g. the peak ISD) exceeds a certain threshold, it is assumed that the structural model has reached the limit-state, as shown in Fig. 2.21a. The alternative IM-based rule focuses on accurately assessing the collapse capacity by identifying a specific point on the IDA curve that clearly separates the non-collapse region (lower IM) from the collapse region (higher IM), as shown in Fig. 2.21b. This point, known as the capacity point, is determined as the last point on the curve where the tangent slope is equal to 20% of the elastic slope. The rationale behind this rule is that the widening of the curve indicates dynamic instability, with the DM increasing at ever higher rates and accelerating towards infinity. While this rule provides a clear identification of the collapse region, it can be challenging to consistently define the capacity point for each curve. The composite rules combine both DM-based and IM-based approaches. In cases where a structure has multiple collapse modes that cannot be detected by a single DM, it is advantageous to use an IM indicator to identify global collapse for each individual mode. These rules provide valuable guidelines for assessing different limit-states in PBEE analysis.

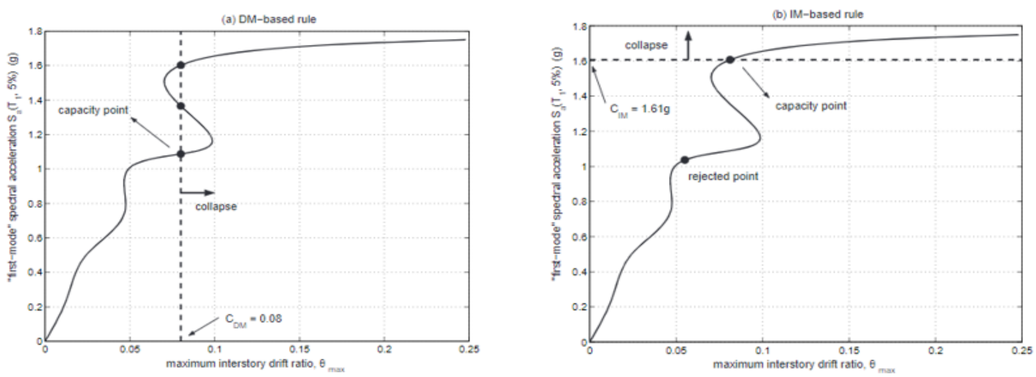

Fig. 2.21. Examples of two different rules producing multiple capacity points (Vamvatsikos and Cornell, 2002)

2.7 Summary

From the literature review it was found that several innovative structural systems were proposed by researchers to mitigate the damage concentration within one or a few floors. Among them is the SBFs, which is composed of a primary ductile system able to dissipate the input energy and an elastic vertical truss (strongback) that prevent the occurrence of dynamic instability. Although this system was envisioned three decades ago (Khatib et al., 1988) it was not widely investigated due to the difficulty of proposing a design method to size members of strongback. It was shown that higher-mode forces are not limited by the yield mechanism of ductile system which leads to large inertial effects relative to the first-mode response. Currently, the available studies are low-rise buildings, and the SB is placed interior to the ductile braced frame. Different configurations of SB can be considered.

CHAPTER 3. SEISMIC DESIGN OF TRADITIONAL CONCENTRICALLY BRACED FRAME

3.1 Introduction

In this chapter, the traditional concentrically braced frame (CBF) is presented for comparison purpose. The traditional CBF system has several drawbacks: i) once braces have buckled they possess only the post-buckling compression strength, and ii) the CBFs are not able to redistribute damage among floors; hence, CBFs are prone to weak-storey mechanism. To emphasize on these drawbacks, a 4-storey prototype office building is presented herein. The design is conducted in accordance with the Canadian Building Code (NBC, 2015) and the CSA S16 2014 steel design standard. To examine the seismic response of the 4-storey CBF office building, the nonlinear time history analysis and the incremental dynamic analysis were employed using two sets of ground motions. The prototype building is located on Site Class C, in Victoria, B.C.

3.2 Building Design Criteria According to NBCC & CSA Standard

Both the vertical and lateral loads applied to the whole building structure are analysed. The vertical loads include dead load, live load, and snow load, while the lateral loads include wind load and earthquake load.

Two limit states are presented in NBC 2015: (a) the ultimate limit state (ULS) considered to assess the members' strength, and (b) the serviceability limit state (SLS), to verify lateral deflection.

Moreover, the ULS is used to compute the factored load and check if the factored resistance of the system exceeds the values of factored loads.

3.2.1 Gravity Loads

The following load combinations are considered to compute the forces assigned to gravity system. The critical combination that leads to maximum load is used to design the gravity system:

1) 1.4D (3.1)
2) 1.25D + 1.5L + 1.0S (3.2)
3) 1.25D + 1.5S + 1.0L (3.3)

where D is the dead load, including the self-weight of members, L is the live load, obtained from NBCC 2015 for different building occupancies, and S is the snow load. A live load reduction factor is calculated and used in design. Then, the snow load, is calculated as:

$$S = I_s[S_s(C_b C_w C_s C_a) + S_r] \tag{3.4}$$

where I_s is importance factor, S_s is 1-in-50-year ground snow load, C_b is basic roof snow load factor, C_w is wind exposure factor, C_a is accumulation factor, and S_r is 1-in-50-year associated rain load.

The following load combinations are considered to design the lateral force resisting system (LFRS).

4) 1.25D + 1.4W + 0.5L **or** 0.5S (3.5)
5) 1.0D + 1.0E + 0.5L + 0.25S (3.6)

Herein, W is the wind load and E is the earthquake load.

For an office building, the typical live load is $L = 2.4\ kPa$, and for the building in Victoria, $S_s = 1.1\ kPa$, $S_r = 0.2\ kPa$, which leads to $S = 1.08\ kPa$.

3.2.2 Seismic Load

The equivalent static force procedure (ESFP) is used to calculate the lateral base shear from earthquake load as per the equation below:

$$V = S(T_a)M_v I_E W/(R_d R_0) \tag{3.7}$$

where $S(T_a)$ is the 5%-damped spectral acceleration associated to the fundamental period T_a, M_v is the higher mode factor, I_E is the importance factor, W is the building seismic weight computed by considering additional 25% of snow load, and R_d and R_0 are the ductility related-force modification factor and overstrength related-force modification factor, respectively. For braced frame structures, the fundamental period is calculated as:

$$T_a = 0.025h_n \textit{ but not more than } 0.05h_n \tag{3.8}$$

where h_n is the total height of the building in meters and T_a can increase up to two time if dynamic analysis is used in design. As per the NBC (2015), the acceleration response spectra ordinates are determined based on design spectrum associated with 2% probability of exceedance in 50 years (2475-year return period).

For the distribution of seismic base shear along the building height, the following equation is used:

$$F_x = (V - F_t)W_x h_x/(\sum W_i h_i) \tag{3.9}$$

where F_t is the top storey concentration force computed as $F_t = 0$ for buildings with $T_a \leq 0.7s$ and $F_t = 0.07\,T_a V$ but not greater than 0.25V for building with $T_a > 0.7s$, where T_a is the fundamental period.

Considering the P-δ effects, the amplification factor U_2 is computed as per Eq. (3.10) and is used to amplify the storey shear force.

$$U_2 = 1 + \theta_x \tag{3.10}$$

where:

$$\theta_x = \frac{\sum C_f}{V_f} \frac{R_d \Delta f}{h_s} \tag{3.11}$$

Herein, θ_x is the stability factor, $\sum C_f$ is the factored axial force, V_f is the design storey shear force at the level under consideration, Δf is the interstorey drift at the same floor level, R_d is the ductility-related factor and h_s is the storey height at the calculation level.

The notional lateral loads, V_{Nx}, required in design according to CSA-S16-14, are considered. It is calculated as 0.005 times the factored gravity loads in each floor $\sum C_{D+0.5L+0.25S}$ as per Eq. (3.12). Live load reduction factor is applied in the calculation of factored gravity loads.

$$V_{Nx} = 0.005 \sum C_{D+0.5L+0.25S} \tag{3.12}$$

The torsional effect caused by accidental eccentricity is not considered in this study.

3.2.3 Design of Tension-compression Bracing Members of MD-CBFs

All braces are made of hollow structural sections. To prevent local buckling, all braces are Class 1. For CBF buildings in seismic areas with $I_E F_a S_a(0.2) \geq 0.35$, Class 1 HSS braces with slenderness ratio is $KL/r < 100$ is associated with the width-to-thickness ratio lower than $330/\sqrt{Fy}$. However, when the slenderness ratio is $KL/r = 200$, Class 1 sections shall be used. If the slenderness ratio is between 100 and 200, linear interpolation can be considered. Herein, KL is the effective brace length and *r* is the radius of gyration in the direction of bending. For CBF buildings in seismic areas with $I_E F_a S_a(0.2) \geq 0.75$ or $I_E F_v S_a(1.0) \geq 0.3$, HSS braces shall also comply to $KL/r > 70$.

Designing HSS braces to behave in tension and compression, requires that: $C_f \leq C_r$ and $T_f \leqslant T_r$, where C_f and T_f are the factored axial compression force and axial tensile force in brace, respectively, while C_r and T_r are the brace compression and tensile resistance, respectively, computed with Eqs. (3.13) and (3.14).

$$C_r = \phi A_g F_y (1 + \lambda^{2n})^{-1/n} \quad \text{and} \quad \lambda = (KL/r)\sqrt{F_y/\pi^2 E} \tag{3.13}$$

where $\phi = 0.9$ for steel members, A_g is the gross area of brace cross-section, n =1.34 for the type of braces selected, λ is the slenderness parameter, F_y is the yielding stress of steel and E is the modulus of elasticity.

$$T_r = \phi A_g F_y \tag{3.14}$$

3.2.4 Design of Beam and Column of MD-CBF

Capacity design principle is used to design the beams and columns of moderately ductile concentrically braced frames (MD-CBFs). Two loading conditions in CSA/S16-14 are considered so that the beams and columns could resist axial forces transferred by brace members. Thus:

a) compression acting braces achieving their probable compressive resistance C_u in conjunction with tension acting braces developing their probable tensile resistance T_u and
b) compression acting braces achieving their probable post-buckling resistance $C_u{}'$ in conjunction with the probable tensile resistance T_u of tension acting braces.

To calculate T_u, C_u and $C_u{}'$, the following equations are used:

$$T_u = A_g R_y F_y, \text{ where } R_y F_y = 460 \text{ MPa} \tag{3.15}$$

$$C_u = 1.2 C_r R_y/\phi \tag{3.16}$$

$$C_u{}' = \min\,(0.2A_gR_yF_y; C_rR_y/\phi) \tag{3.17}$$

Herein, $R_yF_y = 460\ MPa$ is the probable yield stress for HSS sections.

For MD-CBF beams design, the following Eqs. are used:

$$\frac{C_f}{C_r} + \frac{0.85U_1M_f}{M_r} \leq 1.0 \tag{3.18}$$

$$\frac{T_f}{T_r} + \frac{M_f}{M_r} \leq 1.0 \tag{3.19}$$

Cross-sectional strength (CSS), overall member strength (OMS), and combined axial tensile force and bending moment (AT&B) of beams are checked in the equations above.

To be noticed, the probable tensile resistance of braces could be taken as 0.6 T_u for low-rise buildings (no more than four storeys) if the beam's section is Class 1.

When chevron braces are considered, these are connected to the beam and the frame, where beams are continuous between columns. At the brace-to beam connection, both top and bottom flanges are laterally braced, so that they can resist bending moment from related gravity load component and the vertical load due to the unbalance T_u and C_u' brace components, assuming no vertical support is provided by braces. The MD-CBF beams are designed as beam-column elements and Class 1 sections.

Columns of MD-CBF are designed as beam-column elements of Class 1 or Class 2 sections. Columns shall resist gravity loads in addition to the projection of brace forces associated to C_u and T_u scenario. However, the transfer of axial forces associated with the probable brace resistances to columns may be larger due to some other criteria such as with-to-thickness ratio, availability of HSS sizes, etc.; however, these forces shall be limited to the projection of factored loads corresponding to elastic design where $R_dR_o = 1.3$. Columns shall be continuous over two storeys and of constant section. Columns are designed as beam-column, where the bending moment in the direction of applied lateral forces is considered to be 0.2 times the plastic moment (M_p) of column cross-section.

Similar with the beam elements, the CBF columns should also check the Cross-sectional strength (CSS), overall member strength (OMS), lateral torsional buckling (LTB) and combined axial force and bending moment (AT&B) as per the CSA/S16 standard requirements. Thus, for these criteria, C_r is considered as follows: (i) for cross-sectional strength, C_r is computed with $\lambda = 0$, (ii) for overall member strength, C_r is computed based on the axis of bending, and (iii) for lateral torsional buckling strength, C_r is computed based on the weak-axis.

3.2.5 Design of Brace-to-frame Gusset Plate Connections

The capacity design approach is applied to the brace to frame gusset plate connections. Six failure modes are considered, they are 1) shear resistance of fillet welds connecting the HSS brace to the gusset plate, 2) Tensile resistance of filler weld, 3) Tensile yielding of gusset plate, 4) Buckling of gusset plate, 5) Net fracture of braces, and 6) Block shear failure of braces.

Following two cases decide the shear resistance of fillet welds:

i) Fracture of the weld metal through the weld throat, and

ii) Yielding at the weld-to-base metal interface.

Two similar equations are used to determine them separately:

$$V_r = 0.67\phi_w A_w X_u \tag{3.20}$$

$$V_r = 0.67\phi_w A_m F_u \tag{3.21}$$

where,

$$A_w = 0.707D_wL_w \tag{3.22}$$

$$A_m = D_wL_w \tag{3.23}$$

In these equations, A_w is the area of effective fillet weld throat and A_m is the shear area of effective fusion face, ϕ_w is the resistance factor of weld metal which equals to 0.67, and X_u is the electrode ultimate tensile strength and equals to 490MPa for electrode type E49XX. In the later two equations, D_w is the fillet weld size and L_w is the length of the fillet weld, while D_w is limited to the thickness of the thinner element of brace gusset plate connection. To be noticed, the shear resistance of welding should be designed to exceed the probable tensile resistance T_u of the brace.

The tensile resistance of metal base, T_r is obtained by this equation:

$$T_r = \phi t_g L_w F_y \tag{3.24}$$

where t_g is the thickness of gusset plate. The value of T_r should also be not less than the probable tensile resistance T_u of the brace.

The yielding strength of gusset plate is obtained from the following equation:

$$T_r = \phi A_g F_y \tag{3.25}$$

where $A_g = t_gW_w$ and A_g is the gross tension area, t_g is the thickness of the gusset plate, and W_w refers to the Whitmore width, which is defined as a line that runs through the base of the HSS brace and is intercepted by two 30-degree lines originating from the intersection of the brace and the gusset plate (Whitmore, 1952). This definition is illustrated in Fig. 3.1. To be noticed, that the gusset plate yielding strength T_r should also exceed the probable tensile resistance T_u of brace.

The compressive resistance of gusset plate, $C_{rg.p.}$, is calculated using Eq. (3.13), where λ is calculated as per Eq. (3.26). $C_{rg.p}$ shall exceed or equate the probable compressive resistance of brace, C_u.

$$\lambda = (KL_{ave}/r)\sqrt{F_y/\pi^2 E} \tag{3.26}$$

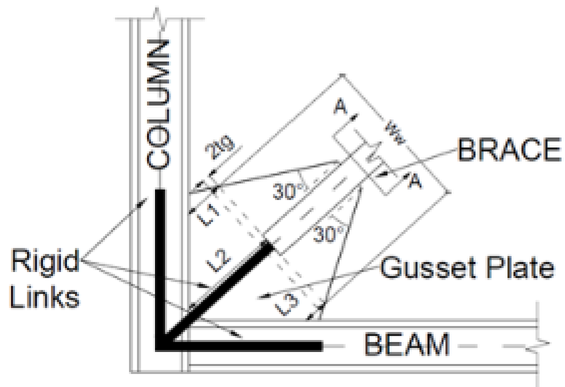

Fig. 3.1. Brace -to-frame connection and parameters considered

As per Fig. 3.1, L_{ave} is the average of L_1, L_2 and L_3 while r is the radius of gyration of gusset plate Whitmore width section, calculated in following equation:

$$r = (\frac{I_g}{A_g})^{0.5} \tag{3.27}$$

where I_g is the moment of inertia of gusset plate as calculated below:

$$I_g = \frac{W_w {t_g}^3}{12} \tag{3.28}$$

The net fracture resistance of HSS braces is verified as following:

$$T_r = \phi_u A_{ne} F_u \tag{3.29}$$

where A_{ne} is the effective net area calculated as per Eq. (3.30), ϕ_u is 0.75 and, F_u is the specified minimum tensile strength. To be noticed, the shear lag effect is considered. As shown in Fig. 3.2, he effective net area A_{ne} is reduced by the shear lag factor according to Cls. 12.3.3.4 of S16-14.

- when $\frac{\bar{x}'}{L_w} > 0.1,\ A_{ne} = A_n\left(1.1 - \frac{\bar{x}'}{L_w}\right) \geq 0.8A_n$
- when $\frac{\bar{x}'}{L_w} \leq 0.1,\ A_{ne} = A_n$ (3.30)

where $\bar{x}'$ is the distance between the center of gravity of half of the HSS cross section and the edge of the connection plate as shown in Fig.3.2, while L_w is the length of a single weld segment for welding the HSS brace and the connection. The total weld length usually should be $4L_w$.

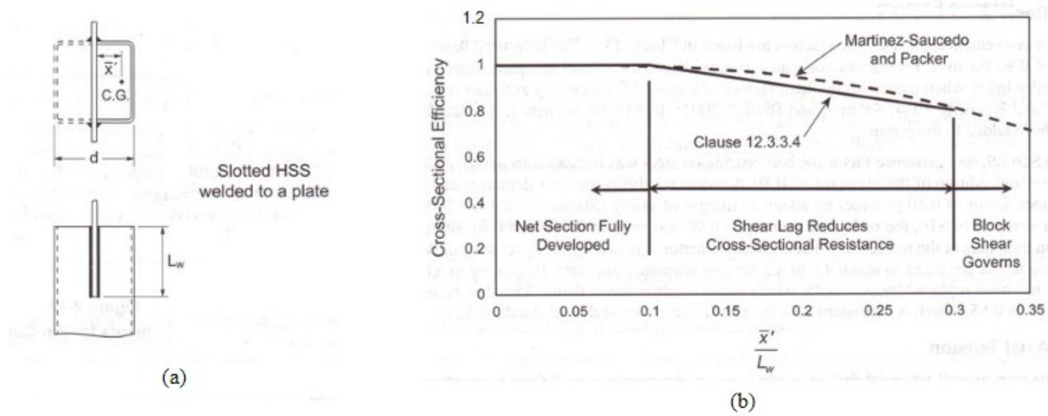

Fig. 3.2. Shear lag effects on slotted HSS brace ends (CSA/S16-14)

The block shear resistance is calculated by the following equation:

- $T_{r-BS} = \phi_u[U_t A_n F_u + 0.6A_{gv}\frac{F_y+F_u}{2}]$ (3.31)

where the efficiency factor $U_t = 1$ for symmetrical blocks, A_n is the net area in tension, and A_{gv} is the gross area in shear. According to CSA/S16 CL 13.11, the block shear resistance T_{r-BS} should exceed or equal to the probable tensile resistance, T_u, of the brace.

3.3 Case Study

3.3.1 Building Description

In this study, a 4-storey braced frame office building located on Site Class C in Victoria, B.C., is designed and analysed. As shown in Fig. 3.3, the building floor area is 30.5 m x 60.5 m with 0.25 m of extension from the perimeter gridlines. Composite decks which behave as rigid horizontal diaphragms are considered for all floors and roof. Because of the symmetric characteristics of the building, the seismic force resisting systems (SFRS) should carry the same horizontal forces in both orthogonal directions. Therefore, in each orthogonal direction, four MD-CBFs with symmetric split-X braces are placed as in Fig. 3.4. The total building height is 14.8 m, while the height of the ground is 4.0 m and that of typical floor is 3.6 m.

For design, the NBC 2015 and CSA/S16-14 standard are used. Then, ETABS software is used for dynamic response analysis and OpenSees for nonlinear response history analysis (NRHA).

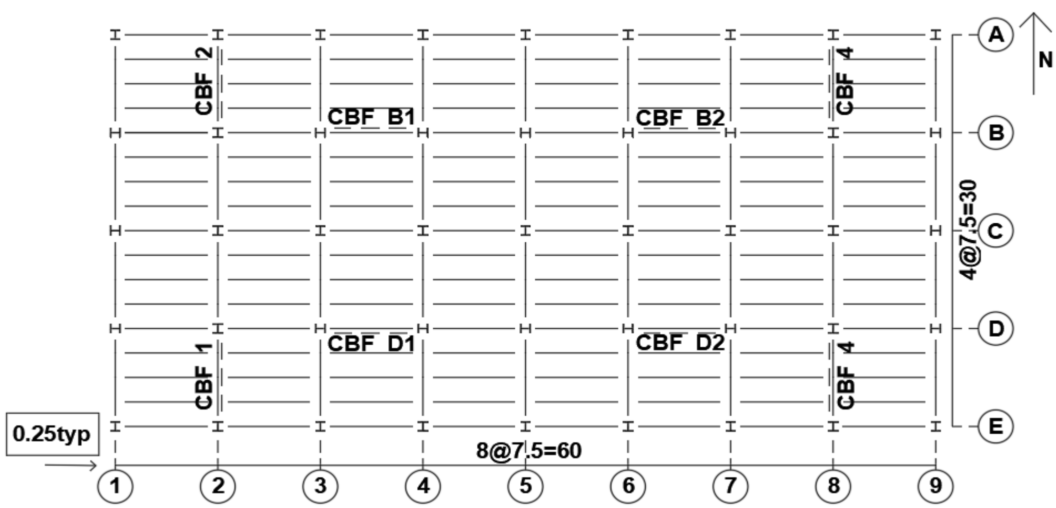

Fig. 3.3. Building plan view

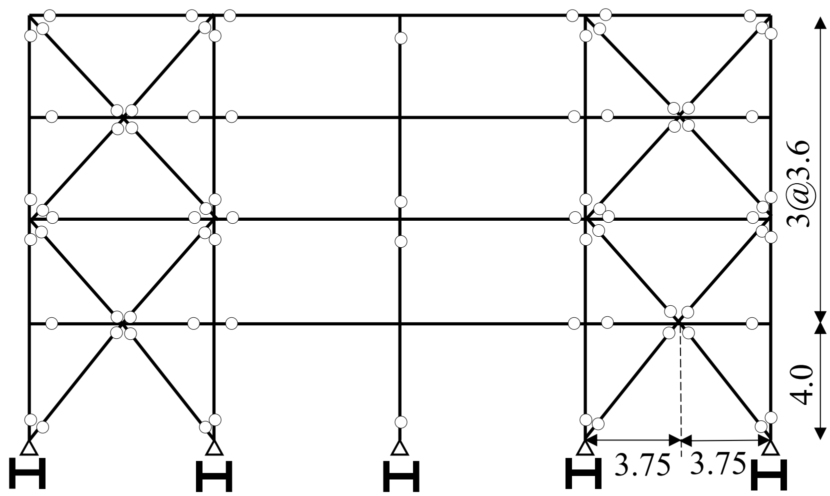

Fig. 3.4. Elevation of gridline “2”

3.3.2 Gravity System

The gravity system is designed to carry the gravity loads considering the load combination cases presented in Section 3.2.1. For typical floors and roof is considered DL_{floor} = 4.0 kPa including 1.0 kPa partition wall and DL_{roof} = 3.3 kPa, respectively. The live load (LL) at roof and typical floor is LL_{roof} = 1.0 kPa, and LL_{floor} = 2.4 kPa, respectively, while cladding is 1.5 kPa. According to Eq. (3.4), the snow load is calculated as 1.08 kPa for Victorica, B.C. The member sections for the gravity system are shown in Table 3.1.

Table 3.1 Member section of gravity system

Storey	Secondary Beam	Girder	Interior Column	Exterior Column	Corner Column
4	W310X21	W460X60	W200X46.1	W150X37.1	W150X37.1
3	W310X28	W530X66	W200X46.1	W150X37.1	W150X37.1
2	W310X28	W530X66	W200X86	W200X46.1	W150X37.1
1	W310X28	W530X66	W200X86	W200X46.1	W150X37.1

For column design, the live load reduction factor was considered according to NBC 2015. Secondary beams, girders, and columns are made of W-shape sections complying with CSA G40.21, where the yield strength and tensile strength are $F_y = 345MPa$ and $F_u = 450\ MPa$, respectively. In this case study, gravity columns are designed continuous over each two floors with the same section.

3.3.3 Lateral Force Resisting System

The Lateral force resisting system is designed according to the load combination cases shown in Section 3.2.1. Because among the earthquake and wind load, the earthquake load governs in Victoria, all MD-CBFs are designed based on the seismic load.

According to Eq. (3.7), the base shear from earthquake load is obtained using the equivalent static force procedure (ESFP). Using Eq. (3.8), $\boldsymbol{T_a}$ is calculated as 0.37s. If a dynamic analysis is considered, $\boldsymbol{2T_a}$ = 0.74 s can be used which leads to S(0.74) =0.92g computed from linear interpolation of spectral ordinates given in Table 3.2. Then, $\boldsymbol{M_v = 1}$ as the higher mode factor, $\boldsymbol{I_E = 1.0}$ for normal importance category, and, for MD-CBF, $\boldsymbol{R_d}$ and $\boldsymbol{R_0}$ are 3 and 1.3, respectively. The building seismic weight including 25% of snow load, W, is given in Table 3.3.

Table 3.2 Acceleration response spectra ordinates for site Class C in Victoria

T (s)	T = 0.2	T = 0.5	T = 1.0	T = 2.0	T = 5.0
$S_a(T)$, g	1.30	1.16	0.676	0.399	0.125

The base shear V = 0.92 x29457x1x1/(3x1.3) = 7007 kN. The distribution of the base shear along the building height follows Eq. (3.9) and the results are presented in Table 3.4.

Table 3.3 Seismic weight of 4-storey MD-CBF office building

Storey	D*) (kPa)	Area (m^2)	D of floor (kN)	25% of S (kN)	Cladding (kN)	W_x (kN)
4	3.3	1845.3	6089	498	491	7079
3	3.5	1845.3	6459	-	983	7441
2	3.5	1845.3	6459	-	983	7441
1	3.5	1845.3	6459	-	1037	7496
Sum						29457

*) Partition load is reduced to 0.5 kPa when calculating the seismic weight as per NBC 2015

The notional lateral loads, V_{Nx}, are calculated as per Eq. (3.12). The notional lateral loads are provided in Table 3.5 and the summation of lateral forces associated to half of building floor

Table 3.4 Storey force from base shear distribution

Storey	h_x (m)	W_x (kN)	$W_x h_x$ (kN-m)	F_x (kN)	Storey shear (kN)
4	14.8	7079	104769	2898	2898
3	11.2	7441	83339	2016	4914
2	7.6	7441	56552	1368	6282
1	4	7496	29984	725	7007
Sum		29457	274644	7007	

resulted from Tables 3.4 and 3.5 are presented in Table 3.6. Due to the building symmetry and symmetrical distribution of MD-CBFs with respect to center of mass (Fig. 3.3), only MD-CBF 1 and the gravity columns laterally supported by this frame are consider in the numerical model.

Table 3.5 Notional loads

Storey	V_{Nx} (kN)	$V_{Nx}/2$ (kN)
4	40	20
3	88	44

2	134	67
1	178	89

Table 3.6 Storey force associated to half of building floor and that per MD-CBF1

Storey	V/2 (kN)	V/2 + V_{NX}/2 (kN)	V $_{MD\text{-}CBF\ 1}$ (kN)
4	1449	1469	734
3	2457	2501	1251
2	3141	3208	1604
1	3503.5	3592	1796

The P-Δ effect is also considered. However, calculations showed that $U_2 < 1.1$ in both orthogonal direction, which means that P-Δ effect does not amply the storey shear resulted from the ESFP.

Braces of MD-CBF are made of square Hollow Structural Sections (HSS) and comply with G40.21-350W Class C steel (cold formed) with $F_y = 350\ MPa$, $F_u = 450\ MPa$, and $E = 200\ GPa$. Following Eqs. (3.13) and (3.14), as well as the storey shear force from Table 3.5 and gravity loads presented in Section 3.3.2, the sizes of all bracing members, slenderness ratio, class section verification and compression resistance are provided in Table 3.7.

Table 3.7 Sizes and characteristics of HSS braces of MD-CBF1

St	C_f (kN)	Brace sections	A_{br} (mm^2)	$L_{br\ c\text{-}c}$ (mm)	KL/r	C_r (kN)	(b-4t)/t ≤ 330/$F_y^{0.5}$	Class
4	470	HSS127X127X13	5390	5198	102.4	697	5.77	1
3	1025	HSS152X152X13	6680	5198	83.4	1121	7.70	1
2	1105	HSS178X178X9.5	6180	5198	68.8	1260	14.74	1
1	1482	HSS203X203X13	9260	5483	64.2	2002	11.62	1

To design the beams and columns of MD-CBF, the probable tensile, probable compression and post-buckling resistance of brace members are calculated as per Eqs. (3.15), (3.16), and (3.17), respectively and are provided in Table 3.8.

Table 3.8 Probable resistance of HSS braces of 4-storey MD-CBF1

St.	Brace sections	T_u (kN)	$0.6T_u$ (kN)	C_u (kN)	C_u' (kN)
4	HSS127X127X13	2471	1483	1218	494
3	HSS152X152X13	3063	1838	1959	613
2	HSS178X178X9.5	2834	1700	2201	567
1	HSS203X203X13	4246	2547	3497	849

Then, using the capacity design principle and Eqs. (3.18) and (3.19), the beam and column members of MD-CBF 1 are presented in Table 3.9.

Table 3.9. Preliminary design of MD-CBF1 members of 4-storey building

St.	Brace	Column	Beam
4	HSS127X127X13	W250X67	W460X106
3	HSS152X152X13	W250X67	W460X128
2	HSS178X178X9.5	W310X179	W460X128
1	HSS203X203X13	W310X179	W460X128

3.3.4 ETABS model

After the application of ESFP, dynamic analysis by means of the Response spectrum analysis (RSA) using the ETABS software (edition 2016), is employed. Through this method, the dynamic distribution of storey forces along the building height, the first mode period (T_1) and the associated base shear are obtained. The 3D view of numerical model is shown in Fig. 3.5. In Table 3.10, the first mode period and base shear are compared with that resulted from the ESFP. Only the calculation in N-S direction is shown.

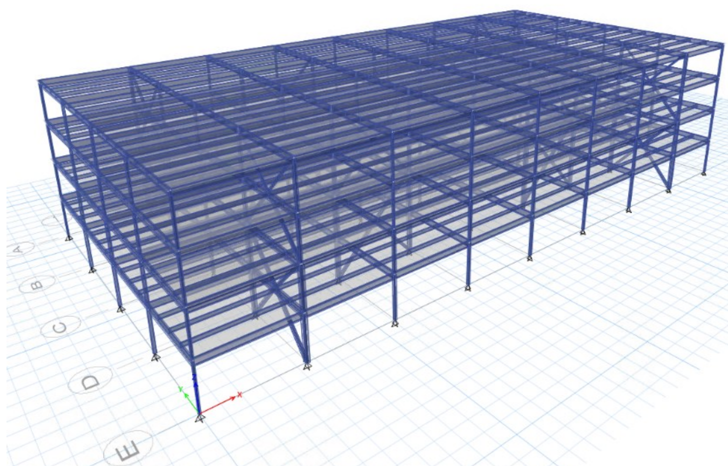

Fig. 3.5. Three-dimensional (3D) model using ETABS

From Table 3.10 it results that T_1 from RSA is less than $2T_a$ considered in the ESFP; thus, $V_{dyn.}$ is larger than the base shear, V, obtained from preliminary design. This means that the design of

Table 3.10 Characteristics of MD-CBF building from ESFP and RSA (N-S directions)

h_m (m)	W (kN)	ESFP		RSA from ETABS	
		$2T_a$ (s)	V (kN)	T_1 (s)	$V_{dyn.}$ (kN)
14.8	29457	0.74	7007	0.551	8477

MD-CBF members should be revised based on the dynamic base shear $V_{dyn.}$ from RSA. This iterative process is repeated until $V_{dyn.}$ is reached; hence, as a result, the stiffness of MD-CBFs increases. The sizes of re-designed MD-CBF members are presented in Table 3.11, where in the

2^{nd} and 3^{rd} floors the sizes of section were increased, when comparing with the preliminary design. The recalculated probable resistances of braces are shown in Table 3.12.

Table 3.11 Final design of MD-CBF 1 members of 4-storey building

St.	Brace	Column	Beam
4	HSS127X127X13	W250X67	W460X106
3	HSS178X178X9.5	W250X67	W460X128
2	HSS203X203X9.5	W310X202	W460X128
1	HSS203X203X13	W310X202	W460X128

Table 3.12 Probable resistance of re-designed HSS braces of MD-CBF1

St.	Brace sections	T_u (kN)	$0.6T_u$ (kN)	C_u (kN)	$C_u{}'$ (kN)
4	HSS127X127X13	2471	1483	1218	494
3	HSS178X178X9.5	2655	1593	2070	531
2	HSS203X203X9.5	3077	1846	2682	615
1	HSS203X203X13	3994	2396	3299	799

3.3.5 Gusset plate connection details

Following Eqs. (3.20) to (3.31) given in Section 3.2.5, the brace-to-frame gusset plate connections are calculated and detailed in Table 3.13.

Table 3.13 Gusset plate connection details of HSS braces to frame

St.	Brace sections	D_w (mm)	L_w (mm)	W_w (mm)	t_g (mm)	L_{ave} (mm)
4	HSS127X127X13	8	260	483	9.54	163
3	HSS178X178X9.5	8	330	602	15.9	197.5

2	HSS203X203X9.5	8	400	708	15.9	198
1	HSS203X203X13	11	400	708	19.05	262.3

3.3.6 Modelling MD-CBF building using OpenSees

The 4-storey building's symmetrical feature on both orthogonal directions allows simulation in OpenSees of only a quarter of the building plan, as depicted in Fig. 3.6 and 3.7. In Fig. 3.7, the gravity columns are modelled as leaning columns to mimic their stiffness and account for P-delta effects. Herein, all CBF columns and gravity columns have constant section over two storeys, while beams are pinned to column faces. CBF members such as braces, beams, and columns were simulated using nonlinear force-based beam-column elements with distributed plasticity and fiber cross-section formulation. The *Steel*02 uniaxial material known as Giuffre-Menegotto-Pinto steel material that considers isotropic strain hardening (Menegotto and Pinto, 1973) was assigned to CBF members. This material is able to capture the Bauschinger effect and residual stresses (Lamarche and Tremblay, 2008). Parameters for defining *Steel*02 material were selected according to Aguero et al. (2006).

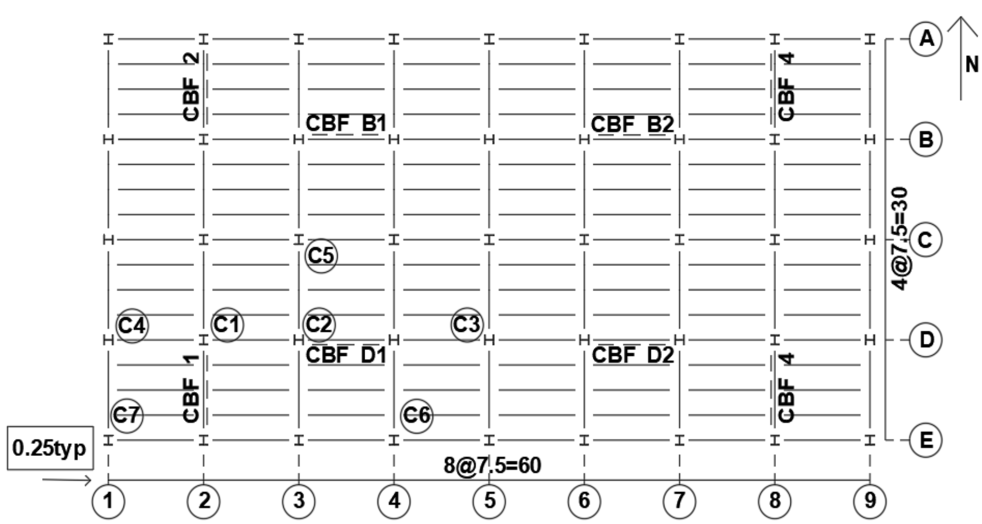

Fig. 3.6. OpenSees model of ¼ building plan, with gravity columns marked

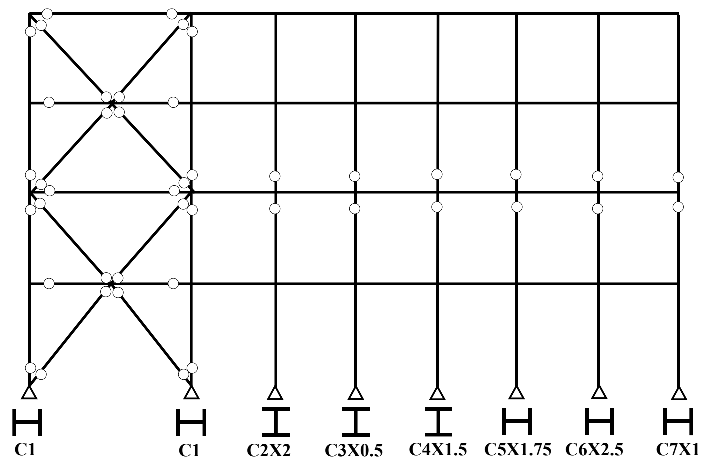

Fig. 3.7. OpenSees model of ¼ of building plan (N-S direction)

To model the fracture of HSS brace, the low-cycle fatigue was implemented in OpenSees by Uriz (2005) and detailed in Uriz and Mahin (2008). However, the predicted parameters introduced by users in the OpenSees model were those proposed by Tirca and Chen (2014), where the predicted fatigue ductility coefficient, $\varepsilon_{0,pred}$ results from equation below and the fatigue ductility exponent is m= -0.5.

$$\varepsilon_{0,pred} = 0.006(\frac{kL}{r})^{0.859}(\frac{b_0}{t})^{-0.6}(\frac{E}{F_y})^{0.1} \quad (3.32)$$

In this equation, according to the CSA S16 standard, $b_0 = b - 4t$, where b is the effective width and t is the thickness of the HSS brace. It is important to note that the slope of the Coffin-Manson curve is assumed to be m = -0.5, consistent with the value proposed by Uriz and Mahin (2008). Thus, the fatigue parameter $\varepsilon_{0,pred}$ resulted from Eq. (3.32) for selected HSS braces are listed in Table 3.14. To capture the nonlinear behavior of MD-CBF brace members, Hsiao et al. (2013) recommended to consider 16 nonlinear beam-column elements with distributed plasticity and fiber discretization for HSS cross-sections to simulate braces fracture.

Table 3.14 Fatigue ductility coefficient, ε_0 for HSS braces of MD-CBF1

St.	Brace sections	KL/r	b_0/t	ε_0
4	HSS127X127X13	102.4	5.77	0.12741
3	HSS178X178X9.5	68.5	14.74	0.08444
2	HSS203X203X9.5	59.4	17.37	0.06774
1	HSS203X203X13	64.2	11.62	0.08986

To capture the nonlinear behavior of MD-CBF brace members, Hsiao et al. (2013) recommended to consider 16 nonlinear beam-column elements with distributed plasticity and fiber discretization for HSS cross-sections to simulate braces fracture. In each element, three Gauss-Lobatto integration points are considered. The fiber discretization method considered rounded corners for all HSS braces and used 240 fibers within each cross-section. To simulate the out-of-plane buckling of braces, an initial imperfection of e = (1/500)l_b was assigned to each HSS brace, as buckling of braces, an initial imperfection of e = (1/500)l_b was assigned to each HSS brace, as shown in Fig. 3.8.

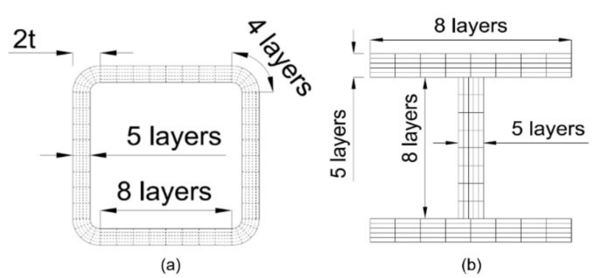

Fig. 3.8. Modelling: (a) HSS cross-section fiber discretization; and (b) I-shape cross-section fiber discretization

The beams and columns of CBFs are constructed from I-shape sections and modeled using nonlinear force-based beam-column elements with distributed plasticity and fiber cross-section discretization. Beams are modeled with four elements and columns with eight, each assigned three and four integration points per element, respectively. For I-shaped columns, an initial imperfection of $e = \frac{1}{1000} l$ is considered. As shown in Fig. 3.8 (b), the I-shaped cross-section is divided into 120 fibers, with each flange and web comprising 40 fibers. Gravity columns (C1-C6 as per Fig. 3.7) are modeled with elastic beam-column elements, while leaning columns are connected to each floor by truss elements with large stiffness, simulating the rigid diaphragm effect.

The gusset plate connections are simulated with two rotational springs (one displaced out-of-plane and one in plane) and one torsional spring using a *Zerolength* element, as shown in Fig. 3.9.

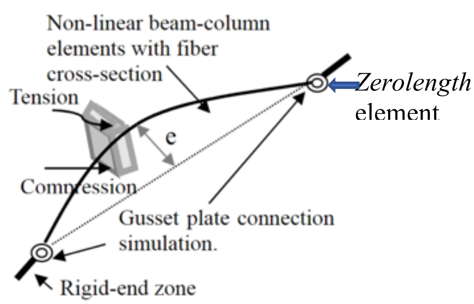

Fig. 3.9. Model of brace with end plate connections using OpenSees (Tirca et al., 2015)

The section of gusset plate is its width, e.g. Whitmore width (W_w), and thickness, *tg*. The stiffness of out of plane rotational spring is given by Eq. (3.33) where L_{ave} is illustrated in Fig. 3.1.

$$K_{out-of-plane} = \frac{E}{L_{ave}}\left(\frac{W_w t_g^{\,3}}{12}\right) \tag{3.33}$$

Another rotational spring is added in the same zero-length element to mimic the in-plane flexural stiffness of the gusset plate, which should exceed the stiffness of the brace. Additionally, a third spring representing the torsional restraint of the gusset is included and calculated using the shear modulus of steel (G) and the torsional constant of the Whitmore cross-section (J):

$$K_{torsional} = \frac{GJ}{L_{ave}} \tag{3.34}$$

These aforementioned parameters are provided in Table 3.15. The flexural springs are modeled using the Giuffre-Menegotto-Pinto steel material, while the torsional spring is made of the elastic uniaxial material.

Table 3.15 MD-CBF1 braces to frame gusset plate connections properties and its spring's models

St.	W_w (mm)	t_g (mm)	L_{ave} (mm)	$K_{out-of-plane}$ (Nm)	M_p (Nm)	J (mm^4)	$K_{tor.}$ (Nm)
4	483	9.54	163	42879	2821	139649	65968
3	602	15.9	197.5	204184	9766	805809	314130
2	708	15.9	198	239605	11485	947696	368624
1	708	19.05	262.3	310998	16487	1629906	478458

Once the OpenSees model was completed, an Eigenvalue analysis was conducted, and the first three mode periods of vibration (in the N-S direction) were obtained and presented in Table 3.16. To compare the results, the periods obtained from an elastic analysis using ETABS were also provided. The comparison showed that the periods obtained from both the 3-D model defined in ETABS and the 2-D model defined in OpenSees were similar.

Table 3.16 Vibration periods of MD-CBF building (N-S direction)

Period	Eigenvalue Analysis	
	ETABS	OpenSees
T1 (s)	0.551	0.554
T2 (s)	0.201	0.205
T3 (s)	0.125	0.138

3.3.7 Ground Motions

Victoria is situated on the Pacific coast of B.C. and is in the vicinity of the Juan de Fuca plate that has the potential to cause a large subduction zone earthquake known as the Cascadia subduction zone. To analyze the seismic behavior of 4-storey MD-CBF building in Victoria, B.C., two sets of ground motions (GMs) were considered: crustal ground motions and subduction ground motions. These GMs were selected based on the expected magnitude (Mw 7-9) and geotechnical profile. For ground motion scaling, the NBC 2015 recommendations are used; hence, the mean spectrum of each set of 7 ground motions shall match or exceed the design spectrum within the period of interest (0.15T_1 to 2T_1) but not be less than 90% of the design spectrum within that same period. In addition, the NBC 2015 allows the consideration of fewer than 11 records per set, if a minimum of 5 records is selected for each set and the total number of records for all sets is not less than 11. The case study is located on Site Class C (very dense soil), where the average shear wave velocity computed for the upper 30.0 m, $V_{s\,30}$, is in the range of $360 < V_{s\,30} < 760\ m/s$.

3.3.7.1 Crustal ground motions

For crustal ground motions, a set of 7 ground motions of Mw 7 was selected from the PEER-NGA ground motion database. Table 3.17 provides information on the selected records, including their identification (NGA), horizontal peak ground acceleration (PGA), peak ground velocity (PGV), PGV/PGA ratio, total record duration (t), Trifunac duration t_d, computed V_{s30}, Joyner-Boore distance R_{jb}, rupture distance R_{rup} (listed in PEER (2018) database), the mean period T_m, principal ground motion period T_p, and the scale factor (SF). Trifunac duration is defined as the time difference between the development of 5% and 95% of the Arias intensity (Trifunac and Brady 1975). Figure 3.10 shows the scaled acceleration response spectrum of each GM, the mean

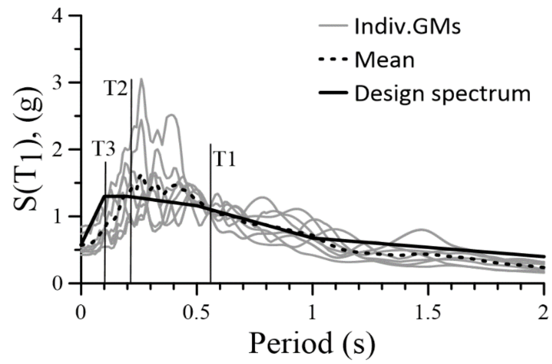

Fig. 3.10. Response spectrum of scaled crustal GMs for 4-storey MD-CBF building (T1 =0.55s; 0.15T1 = 0.08s; 2T1 = 1.1s)

Table 3.17 Seismic characteristics of crustal GMs selected from the PEER-NGA database

ID	NGA - Comp	Event	M	R_{jb}; R_{rup} (km)	PGA (g)	PGV (m/s)	PGV/ PGA	t;t_d (s)	t_p;t_m (s)	$V_{s,30}$ (m/s)	SF
C1	735 -000	Oct. 18, 1989 Loma Prieta	6.9	42; 42	0.16	0.16	0.102	39.99; 16	0.44; 0.64	415	3.4
C2	958 -270	Jan. 17, 1994 Northridge	6.7	35; 40	0.12	0.06	0.049	75; 37.6	0.26; 0.41	351	3.9
C3	1039 -180	Jan. 17, 1994 Northridge	6.7	17; 25	0.27	0.22	0.083	39.5; 16.1	0.26; 0.47	342	3.1
C4	787 -360	Oct. 18, 1989 Loma Prieta	6.9	31; 31	0.27	0.30	0.113	39.65; 12.7	0.32; 0.67	425	1.85
C5	1052 -090	Jan. 17, 1994 Northridge	6.7	5; 7	0.31	0.34	0.111	39.98; 10.1	0.32; 0.67	508	1.5
C6	739 -250	Oct. 18, 1989 Loma Prieta	6.9	20; 20	0.25	0.44	0.181	74.35; 10.9	0.40; 0.90	488	2.0
C7	963 -90	Jan. 17, 1994 Northridge	6.7	20; 21	0.61	0.53	0.089	39.98; 9.1	0.26; 0.53	450	1.22

spectrum, as well as, the 2%/50 yrs. design spectrum for Victoria, Site Class C.

3.3.7.2 Subduction Ground Motions

The subduction ground motions have longer duration, while the Trifunac duration is greater than 60 seconds. Tesfamariam and Goda (2015) concluded that the best available proxy to simulate the effect of a future Cascadia event is the main-shock subduction earthquake records from the M_w9

Tohoku earthquake in Japan (March 11, 2011). Assessing the potential impact of a M_w9 mega-thrust Cascadia subduction earthquake on buildings is of great importance (Tirca et al, 2015).

Table 3.18 Seismic characteristics of subduction ground motions selected from K-NET database

ID	Station-comp	M	$R_{rup}; R_{jb}$ (km)	PGA (g)	PGV (m/s)	PGV/ PGA	$t; t_d$ (s)	$t_p; t_m$ (s)	V_{s30} (m/s)	SF
S1	FKS005-EW	9	175; 58.2	0.45	0.35	0.079	300; 92	0.15; 0.32	469	1.75
S2	FKS009-EW	9	216; 70.8	0.83	0.44	0.054	300; 74	0.2; 0.2	387	1.45
S3	FKS010-EW	9	189; 65	0.86	0.56	0.066	300; 66	0.27; 0.18	409	1.95
S4	MYG001-EW	9	155; 52.1	0.43	0.23	0.055	300; 83	0.26; 0.27	441	2.15
S5	MYG004-EW	9	184; 75.1	1.22	0.48	0.040	300; 85	0.25; 0.26	430	1.25
S6	IBR004-EW	9	273; 71.4	1.03	0.38	0.038	300; 33	0.15; 0.21	382	1.35
S7	IBR006-EW	9	283; 70.8	0.78	0.3	0.039	300; 36	0.12; 0.25	406	1.35

Table 3.18 shows seven M_w9 Tohoku records that match the geotechnical profile of Site Class C in Victoria, B.C. These records were chosen from the K-NET stations in Japan.

All ground motions were scaled according to NBC 2015 requirements mentioned above, and the scaled spectra of subduction ground motions, their mean, and the design spectrum are shown in Fig. 3.11.

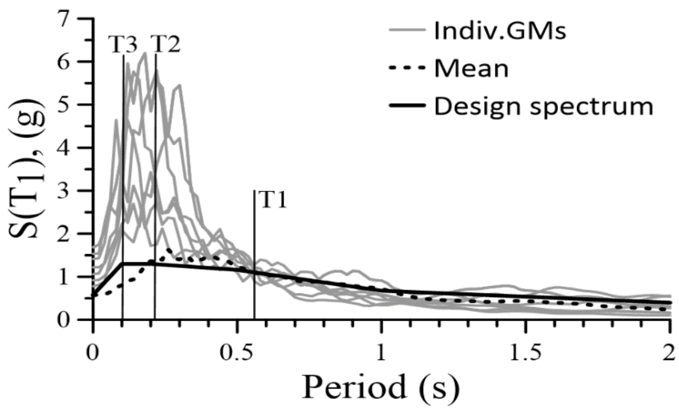

Fig. 3.11. Response spectrum of scaled subduction GMs for 4-storey MD-CBF building (T1 =0.55s; 0.15T1 = 0.08s; 2T1 = 1.1s)

3.3.8 Seismic Response of MD-CBF Building Based on Nonlinear Time-History Analysis

3.3.8.1 Seismic response of 4-storey MD-CBF building under crustal ground motions

After the OpenSees model of MD-CBF building is developed and the ground motions are selected, the nonlinear response history analysis (NRHA) is employed. The building response is expressed in terms of interstorey drift (ISD), residual interstorey drift (RISD), and floor acceleration (FA). An additional 20 second of zero amplitude was added at the end of each record to capture the RISD of the building. These engineering demand parameters (EDP) obtained at each floor under each individual ground motion scaled at the design level are shown in Fig. 3.12. In addition, the values of Mean and Mean+SD (standard deviation) are also presented. Moreover, the shear force distributed along the building height is also plotted in Fig. 3.12. As depicted, the peak of mean FA =1.1 g occurs at top floor, the peak of mean ISD is below 2.5%h_s code limit, and the peak of mean RISD is less than 0.5%h_s which is the reparability threshold. Hence, the peak of mean ISD and RISD is 0.65 %h_s and 0.1 %h_s, respectively and occur at 3rd floor.

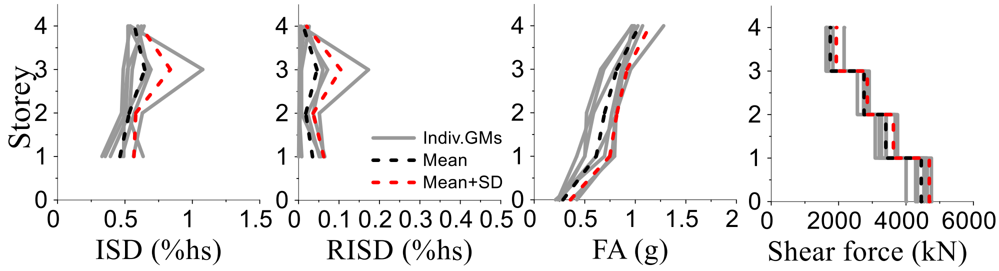

Fig. 3.12. Nonlinear response of 4-storey MD-CBF building subjected to crustal GMs scaled at design level: a) ISD, b) RISD, c) FA, and d) shear force

The mean base shear resulted for ¼ of building floor is much larger than that resulted from ESFP. This is explained by the consideration of probable stress F_y = 460 MPa for HSS braces, as well as larger response spectrum of some scaled GMs as plotted in Fig. 3.10.

The scaled accelerogram #C6 739-250, presented in Fig. 3.13, demands the larger ISD and RISD at the third floor where ISD = 1.08 %h_s, and RISD is about 0.15%h_s. The peak FA occurs at top floor and is near 1.0g. The hysteresis responses of HSS braces under the #C6 GM scaled at design level, are plotted in Fig. 3.14. It can be seen that the right braces in all floors buckled in compression, and the 3rd floor brace shows the largest response with axial deformation in compression of 30 mm. The left braces are neat the elastic response.

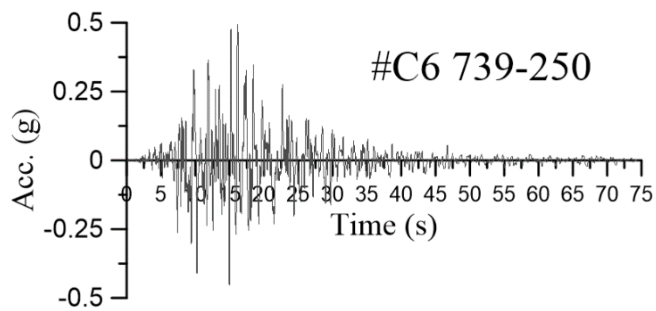

Fig. 3.13. Accelerogram #C6 739-250 scaled at design level

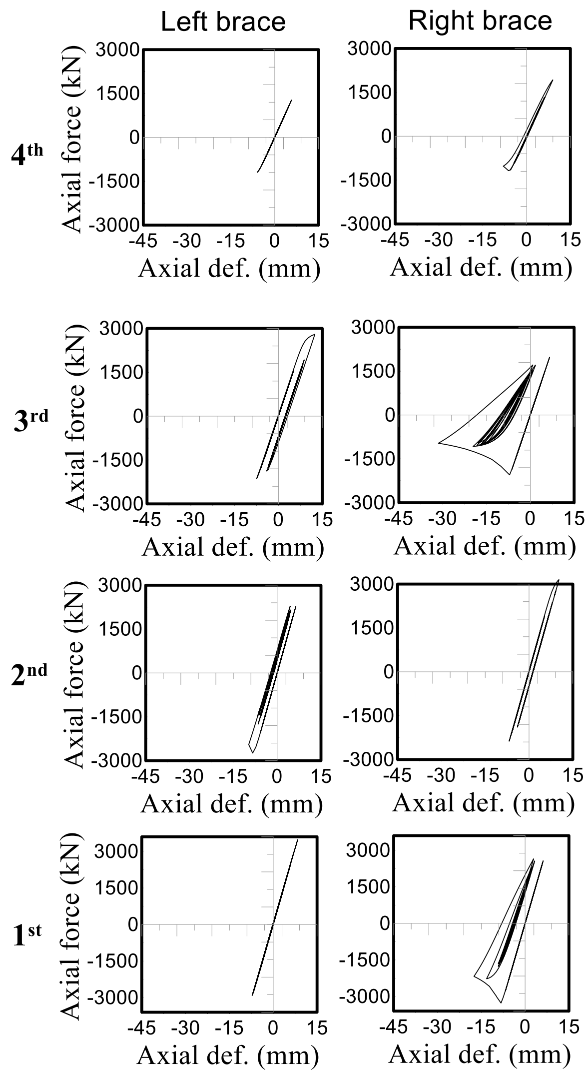

Fig. 3.14. Hysteresis loops of HSS braces of MD-CBF1 under #C6 scaled at design level

3.3.8.2 Seismic response of 4-storey MD-CBF building under subduction ground motions

Considering the 7 subduction ground motions scaled at design level (Fig. 3.11), the seismic response of 4-storey MD-CBF building associated with ¼ of floor area, is presented in Fig. 3.15 in terms of ISD, RISD, FA, and shear force. In addition, the values of Mean and Mean+SD are also presented. As depicted, the peak of Mean ISD and RISD is concentrated at the top floor and the values are 1.1%h_s and 0.1%h_s, respectively. The peak of Mean FA occurs at the 3rd floor and is 1.6 g. However, the peak ISD does not overpass 2.5%h_s, which is the limit value for buildings of normal importance category according to the NBCC code. In addition, the peak RISD is below 0.5h_s. Nonetheless, the large FA values could produce damage of non-structural components that are acceleration-sensitive.

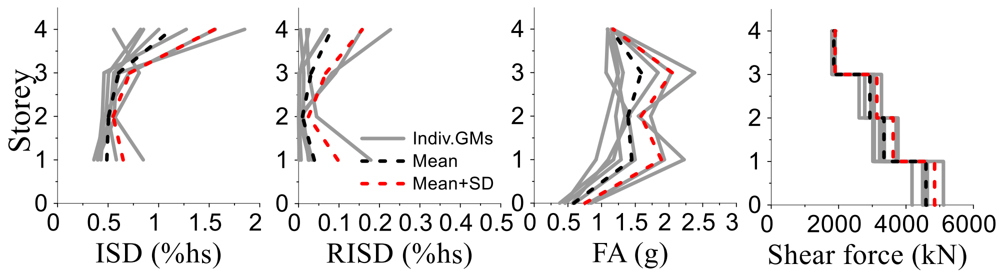

Fig. 3.15. Nonlinear response of 4-storey MD-CBF building subjected to subduction GMs scaled at design level

To analyse in detail the response of MD-CBF braces, the nonlinear response resulted under the scaled accelerogram #S3, plotted in Fig. 3.16, is investigated. The #S3 record was selected because it drives the maximum demand. From Fig. 3.15, it results that #S3 GM demands a peak ISD = 1.85%h_s and a peak RISD = 0.16%h_s at the top floor. This large demand at top floor is caused by the higher mode excitation and large spectral amplitudes in the short period range. The hysteresis response of HSS braces under #S3 GM scaled at design level is plotted in Fig. 3.17.

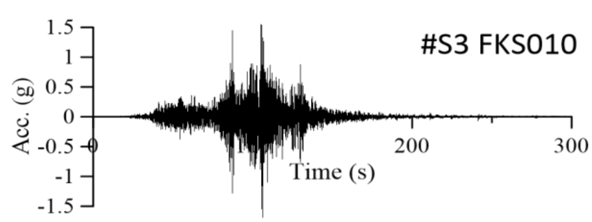

Fig. 3.16. Accelerogram #S3 FKS010 scaled at design level

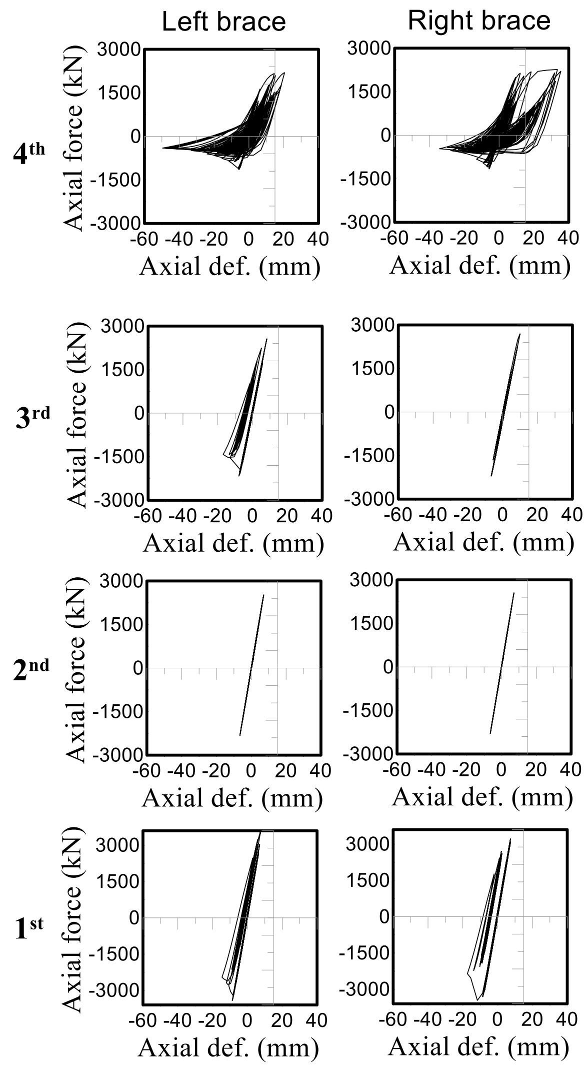

Fig. 3.17. Hysteresis loops of HSS braces under #S3 FKS010 scaled at design level

As depicted, Fig. 3.17 shows yielding in tension of top right brace and bucking in compression of top left brace, while braces of 2^{nd} floor behave elastically.

In general, the building's seismic response under scaled subduction ground motions at design level resulted in larger floor acceleration when comparing to the response under crustal ground motions. This demonstrates that the building's response is influenced by the characteristics of the ground motions. However, in both illustrated cases in Figs. 3.14 and 3.17, it results that damage concentrates at a single floor. To mitigate the formation of weak-storey mechanism that characterizes the CBF seismic response, in the next Chapter, the Strongback Braced Frame system is introduced.

3.4 Summary

The 4-storey MD-CBF office building located on Site Class C in Victoria B.C. was designed according to the NBC 2015 and CSA S16 (2014) standard requirements. From nonlinear analyses using OpenSees resulted that under both sets of crustal and subduction ground motions scaled to match the design response spectrum within the period of interest 0.2T1 – 2T1, the peak of mean ISD is within the 2.5% code limit and the RISD is lower than the 0.5%hs which is the boundary for reparability. The peak of mean floor acceleration is 0.9g under crustal and 1.5g under subduction ground motions, respectively. The tendency of damage concentration within a floor was observed.

CHAPTER 4. SEISMIC DESIGN OF STRONGBACK BRACED FRAME BUILDINGS

4.1 Introduction

Although the Strongback Braced Frame (SBF) system is not new (Khatib et al. ,1988), the system evolution was slow due to the complexity of developing a design method for the elastic truss (strongback) of SBF. Several researchers proposed simplified design methods for the elastic truss and showed the efficiency of the strongback system, but a straightforward design method is not available yet. Hence, the elastic truss shall be designed to possess sufficient strength to re-center the SBF, even when the ductile members (e.g. braces) behave in the inelastic range. It was found that the elastic truss is able to redistribute forces uniformly over the building height and substantially reduces potential dynamic instabilities.

The design method proposed by Simpson (2018, 2020), consisted in considering iterative nonlinear dynamic analysis and the capacity design principle to proportion the strongback's (elastic truss) members. The method also accounted on the higher mode effect for proportioning the strongback elements. In principal, the elastic truss (strongback) shall behave elastically and ensure yielding of ductile members. Demands and details of primary inelastic system can be assessed considering the first mode demand as required by the building code. To assure that the truss members remain elastic during the yielding of ductile members, these elements shall be stronger than the forces assigned from capacity design. However, the capacity design alone is insufficient to bound the forces in the strongback system, although it assures that the strength of the inelastic elements limit the forces transferred to adjacent members of primary ductile system under earthquake loading. Thus, forces in the remaining force-controlled actions are less constrained and strongly depend on the intensity of ground motions. After the yielding of ductile members, the strongback elements resist lateral loads and continue to accumulate higher mode demands while performing in the elastic range until it reaches yielding. These seismic demands are dynamic and constantly changing with time (Simpson, 2018). The lateral deformation of SBF is dominated by the first mode (uniform) response, while the forces triggered in the strongback elements are not bounded and increase under the higher mode (bending) contributions; hence, the increase could be significantly higher than that resulted solely from the application of capacity design method.

It was noted that the elastic nature of the strongback (elastic truss) can be linked to that of pivoting wall or rocking frames (Simpson, 2018). Latter on, Simpson and Torres (2021) proposed a simplified modal pushover analysis to estimate the first- and higher-mode force demands for the design of strongback braced frames. However, the method proposed is not simply to apply and may not be readily implementable in a design office due to extensive data reduction, numerical modeling expertise, and computational expense (Simpson, 2020). Following the paper of Pollino et al. (2017), Simpson (2018) has also recommended exploring different locations for SB as exterior to inelastic braced frame or reversed exterior. It is worth mentioning that Pollino et al. (2017) proposed a reversed exterior SB (elastic truss) connected to a yielding link as that of an eccentrically braced frame with link at one side, where the yielding links was designed to dissipate energy. Meanwhile, Simpson (2018) has also recommended to add the strongback system to other types of steel braced frames rather than Buckling Restrained Braced Frames that she considered in presented analyses.

New developments into the design methodology were released by Chen (2022). He considered offset split-X braces as ductile system and various locations for strongback.

4.2 Case Study

Figure 4.1 shows the same building plan with that presented in Chapter 3. The difference is that the 4-storey office building designed for Site Class C in Victoria B.C. is braced by four SBFs in each orthogonal direction. To analyse the effect of exterior truss location in the SBF response, two locations for the strongback truss are considered: 1) adjacent exterior to the ductile braced frames (SBF-E) as illustrated in Fig. 4.2a; and 2) reversed exterior (SBF-RE) as presented in Fig. 4.2b. Due to the particularity of building geometry, the strongbacks of two SBFs are placed back-to-back and the truss system was labelled diamond shape (SBF-DS) as presented in Fig. 4.2b.

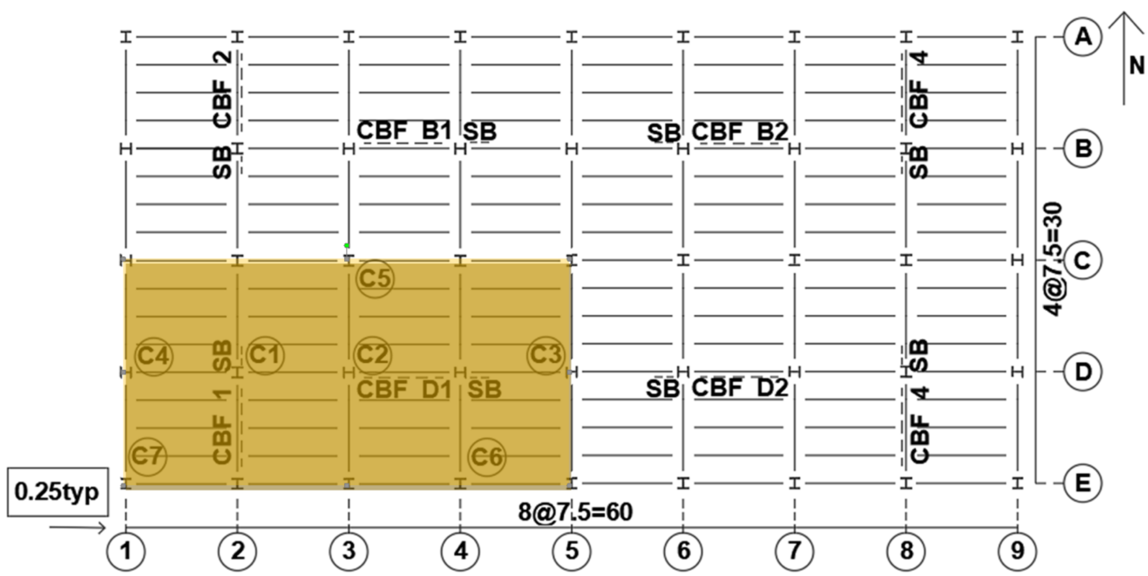

Fig. 4.1. Plan view of 4-storey SBF building with exterior strongback system

In Fig. 4.2, the primary ductile system is the traditional MD-CBF plotted in black, while the strongback truss (SB) is presented in blue. Simpson (2018) suggested considering the width of strongback truss between L/3 and L/4, where L is the span. Herein, the width of strongback truss is considered L/4.

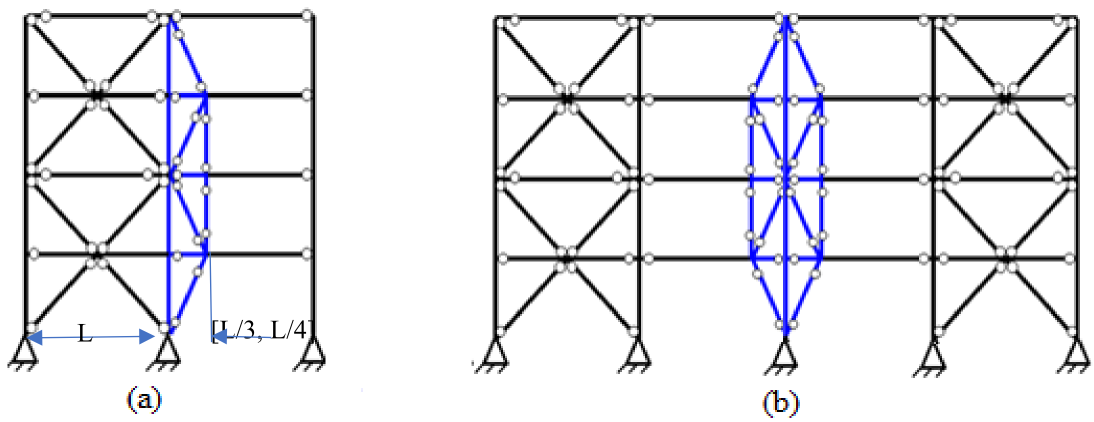

Fig. 4.2. Elevation of SBF: a) SBF-E; and b) SBF-DS

By pivoting-like behaviour under loading/unloading ground motion cycles, the strongback truss is able to redistribute internal forces over the height of the building, re-center the structural system, and provide dynamic stability when the ductile tension-compression braces behave inelastically. Thus, to engage every storey in a pivoting displaced shape, the strongback truss shall be relatively stiff and act as a strong vertical backbone. Conversely, the ductile tension-compression braces of a regular MD-CBF are not able to redistribute damage along the building height and the system is prone to storey mechanism.

4.2.1 Higher mode effect

Designing the members of steel SBF requires a novel approach; hence, the application of capacity design principle is not sufficient to size the members of strongback truss such that they remain essentially elastic in all vibration modes (Lai and Mahin, 2015). The investigation of higher mode effect was initially focused on reinforced concrete shear walls, then extended to rocking braced frames (Wiebe et al., 2013), strongback braced frames (Simpson 2018 and 2020), and spinal braced frames (Chen et al., 2019). Rutenberg (2013) noted that "the longer the initial period of a structure has, the greater is the ductility demand and implicitly the effect of higher modes."

In concrete shear walls and rocking braced frames, the higher modes have a greater influence on the storey shears and moments developed above the base, whereas the first mode governs the base-overturning moment. Similarly, the higher mode effect plays an important role when designing and analyzing the SBFs. Considering only the first mode response in the design of SBF members, could lead to underestimating the forces transferred in the elastic truss if the contribution of higher modes is not accounted for (Simpson, 2018).

To design the traditional braced frame members, either the static approach (e.g. the inverted triangular distribution of lateral forces) or the dynamic distribution of lateral forces along the building height is considered in addition to capacity design, as required by the building code and steel design standard. However, after the yielding of braces, the forces resulted from nonlinear dynamic analysis that account for higher mode effect are greater than those resulting from response spectrum analysis (Blakeley et al., 1975, and others). Thus, forces triggered in the strongback truss members associated to the first mode response are not sufficient to assure its elastic response (Simpson, 2018) and a novel design method is required.

4.2.2 Design methods accounting on higher mode contribution

In the Modal Pushover Analysis (MPA) developed by Chopra and Goel (2002), the building is subjected to lateral forces that increase monotonically with an invariant distribution along the building height, until a pre-determined target displacement is achieved. The MPA method assumed that the force distribution and target displacement rely on two assumptions: i) the fundamental vibration mode controls the response, and ii) the mode shape remains unchanged after the structure yields. Meanwhile, the MPA approach was developed *for linearly elastic structural systems* and is equivalent to the response spectrum analysis (RSA) in addressing assumption i). However, it considers the contributions of all vibration modes. The peak modal response resulting from the first mode (r_1) and higher modes (r_2, r_3, … r_n) are combined using either the square-root-of-sum-of-squares (SRSS) or the complete quadratic combination (CQC). The SRSS method, which is valid for uncoupled modes in building structures, provides an estimate of the peak value of total response, r, according to Eq. (4.1).

$$r = \left(\sum_{i=1}^{n} r_n^2\right)^{1/2} \tag{4.1}$$

The MPA lacks a theoretical basis when applied to inelastic systems. It also assumes that the coupling of elastic modes upon the initiation of inelastic behaviour is negligible, and it allows combining the inelastic response using the elastic modes (Chopra and Goel, 2002).

The Modified Modal Pushover Analysis (MMPA) introduced by Chopra et al. (2004), calculates the seismic demands from higher modes while assuming the structural system to be elastic. This is done by analyzing the response *of the first mode when it is inelastic and the response of higher modes when the system is elastic.* The total response is then determined by adding the gravity response, r_g to the peak modal responses obtained using the SRSS combination rule. Thus, the total response is calculated as the sum of the gravity response and the peak modal responses obtained by combining the responses from all modes using the SRSS rule:

$$r = r_g + \sqrt{{r_1}^2 + {r_2}^2 + {r_3}^2 + \cdots + {r_n}^2} \tag{4.2}$$

The equation provided calculates the total response of a building by adding the peak modal responses from the pushover analysis to the response from gravity loading alone. The modal response is obtained from the pushover analysis at the target displacement, including gravity loading and P-Δ effects. For example, in the case of a 9-storey MRF building in Seattle and Los Angeles (SAC project), it was found that the first mode pushover analysis is capable of detecting damage at lower floors but fails to identify damage in the upper floors, where the higher modes' contribution is crucial. Using the MMPA procedure resulted in a better estimation of higher modes demand.

Wiebe et al. (2015) and Steele and Wiebe (2016) proposed a computation method to determine forces in the Rocking braced frame system for practical engineering applications. This method involved using the prescribed lateral forces from building codes to calculate the first mode response, r_1, and the elastic higher mode response, r_2 through r_M, using the MPA method. Chen et al. (2019) proposed a similar procedure, but the elastic higher mode demand was estimated using the MMPA method. Thus, it is assumed that the spine or SB oscillates due to higher mode excitations, while the ductile fusses of steel braced frame experienced yielding in the first-mode response. It is also assumed that the higher modes are uncoupled or weakly coupled. To estimate the total response due to the first and higher modes, the superposition modal combination rule is used. As considered by Chen et al (2019) and Simpson (2018, 2020), the modal combination rule superposes the SRSS of higher modes with the response in the first mode as per Eq. (4.3).

$$r = r_g + |r_{1,pl}| + \sqrt{{r_{2,el}}^2 + r_{3,el}^2 + \cdots + r_{M,el}^2} \tag{4.3}$$

Later on, Simpson and Torres (2021) presented a simplified MPA approach for the design of strongback truss. Instead of using the target displacement as proposed by Chopra and Goel (2002), they use the target base shear. The proposed method is limited to the case study where the strongback is located interior to braced frame and the ductile braces are BRBs.

4.2.3 Deformation Compatibility

According to Simpson (2018) and Palermo et al. (2018) there is interaction between the inelastic primary frame and the SB truss which behaves in combined shear and bending. The magnitude of the interaction between the SB and the braced frame that behaves in shear depends on the relative stiffness of the SB to the inelastic frame which changes as it yields under the ground motion demand. Hence, Simpson (2018) noted that the SB behaviour is similar to that of a "beam-like bending behaviour… and the strongback could be modeled as a simply-supported beam of equivalent lateral stiffness."

From modal analyses results, Simpson (2018) highlighted that the SB exhibited significant stiffness and strength in the second and higher modes even after yielding of ductile members. In the second and higher modes, the SB truss remains elastic and attracted larger forces even after yielding of ductile members and/ or increase of ground motion intensity. Furthermore, the contribution of higher modes on the SB truss member sizes is limited by the ground motion intensity, rather than it's bending capacity.

4.2.4 Design Methodology Developed for SBFs

The design approach presented in this study is based on the MMPA (Chopra and Goel, 2004) while the superposition modal combination rule as per Eq. (4.3) is used. This is similar to the method proposed by Chen et al. (2019) for the Tied Braced Frames. Herein it is assumed that the SB truss oscillates due to higher modes excitations, while the braced frames withstand the yielding of braces in the first-mode response. It also assumes that higher modes are uncoupled or weakly coupled. Although the nonlinear second mode response can develop lower inelastic forces due to the bending of strongback, these forces are neglected. The graphical representation of Eq. (4.3) adapted for the 4-storey SBF-E case study presented in Fig. 4.2a is illustrated below (Fig. 4.3).

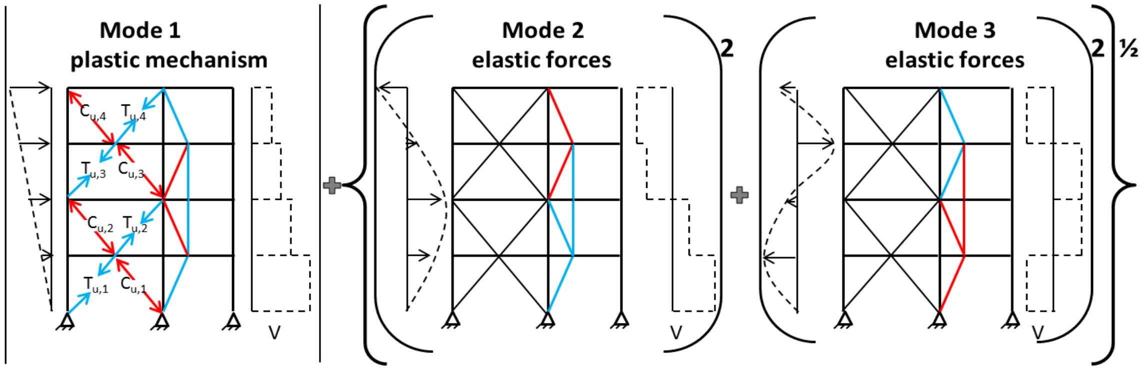

Fig. 4.3. Graphical illustration of adapted Eq. (4.3) for the 4-storey SBF-E case study (Chen et al., 2022)

The design methodology employed for the case study is similar to that proposed by Chen et al. (2022). The design steps are:

1. Use the Equivalent Static Force Procedure (ESFP) according to building code and design the braces of traditional MD-CBF. The system is proportioned to resist 100% base shear. Then, used the capacity design approach to size the beams and columns of MD-CBF (primary system). It is noted that the MD-CBF column that support the strongback truss is continuous.
2. Compute the brace member forces assuming that the full plastic mechanism forms in the first mode (Fig. 4.3a) and consider equilibrium of forces to compute the axial forces transferred into SB members. The resulted member forces are applied as static forces to estimate the truss member sections.
3. For preliminary design, use member sections of primary system resulted from step 1 and member sections of strongback from Step 2. Determine the elastic natural periods and modes from Eigenvalue analysis.
4. To account on higher modes contribution on strongback truss, employ the truncated elastic design spectrum (Fig. 4.4) and compute independently the storey forces associated to the

2nd and 3rd mode as exemplified in Fig. 4.3b and c. Compute the higher mode forces triggered in strongback truss members using the SRSS combination rule (see Eq. 4.3).

5. Using the MD-CBF sections from step 1 and the strongback truss sections from step 4, calculate the total response according to Eq. (4.3).
6. Verify the accuracy of design members against nonlinear dynamic response analysis.

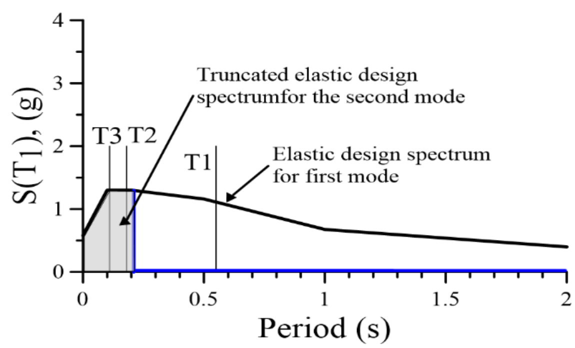

Fig. 4.4. Elastic Design spectrum for Site Class C, Victoria, BC as per NBC 2015 and the truncated elastic design spectrum associated to 2nd mode (shaded area)

4.2.5 Preliminary design of SBF-E

The calculation of seismic weight, W =29457 kN, was provided in Chapter 3, as well as the first mode period of MD-CBF building resulted from eigenvalue analysis, which is T1=0.55 s. Accordingly, the associated S(T1) is 1.11g computed for Site Class C in Victoria, BC. Considering the same coefficients R_d =3 and R_0=1.3 as per the MD-CBF system, the base shear is V = 1.11x29457x1.0x1.0/(3x1.3) = 8384 kN. It is worth mentioning that this value is lightly smaller than V_{max} = max(2/3S(0.2)$I_E M_v W/R_d R_0$; S(0.5)$I_E M_V W/R_d R_0$) =8762 kN; hence, use in design V = 8384 kN. The shear resulted from the contribution of notional loads and P-delta effect was also added, while the torsion caused by accidental eccentricity was neglected. As per Fig. 4.1, the building is symmetric and the SFRSs are placed symmetric with respect to the center of mass. Conducting the design in N-S direction and considering ¼ of building floor area due to building symmetry, the base shear associated to SBF1 is 8384/4=2096 kN. The notional load and P-Δ effect were also considered. However, the seismic forces were not affected by P-Δ because the stability factor θ was smaller than 0.1. The MD-CBF brace sizes and their probable tensile (T_u) and compression (C_u) resistance are provided in Table 4.1. According to the CSA S16 standard, for buildings shorter than 4 storeys, the probable tensile strength of HSS braces, T_u, could be considered as 0.6 T_u but not less than C_u.

Applying the capacity method, two scenarios are considered: a) all ductile braces reached the probable tensile force T_u and the probable compression force, C_u, and b) all braces reached the probable tensile force T_u and the probable postbuckling force C_u'. Scenario a) is depicted in Fig. 4.5, where the direction of lateral loads is left-to-right (Fig. 4.5a) and right-to-left (Fig. 4.5b).

Table 4.1 Brace member sizes of MD-CBF and their probable resistances

St.	Inelastic braces				
	Brace sizes	C_u	T_u	$T_{u,used}$ = max (0.6T_u; C_u)	C_u'
4	HSS127X127X13	1000	2479	1488	496
3	HSS178X178X9.5	1810	2843	1810	568
2	HSS203X203X9.5	2358	3289	2358	658
1	HSS203X203X13	2891	4260	2891	852

Using the equilibrium of forces, the preliminary estimation of axial forces transferred in the external SB members of SBF-E, conducted for both loading directions is also presented. The example is for Elevation "2" (SBF 1) of floor plan shown in Fig. 4.1.

To design the strongback truss members, Simpson (2018) considered the nonlinear response time-history analysis (NRHA) and performed several iterations. Based on the results, Simpson (2018) observed that the SBF responds in the 2nd mode in bending and the members of strongback truss could be estimated considering the truss as a simply supported structure. Based on this observation, a 2D model of strongback truss considered pinned at the base and simply supported at the roof through a roller was analysed. Both sets of loads given in Figs. 4.5a and b were considered and the plots are shown in Figs. 4.6a and b.

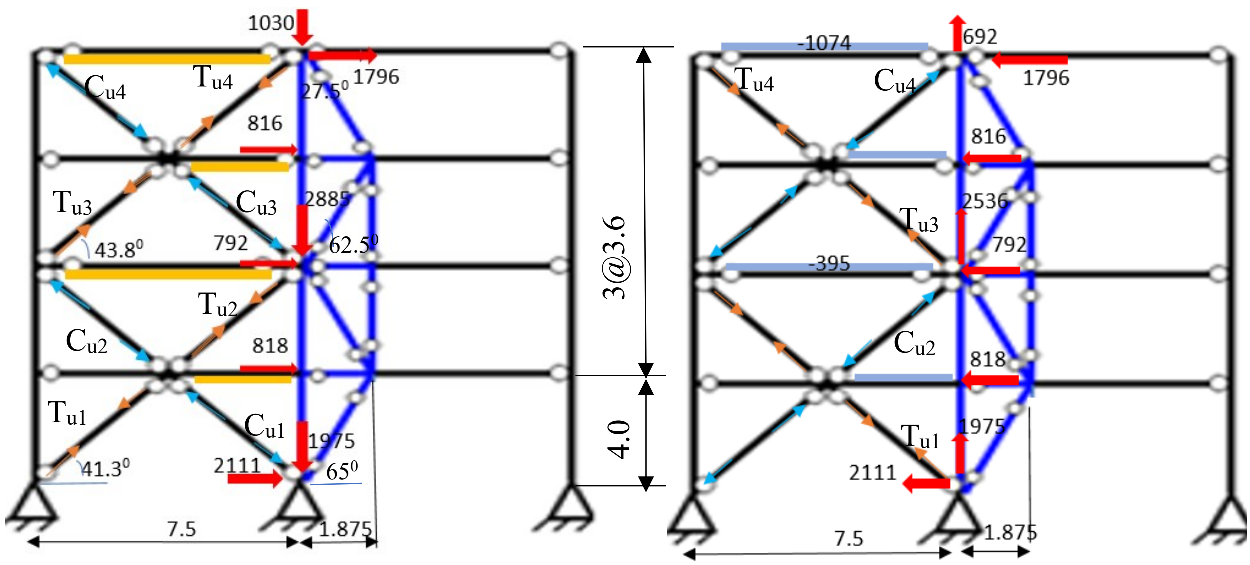

Tw

Fig. 4.5. Forces triggered in SB truss considering T_u, C_u scenario and direction of lateral force: a) left-to-right, and b) right-to-left

A summary of axial forces developed in truss members considered as a simply supported truss and presented in Fig. 4.6 are given in Table 4.2. The length of braces (c/c) of strongback truss is 4.0 m at typical floors and 4.4 m at bottom floor, while the effective length is 3.2 m and 3.5 m, respectively. The effective length of a tie is 2.8 m. The sections selected for 2nd and 3rd floor braces could be smaller, while the tie sections could be HSS 203x203x16 with C_r = 3185 kN. Thus, the larger forces are triggered in ties and top and bottom braces of SB. Using the braces and ties section of SB presented in Table 4.2, the 3D ETABS model is prepared and plotted in Fig. 4.7.

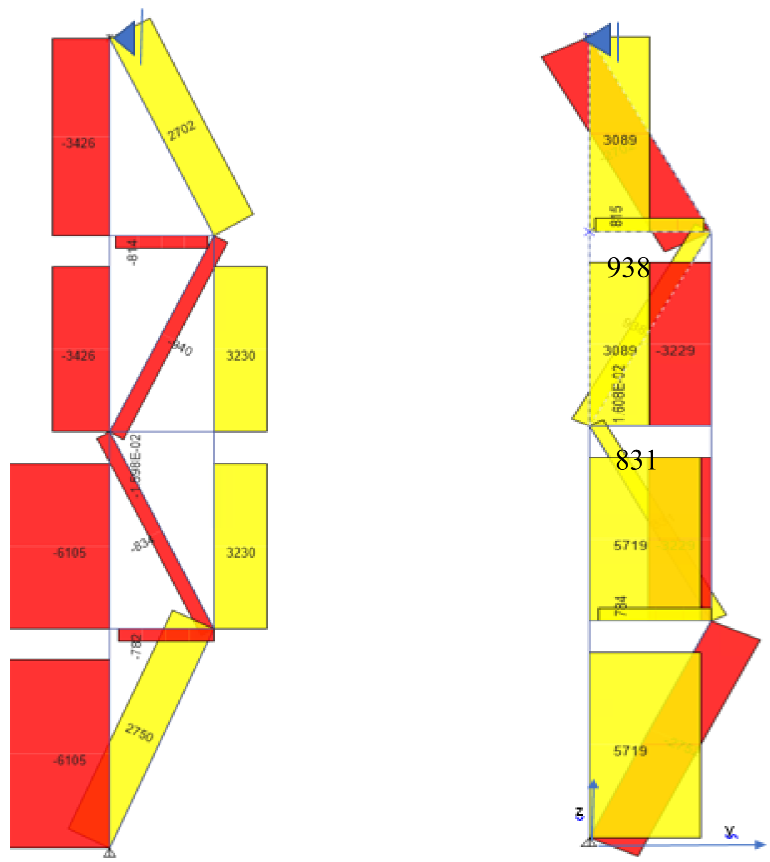

a) b)

Fig. 4.6. Preliminary forces in strongback truss considered as a simply supported truss structure resulted under forces illustrated in Figs. 4.5a and b

Table 4.2 Forces triggered in truss members (Fig. 4.6) for preliminary design

St.	$0.6T_u$ & C_u	C_u &$0.6T_u$	C_f	Sections*	C_r (Φ=0.9)	C_r (Φ=1.0)
Forces in braces of SB [kN]						
4	2702	-2702	-2702	HSS203X13	2520	2800
3	-940	938	-940	HSS203X9.5	1960	2177
2	-834	831	-834	HSS203X9.5	1960	2177
1	2750	-2750	-2750	HSS203X13	2450	2722
Forces in ties of SB [kN]						
2-3	3238	-3239	-3239	HSS203X13	2650	2945

*) Read HSS 203X203X13

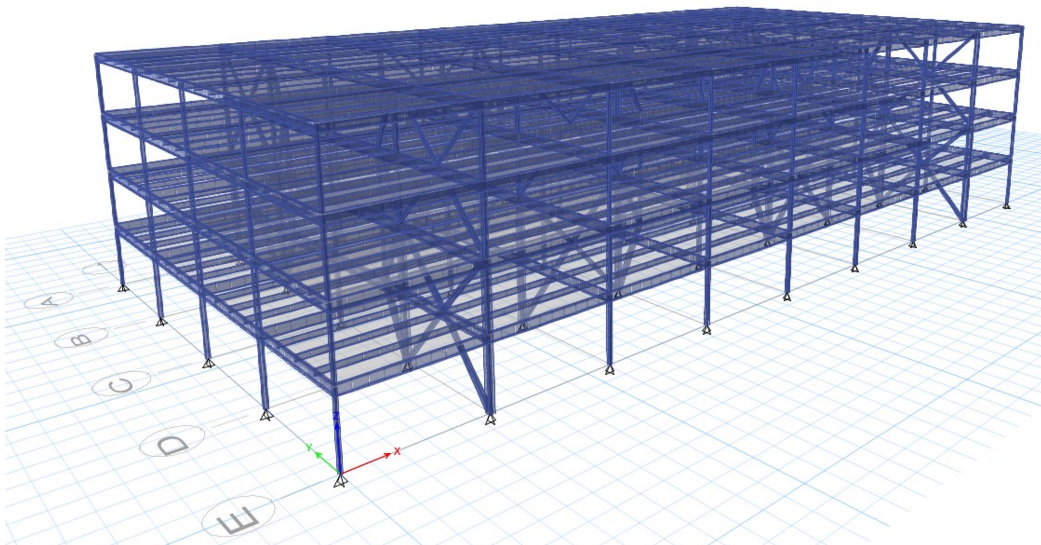

Fig. 4.7. Three dimensional (3D) ETABS model of 4-storey SBF-E building

From Eigenvalue analysis using the 3D building model in ETABS, the first, second, and third mode periods are presented in Table 4.3 along with the base shear.

Table 4.3 Base shear and first, second and third mode periods

Building	Base shear (kN)	T1 (s)	T2 (s)	T3 (s)
SBF-E	8384	0.522	0.174	0.105

As resulted from Table 4.3, the increase of base shear with respect to the benchmark MD-CBF building is only 4%. The deformed shape (ETABS plots) associated with modes 1st, 2nd, and 3rd resulted under the N-S direction forces from response spectrum analysis is presented in Fig. 4.8. From Fig. 4.8 can be concluded that the 1st and 3rd modes are in shear, while the 2nd mode is in bending due to the effect of strongback placed adjacent exterior to the braced frame. When buckling braces are used, is not recommended to integrate the SB inside the braced frame because the lateral forces are not fully sustained after braces experienced buckling.

To capture the elastic higher modes, the response spectrum analyses are carried out using a truncated elastic design spectrum defined by the user in ETABS for the 2nd and 3rd modes, independently (see the shaded area in Fig. 4.4 for the definition of 2nd mode consideration).

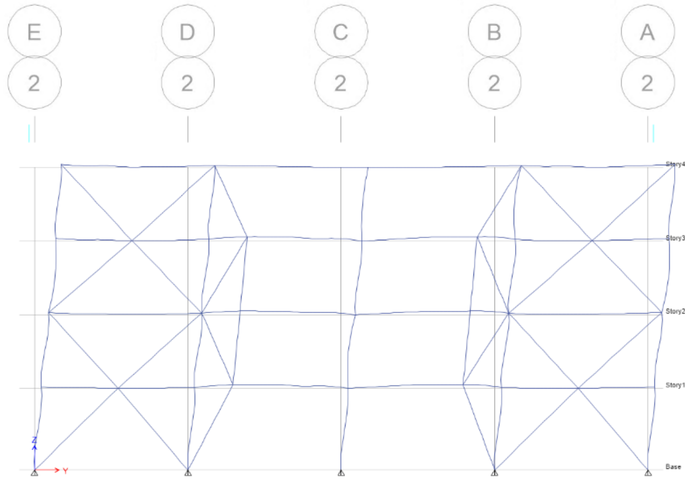

(a)

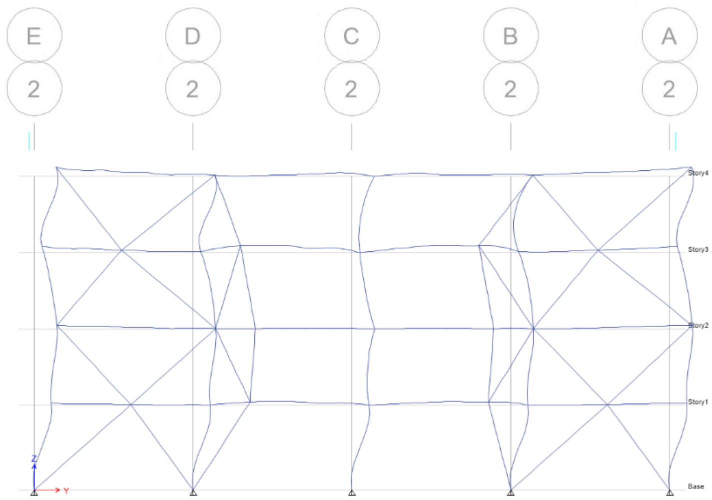

(b)

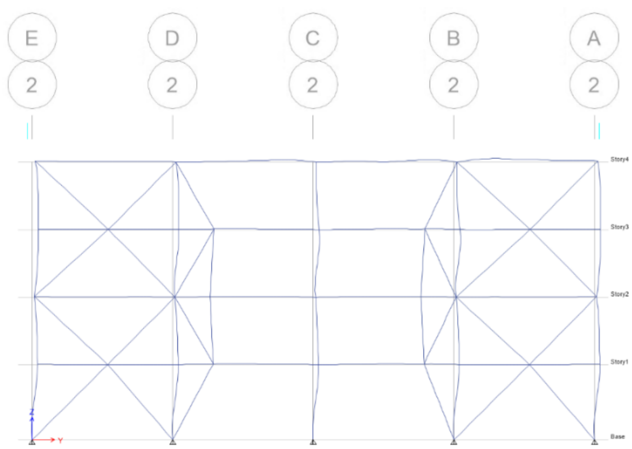

(c)

Fig. 4.8. Deformed shapes: a) first mode, b) second mode, and c) third mode

Using the truncated elastic response spectrum independently for 2nd and 3rd modes, the storey forces resulted from storey shear obtained from 3D model in ETABS are given in Tables 4.4 and 4.5, respectively. Then, these storey forces associated with one SBF-E are plotted in Fig. 4.9.

Table 4.4 Storey shear forces associated with 2nd mode from RSA with truncated spectrum

St.	Shear force per building from ETABS (kN)	Storey force per building (kN)	Storey force per ¼ of building (kN)
4	4990	4990	1248
3	3708	-1282	-320
2	2360	-1348	-337
1	5972	3602	900

Table 4.5 Storey shear forces associated with 3rd mode from RSA with truncated spectrum

St.	Shear force per building from ETABS (kN)	Storey force per building (kN)	Storey force per ¼ of building (kN)
4	1440	1440	360
3	1568	128	32
2	1451	-117	-29
1	1485	35	9

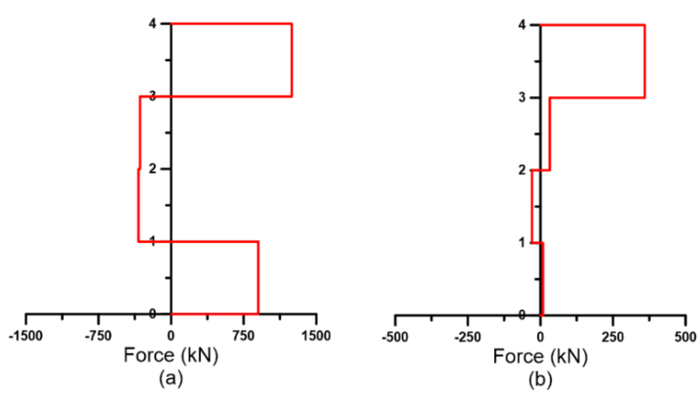

Fig. 4.9. Storey force distribution per one SBF-E associated to: (a) 2nd mode; (b) 3rd mode

Due to the building symmetry and the location of SBFs at equal distances with respect to the center of mass, the storey forces per building were divided by the number of SBFs displaced in the direction of calculation. As expected, larger storey force is triggered at top floor.

Next, the storey forces from Tables 4.4 and 4.5 that are also plotted in Fig. 4.9 were applied as static forces in both positive and negative direction in the 3D ETABS model. The results associated with the 2nd and 3rd mode contributions are presented in Appendix A in Figs. 1 and 2, while the forces triggered in SB members due to the first mode response that are summarized in Table 4.6 are from Fig. 3 provided in Appendix A. Then, the forces from the 2nd and 3rd mode were combined using the SRSS modal combination rule. The summary of compression resistances of selected sections for SB truss members and some observations are presented in Table 4.7.

Table 4.6 Axial forces in braces and ties of SB from higher and 1st mode using 3D ETABS model

Forces in braces of SB (kN)										
St.	Right-to-left direction			Left-to-right direction			C_f due to higher modes	Axial forces due to 1st mode inelastic (right-left direction)	Axial forces due to 1st mode inelastic (left-right)	C_f as per Eq. (4.3)
	2nd	3rd	SRSS	2nd	3rd	SRSS				
4	-1681	-449	1740	1681	449	1740	-1740	-1338	1325	3078
3	141	191	238	-141	-191	238	-238	394	-410	648
2	1059	154	1070	-1059	-154	1070	-1070	105	-158	1228
1	-748	-476	886	748	476	886	-886	-1593	1545	2479
Forces in ties of SB (kN)										
2-3	-1617	-567	1714	1617	567	1714	-1714	-1536	1539	3250

The elastic stiffness of braces of SB and braces of primary system is calculated as (EA/L)cosθ. It is noted that there are two ductile braces per MD-CBF. As can be seen from Table 4.8, the stiffness of SB brace is about half of the stiffness of ductile braces. In addition, the larger relative stiffness of SB brace occurs at top floor where the interaction between the SB and MD-CBF is the highest.

Table 4.7 Design of SB members using axial forces from Table 4.6

St.	HSS sections to satisfy Eq. (4.3)	C_r (Φ=1) (kN)	Observations
Braces of SB truss			
4	HSS203X203X13	2800	A larger section can be selected as HSS 203x203x16. However, no all ductile braces will yield at the same time.
3	HSS203X203X9.5	2177	Smaller section can be selected
2	HSS203X203X9.5	2177	Smaller section can be selected
1	HSS203X203X13	2722	Good
Ties of SB truss			
2-3	HSS203X203X13	2945	A larger section can be selected as HSS 203x203x16 (Cr=3185 kN). However, no all ductile braces will yield at the same time.

Table 4.8 Relative stiffness of SB braces

St.	SB truss braces			Inelastic braces			K_{SB}/ (K_{SB}+2 K_{DB})
	HSS sections of SB members	A (mm^2)	K_{SB}	HSS sections of MD-CBF	A (mm^2)	2K_{DB} (kN/mm)	
4	HSS203X13	9250	269	HSS127X13	5390	2x166	0.45
3	HSS203X9.5	7150	208	HSS178X9.5	6180	2x191	0.35
2	HSS203X9.5	7150	208	HSS203X9.5	7150	2x221	0.32
1	HSS203X13	9250	246	HSS203X13	9250	2x298	0.30

Forces induced in the column supporting the SB are also determined using the SRSS modal combination rule considering higher modes, and these axial forces are given in Table 4.9. For columns W-shape sections are chosen. The column adjacent to SB is continuous over the building height and is also subjected to bending.

Table 4.9 Axial forces in column attached to SB truss

St.	Positive direction (kN)			Negative direction (kN)			C_f (kN)	Capacity design +gravity loads	$\sum C_f$	Column section
	2nd mode	3rd mode	SRSS	2nd mode	3rd mode	SRSS				
4	1491	398	1543	-1491	-398	1543	1543	1259	2802	W250X101
3	1491	398	1543	-1491	-398	1543	1543	1533	3076	W250X101
2	678	431	803	-678	-431	803	803	4676	5479	W310X202
1	678	431	803	-678	-431	803	803	4930	5733	W310X202

In Table 4.10 is provided the factored bending moment triggered in column attached to the SB truss, as well the bending and compression resistance. The column is oriented in strong axis. The capacity of the member required to resist both bending moments and axial compressive force shall be examined for cross-sectional strength, overall member strength, and lateral torsional buckling strength. For column member oriented in strong axis, the lateral torsional buckling verification is the most critical because Cr is calculated in its weak axis. For Class 1 and Class2 sections of I-shape members Eq. (4.4) shall be satisfied. Herein, U_{1x} is considered 1.

$$C_f/C_r + 0.85U_{1x}M_{fx}/M_{rx} \leq 1.0 \qquad (4.4)$$

From Tables 4.9 and 4.10 it can be seen that due to higher modes, greater demand is required in the column adjacent to SB especially at upper floors. Moreover, the beams that support the ties of SB experience additional moment and shear forces. Thus, large W-shape sections are needed for these gravity beams. To conclude, the member sections required for the 4-storey SBF-E building considered in further analyses are listed in Tables 4.11 and 4.12, respectively.

Table 4.10 Bending moment in column of primary system attached to SB

St	2nd mode	3rd mode	SRSS	1st mode (capacity design)	Total M_f [kNm]	Section	M_r [kNm]	C_r* [kN]	Int. Eq. (4.4)
4	39	10	40	30	70	W310X129	671	4534	0.92
3	133	40	139	100	239	W310X129	671	4534	0.98
2	102	35	108	96	204	W310X202	1090	7142	0.93
1	53	11	54	10	64	W310X202	1090	6870	0.89

*C_r is calculated in weak axis

Table 4.11 Final design of inelastic braced frame members of 4-storey SBF-E building

St.	Brace	Column attached to SB[1)]	Beam
4	HSS127X127X13	W310X129	W460X106
3	HSS178X178X9.5	W310X129	W460X128
2	HSS203X203x 9.5	W310X202	W460X128
1	HSS203X203x13	W310X202	W460X128

[1)]At top floors, the column of primary system that is not attached to SB is made of W250x89.

Table 4.12 Sections of SB truss members of 4-storey SBF-E and that of ties support

St.	Elastic truss (SB)		
	Braces	Ties	Exterior beams supporting ties
4	HSS203X203X13	N/A	W460X106
3	HSS203X203X9.5	HSS 203X203x13	W530X248
2	HSS203X203X9.5	HSS 203X203x13	W530X248
1	HSS203X203X13	N/A	W530X248

The preliminary sections of SBF-E members are validated using NRHA and the 2D OpenSees model.

4.2.6 Gusset plate connections

Gusset plate connections of MD-CBF braces are presented in Section 3.2.4. The connections for elastic braces of SB are pin connections.

4.2.7 Preliminary design of SBF-DS

The selection of sections for the SB truss of SBF-DS could be the same as those of SBF-E presented above. However, some differences exist. As plotted in Fig. 4.2b, when the SBs are reversed to the braced frame, they are located back-to-back and form a diamond shape (DS) truss. The forces associated with T_u and C_u scenario that are triggered in the DS truss are given in Fig. 4.10. It is noted that T_u and C_u are the probable tensile and compressive strength of ductile brace members of primary system. Considering the diamond-shape truss as a simply supported that is pinned at the base and supported by a roller at the top, the forces in braces and ties of SB are presented in Fig. 4.11 and are summarized in Table 4.13. Employing the computed truss sections in the 3D ETABS model, the deformed shape associated with first, second, and third vibration modes are plotted in Fig. 4.12. As depicted, the deformed shape of 1st and 3rd mode are similar for SBF-E and SBF-DS, but that of 2nd mode is slightly different.

As presented in Table 4.13, the size of top and bottom braces, as well as the size of ties are about 5-6% lower than required. However, it was decided to maintain the HSS 203X203X13 section for these members for further analyses.

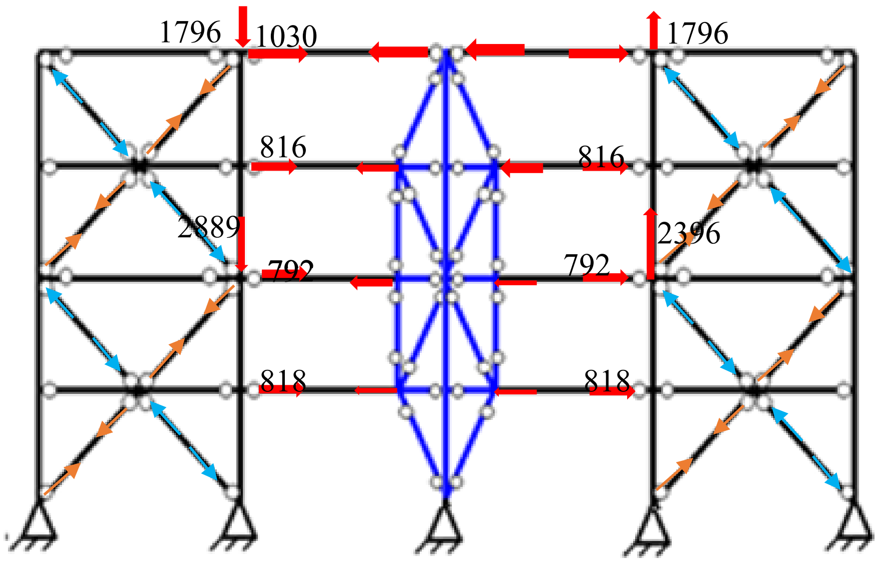

Fig. 4.10. Forces triggered in SB truss of SBF-DS considering T_u, C_u scenario

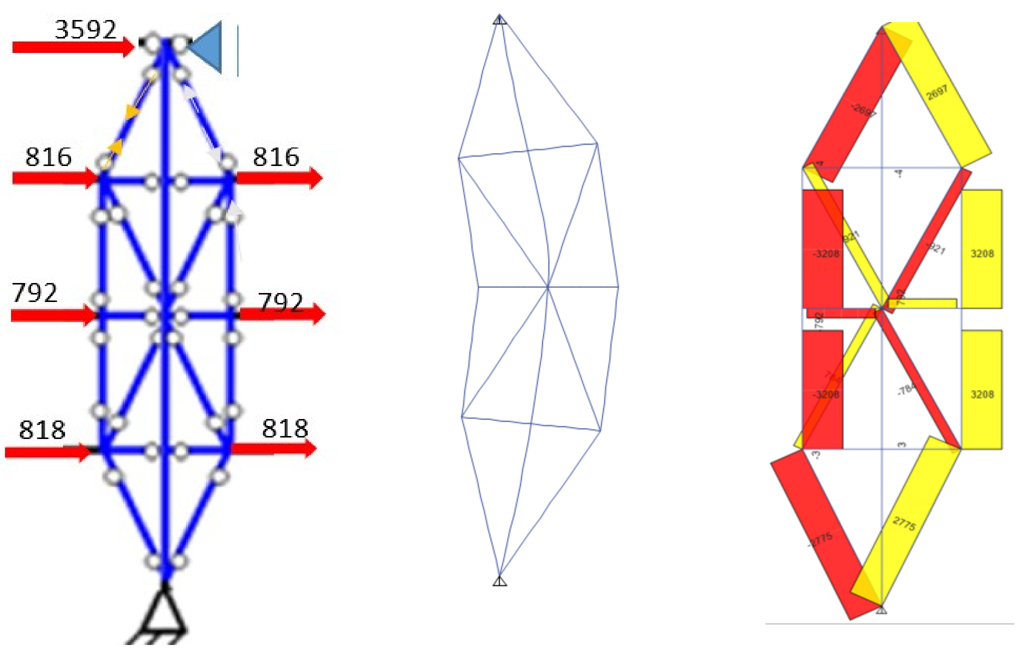

Fig. 4.11. Forces in braces and ties of diamond-shape truss: a) forces associated with 1st mode, b) deformed shape, and c) forces in truss members

Table 4.13 Forces triggered in diamond-shape truss members used for preliminary design

St.	$0.6T_u$ & C_u	C_u &$0.6T_u$	C_f	Sections*	C_r (Φ=0.9)	C_r (Φ=1.0)
Forces in braces of SB [kN]						
4	2967	-2967	-2967	HSS203X13	2520	2800
3	-921	921	-940	HSS203X9.5	1960	2177
2	-784	784	-834	HSS203X9.5	1960	2177
1	2775	-2775	-2775	HSS203X13	2450	2722
Forces in ties of SB [kN]						
2-3	3206	-3206	-3206	HSS203X13	2650	2945

*) Read HSS 203X203X13

Then, the storey forces associated to the 1st mode, presented in Fig. 4.11, were applied in the 3D ETABS model and the plots are presented in Fig. 5 of Appendix A. Next, to compute the forces triggered in SB due to higher modes, the 3D ETABS model was subjected to truncated spectrum associated with the 2nd mode and then to the 3rd mode. A summary of shear forces and storey forces is given in Tables 4.14 and 4.15, respectively. Subsequently, these storey forces were statically applied in the 3D ETABS model and the axial forces in DS truss members are plotted in Table 4.16 while the plots are printed as Figs. 6 and 7 in Appendix A. The sizes of SB diamond shape members are given in Table 4.17 and the summary is provided in Table 4.18.

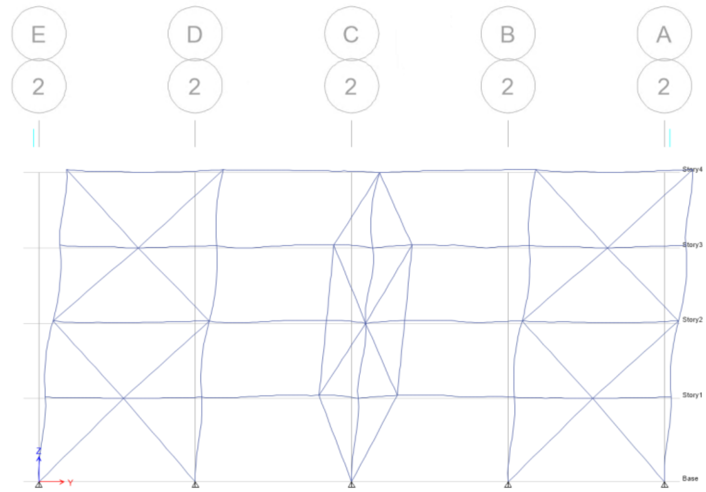

a)

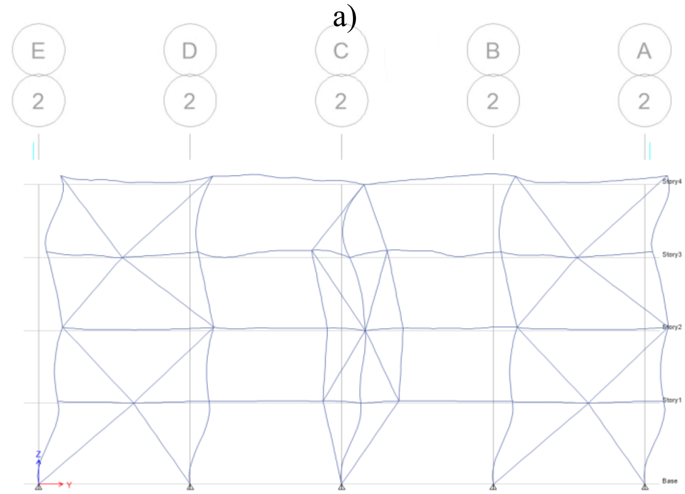

b)

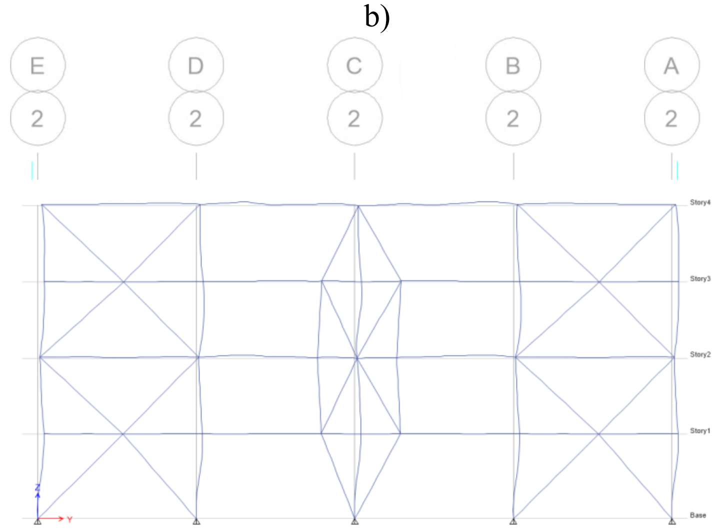

c)

Fig. 4.12. Deformed shapes of grideline 2 of 4-storey SBF-DS building: a) 1st mode, b) 2nd mode, and c) 3rd mode

Table 4.14 Storey shear forces distribution associated with 2nd mode for the SBF-DS

St.	Shear force per building from ETABS (kN)	Storey force per building (kN)	Storey force per ¼ of building (kN)
4	5137	5137	1284
3	3706	-1431	-358
2	2553	-1153	-288
1	6723	4170	1042

Table 4.15 Storey shear forces distribution associated with 3rd mode for the SBF-DS

St.	Shear force per building from ETABS (kN)	Storey force per building (kN)	Storey force per ¼ of building (kN)
4	1471	1471	368
3	1463	-8	-2
2	1422	-41	-10
1	1427	5	1

Table 4.16 Forces in braces and ties of SB type diamond shape from higher modes and 1st mode

Forces in braces of SB type diamond-shape (kN)										
St.	Left brace			Right brace			C_f due to higher modes	Axial forces due to1st mode inelastic (left side)	Axial forces due to 1st mode inelastic (right side)	C_f as per Eq. (4.3)
	2nd	3rd	SRSS	2nd	3rd	SRSS				
4	-2566	-513	2616	2566	513	2616	-2616	-1496	1496	3912
3	195	161	253	-195	-161	253	-253	376	-376	629
2	1427	111	1431	-1427	-111	1431	-1431	40	-40	1471
1	-1307	-551	1418	1307	551	1418	-1418	-1795	1795	3213
Forces in ties of SB (kN)										
2-3	-2449	-597	2520	1617	567	2520	-2520	-1660	1660	4180

Table 4.17 Design of braces and ties of diamond-shape truss using axial forces from Table 4.15

St.	HSS sections to satisfy Eq. (4.3)	C_r (Φ=1) (kN)	Observations
Braces of SB truss			
4	HSS254X254X13	3811	A larger section than HSS 203x203x13 is required and HSS 254x254x13 is selected.
3	HSS203X203X9.5	2177	Smaller section can be selected
2	HSS203X203X9.5	2177	Smaller section can be selected
1	HSS254X254X13	2756	A larger section than HSS 203x203x13 is required and HSS 254x254x13 is selected.
Ties of SB truss			
2-3	HSS254X254X13	3922	A larger section than HSS 203x203x13 is required and HSS 254x254x13 is selected.

Comparing Table 4.17 with Table 4.11, it can be seen that larger sections are required for top and bottom braces, as well as ties of SB diamond-shape truss members than for the adjacent exterior truss presented above. The relative stiffness of SB braces of diamond-shape type is presented in Table 4.18. As depicted, the relative stiffness is larger at top floor and about similar at the remaining floors.

Table 4.18 The relative stiffness of braces of diamond shape truss

St.	SB braces			Inelastic braces			$K_{SB}/(K_{SB}+2K_{DB})$
	HSS sections of SB members	A (mm^2)	K_{SB}	HSS sections of MD-CBF	A (mm^2)	$2K_{DB}$ (kN/mm)	
4	HSS254X13	11800	343	HSS127X13	5390	2x166	0.51
3	HSS203X9.5	7150	208	HSS178X9.5	6180	2x191	0.35
2	HSS203X9.5	7150	208	HSS203X9.5	7150	2x221	0.32
1	HSS254X13	11800	285	HSS203X13	9250	2x298	0.32

The axial force and bending moment triggered in the gravity column that is part of diamond truss are provided in Table 4.19. The axial force triggered in the column is from the associated gravity component of seismic load case DL+0.5LL+0.25SL+E and the bending moment results mostly from higher modes.

The summary of member sizes of SB diamond-shape truss is given in Table 4.20. It is noted that the members of primary system (MD-CBF) are as indicated in Chapter 3.

Table 4.19 Bending moment triggered in gravity column belonging to diamond-shape truss

St	2nd mode	3rd mode	SRSS	1st mode	M_f [kNm]	Cf [kN]	Section	M_r [kNm]	C_r* [kN]	Int. Eq. (4.4)
4	5	1	5	0	5	230	W250X89	382	2920	0.10
3	142	30	145	70	215	522	W250X89	382	2920	0.68
2	140	28	143	88	231	814	W310X107	546	3700	0.61
1	26	17	31	75	64	1110	W310X107	546	3570	0.42

Table 4.20 Summary of diamond-shape truss members and beams supporting ties of 4-st SBF-DS

St.	Elastic truss: diamond-shape type			Beams of supporting ties
	Braces	Ties	Column	
4	HSS254X254X13	N/A	W250X89	W460X106
3	HSS203X203X9.5	HSS 254X254X13	W250X89	W530X248
2	HSS203X203X9.5	HSS 254X254X13	W310X107	W530X248
1	HSS254X254X13	N/A	W310X107	W530X248

4.3 OpenSees model

The 2D OpenSees model of ¼ of SBF building presented in Fig. 4.13 includes the SB truss model adjacent exterior to the MD-CBF discussed in Chapter 3. Although it is expected that all SB truss members behave elastically, to identify their yielding at the near-collapse limit state, both braces and ties were modelled with nonlinear force-based beam-columns elements with distributed plasticity, fiber section discretization and *Steel02* uniaxial material. Ties and braces of SB were connected to beams and respectively column through pin connections and are made of HSS sections with $F_y = 350$ MPa.

As presented in Chapter 3, the inelastic braces, beams, and columns of primary system (MD-CBF) were modeled with nonlinear force-based beam-column elements with distributed plasticity and fiber section discretization. *Steel02* uniaxial material was assigned to MD-CBF members. To simulate the HSS brace fracture due to low-cycle fatigue, the fatigue material was wrapped around the parental *Steel02* material as explained in Chapter 3. For HSS sections of ductile braces, the probable yield stress is $R_yF_y = 460$ MPa. To allow braces to buckle out-of-plain, the brace to frame connections were modelled using two nonlinear rotational springs and one elastic torsional spring. All columns supporting the inelastic MD-CBF braces and the elastic truss were modeled as continuous from top to bottom. The columns on the other side of the inelastic braces were modeled continuous over two storeys. All gravity columns that are laterally supported by braced frame were modeled using the elastic steel material (*Steel01*) with $F_y = 345$ MPa. A 2% Raleigh damping was calculated for the first and third mode and assigned to elastic members only.

From Eigenvalue analysis in N-S direction, using OpenSees, resulted that the vibration periods of the 4-storey SBF building are similar to those of the 4-storey MD-CBF building, indicating that the SB contributed very little to building stiffness by approximately 5%. The vibration periods from the 2D OpenSees model and the 3D ETABS model were almost the same, implying that the 2D OpenSees model was accurate. The vibration periods are summarized in Table 4.21. As resulted, the SBF-E and SBF-DS have similar periods; hence, the first mode period is slightly shorter (~5%) of that of MD-CBF.

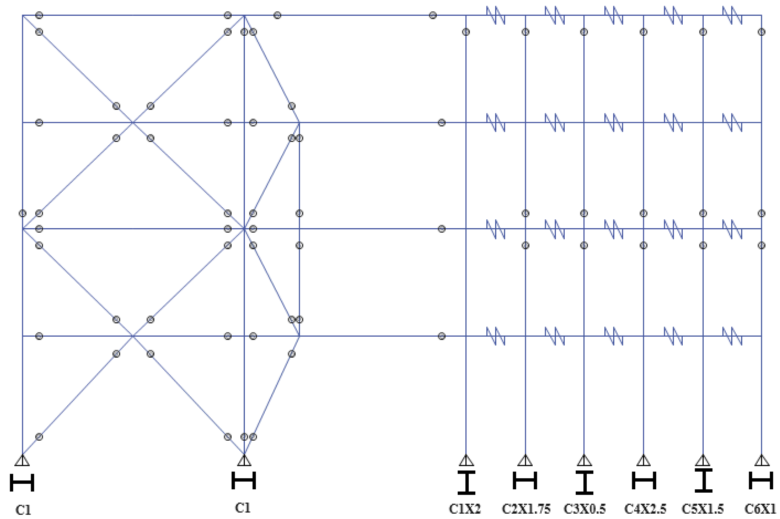

Fig. 4.13. 2D OpenSees model of ¼ 4-storey SBF-E building

Table 4.21 Vibration periods for 4-storey SBF *vs*. the MD-CBF

Type	Vibration periods					
	ETABS			OpenSees		
	T1	T2	T3	T1	T2	T3
MD-CBF	0.551	0.201	0.125	0.554	0.205	0.138
SBF-E	0.520	0.169	0.102	0.522	0.171	0.105
SBF-DS	0.527	0.175	0.104	0.528	0.176	0.111

4.4 Seismic response of SBF buildings at design level using time history analysis

4.4.1 Seismic response of 4-st. SBF-E and SBF-DS buildings under crustal GMs

To evaluate the seismic response of 4-storey SBF-E and SBF-DS, the same set of seven crustal ground motions used in Chapter 3 are employed. The seismic response is expressed in terms of interstorey drift (ISD), residual interstorey drift (RISD), floor acceleration (FA), and shear force. Figs. 4.14 and 4.15 present these seismic response of 4-storey SBF-E and 4-storey SBF-DS, respectively, under crustal ground motions scaled at design level (DL).

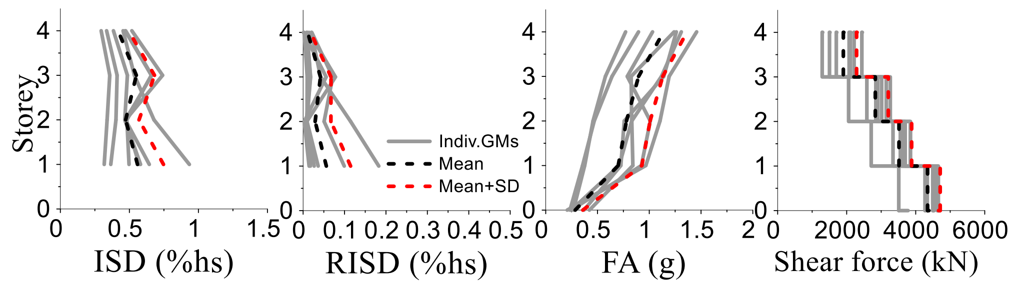

Fig. 4.14. Nonlinear response of 4-storey SBF-E building under crustal GMs scaled at DL

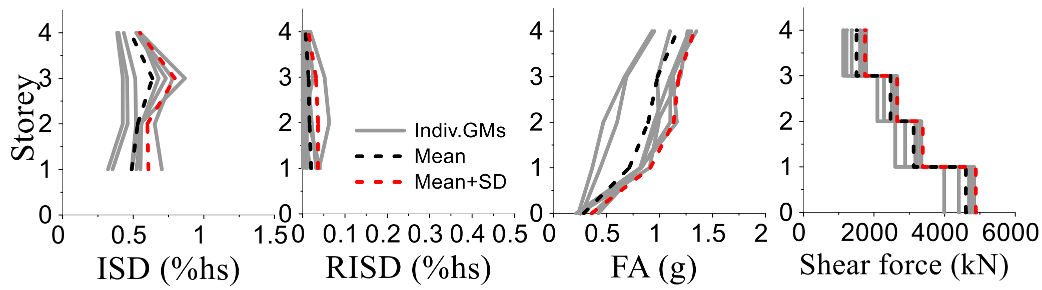

Fig. 4.15. Nonlinear response of 4-storey SBF-DS building under crustal GMs scaled at DL

The nonlinear responses provided in Figs 4.14 and 4.15 are discussed against the 4-storey MD-CBF building response (blue line) in Fig. 4.16. These results indicate that both SBFs show an even distribution of interstorey drift (ISD) along the building height when comparing to MD-CBF response. The SB is able to decrease the peak ISD; hence, a large reduction particularly occurred when the building is subjected to #C1 and #C6. Residual interstorey drift is also reduced in SBFs and is below 0.25%h_s. In general, the floor accelerations and storey shear forces are larger for BBF-E and SBF-DS buildings. It is worth mentioning that storey shear is associated with the projection of brace member forces. For example, the responses resulted under #C2 and #C4 GMs showed the larger FA demand.

The design method for the SBF was done to assure that members of SB respond elastically under seismic ground motion. Such example involving the hysteresis loops of ductile braces and SB members of SBF-E under the #C6 GM is illustrated in Fig. 4.17. As depicted, the larger shear demand in the SBF-E model is concentrated at the bottom floor, while in the case of MD-CBF

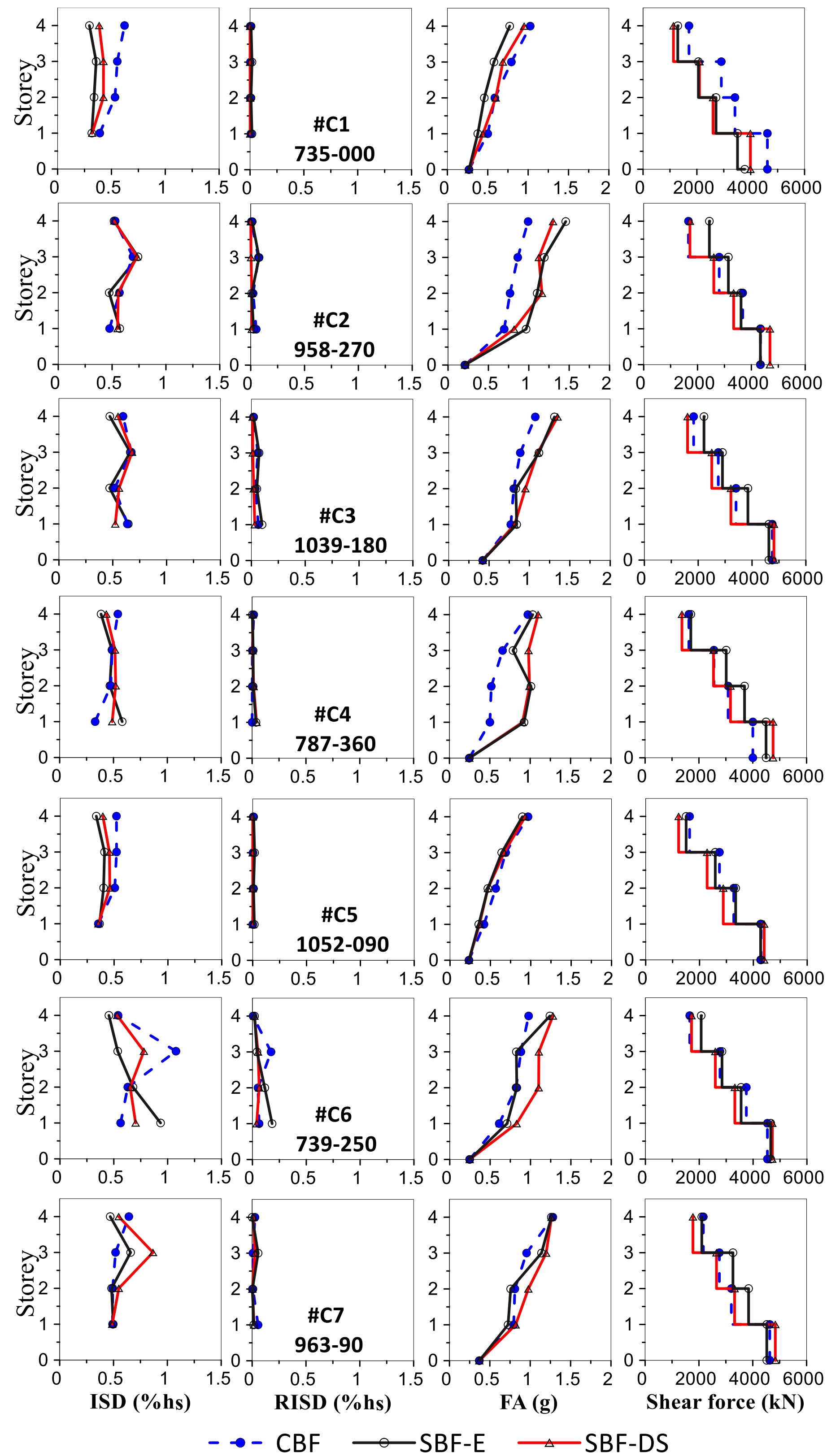

Fig. 4.16. Nonlinear responses of 4-storey SBF-E and SBF-DS buildings subjected to crustal GMs scaled at DL against the response of 4-storey MD-CBF building

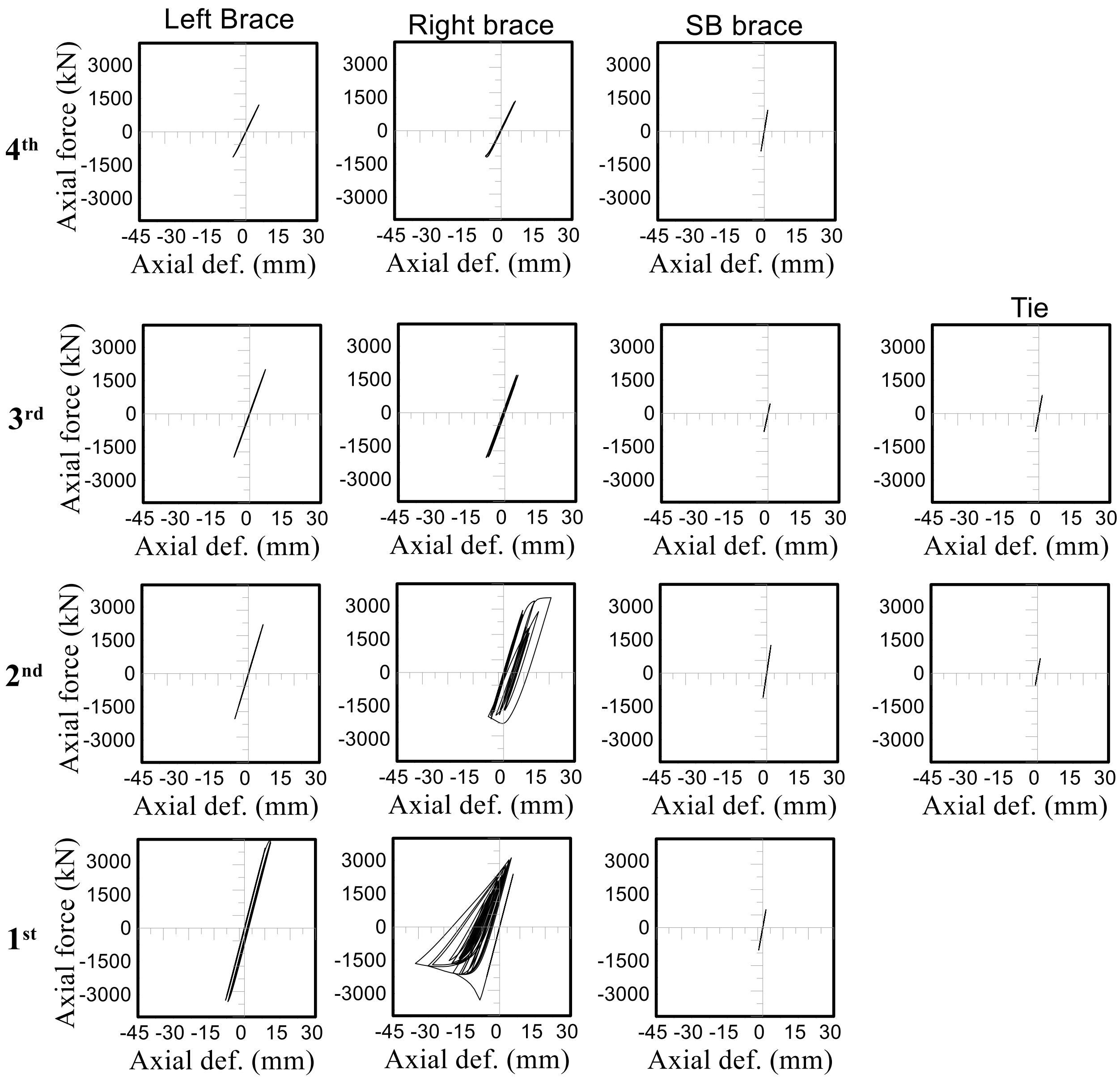

Fig. 4.17. Hysteresis loops of SBF-E braces and SB members under #C6 739-250 scaled at DL

(Fig. 3.14), the demand was concentrated at middle floors. It is noteworthy that the SB braces and ties did not undergo yielding, indicating that the SB member sections are adequate.

The OpenSees model of SBF-DS represents half of the building floor area. In this case, the model contains one diamond-shape truss and two MD-CBFs displaced in each side (see gridline 2 in Fig. 4.12). The hysteresis loops of the left ductile braces of primary system and the members of DS truss of the SBF-DS building resulted under #C6 ground motion are plotted in Fig. 4.18. As expected, the hysteresis response of all ductile braces of the left and right braced frame is almost similar. The dissipation of energy occurred at all floors but not at the top floor, while in the benchmark MD-CBF model, it is primarily concentrated at the third floor. No yielding of members of SB was observed.

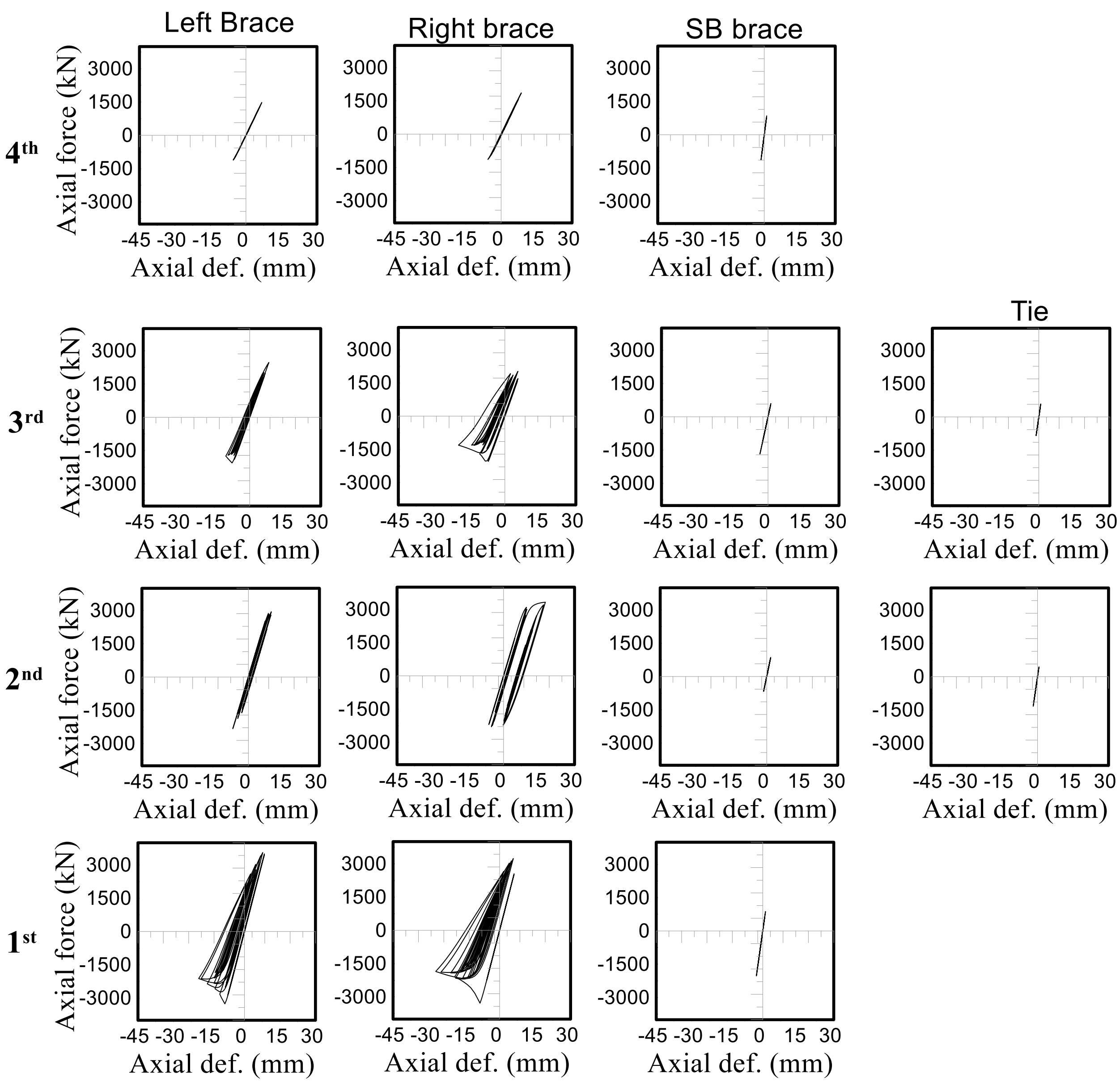

Fig. 4.18. Hysteresis loops of left side SBF-DS braces and SB members under GM #C6 739-250 scaled at design level

4.4.2 Seismic response of 4-storey SBFs under subduction ground motions

To evaluate the seismic response of 4-storey SBFs buildings, the same set of seven subduction ground motions used in Chapter 3 were employed. Figs. 4.19 and 4.20 present the seismic response of SBF-E and SBF-DS resulted under subduction ground motions. The seismic response is expressed in terms of ISD, RISD, FA and storey shear force. Figure 4.21 shows a comparison of these parameters plotted along the building height when the SBF buildings were subjected to subduction ground motion scaled at design level (DL). The responses of SBFs are plotted in red (SBF-DS) and black (SBF-E) against the results obtained for the benchmark MD-CBF building represented in blue. As depicted, using the SBFs, the concentration of damage experienced at top floor by the MD-CBF was mitigated. Meanwhile, the top ISD was substantially decreased when the SBF is used. However, the FA was slightly increased under few GMs. For example, under the #S3 GM, the peak ISD decreased from 1.8%h_s recorded for MD-CBF to 0.7%h_s for SBFs. However, the reduction in RISD was not as noticeable since the values were already low for both MD-CBF and SBF models. In terms of floor accelerations, under all GM but no #S7, the SBFs displayed a smoother distribution across the building height than the MD-CBF.

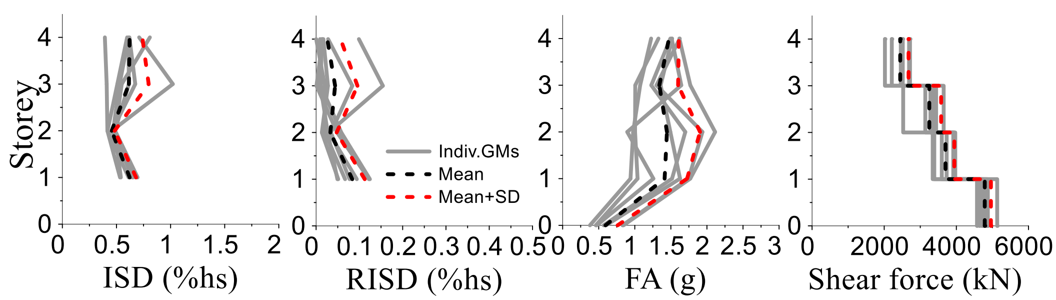

Fig. 4.19. Nonlinear response of 4-st. SBF-E building subjected to subduction GMs scaled at DL

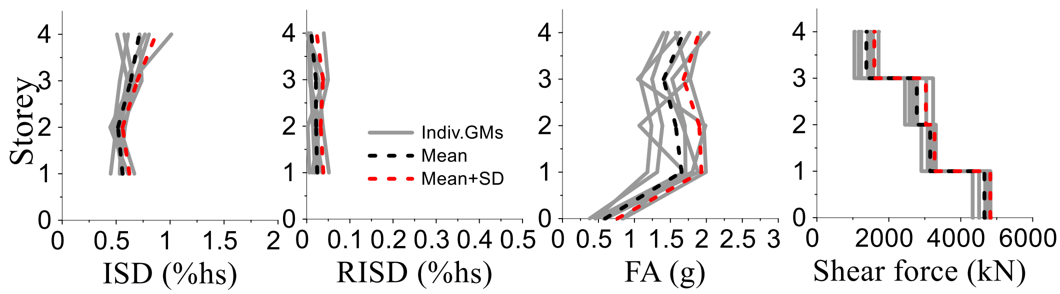

Fig. 4.20. Nonlinear response of 4-st. SBF-DS building under subduction GMs scaled at DL

Regardless of ground motion signature, the maximum storey shear forces at roof were lower for the SBF-DS and larger for the SBF-E with respect to MD-CBF building. In all cases, the SBF-E develops larges storey shear forces than the SBF-DS. This is explained by different contributions of higher modes in the case of SBF-E versus the SBF-DS.

Fig. 4.22 shows the hysteresis loops of ductile braces and the elastic response of SB members of 4-storey SBF-E building under #S3 GM scaled at DL demand.

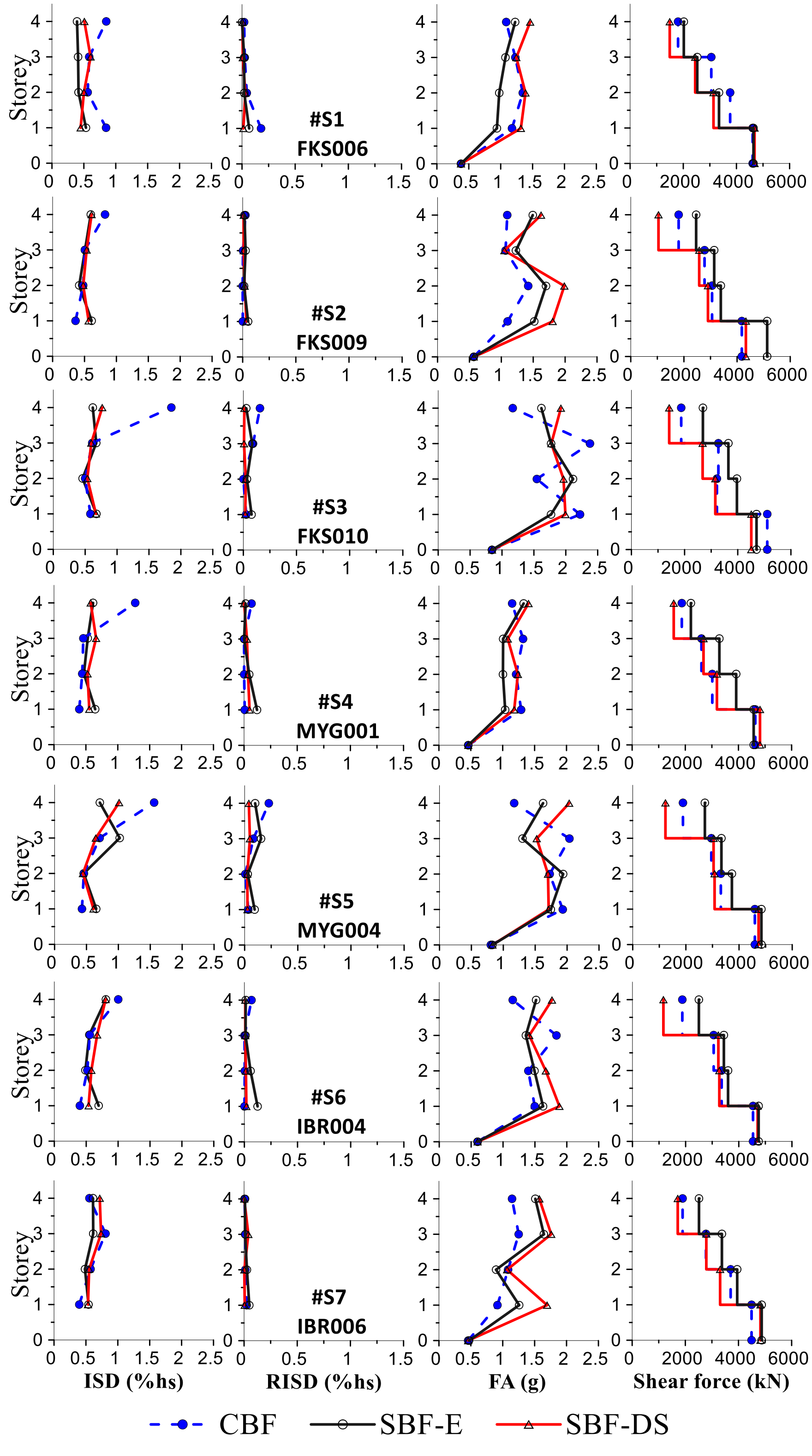

Fig. 4.21. Nonlinear responses of 4-storey SBF buildings subjected to subduction GMs scaled at design level against the response of 4-storey MD-CBF building

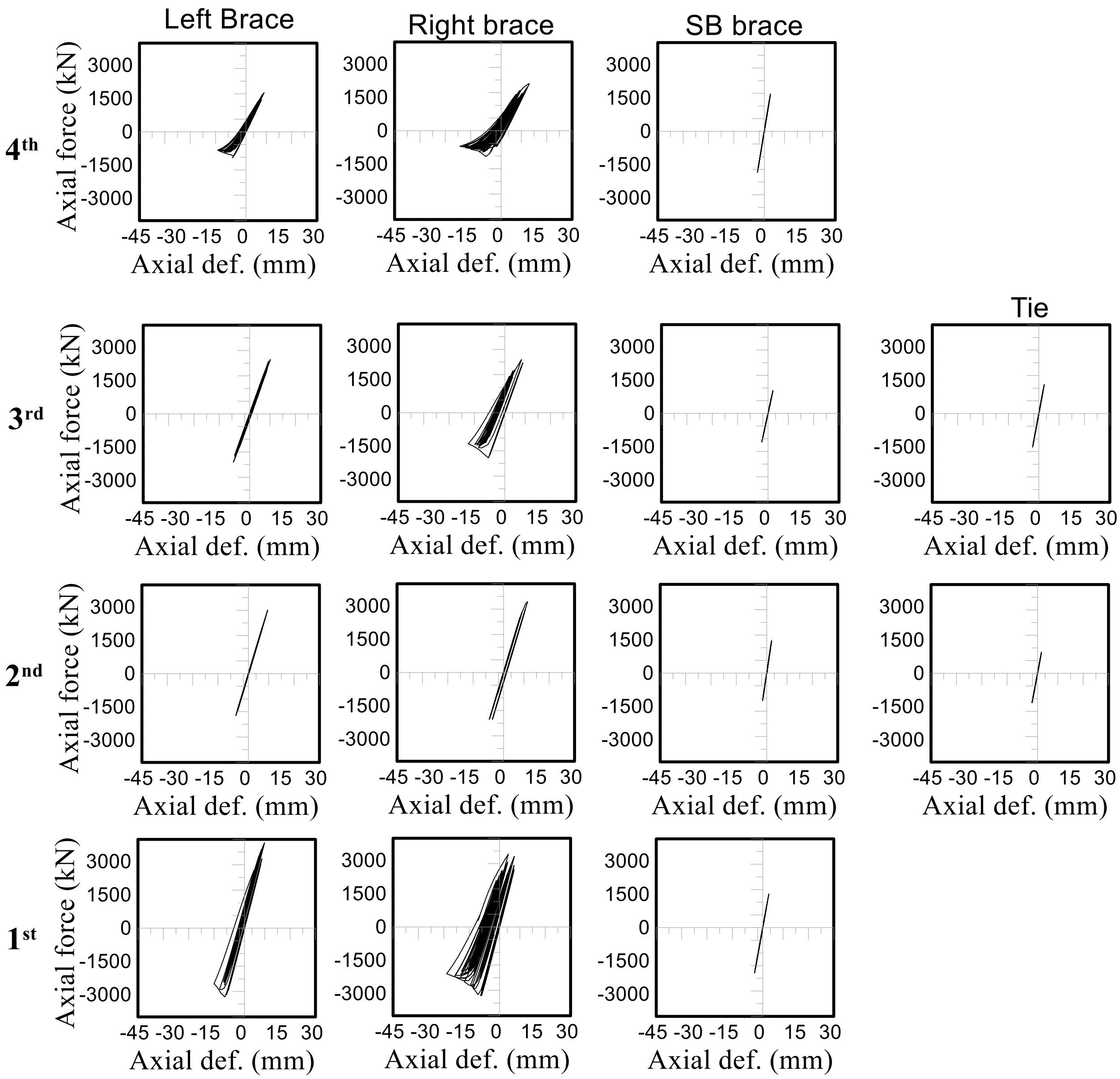

Fig. 4.22. Hysteresis loops of SBF-E braces and SB members under GM #S3 FKS010 scaled at design level

As depicted, the SB truss was able to activate the nonlinear response of almost all ductile braces and to mitigate the formation of storey mechanism. A similar behaviour was observed in the case of SBF-DS illustrated in Fig. 4.23.

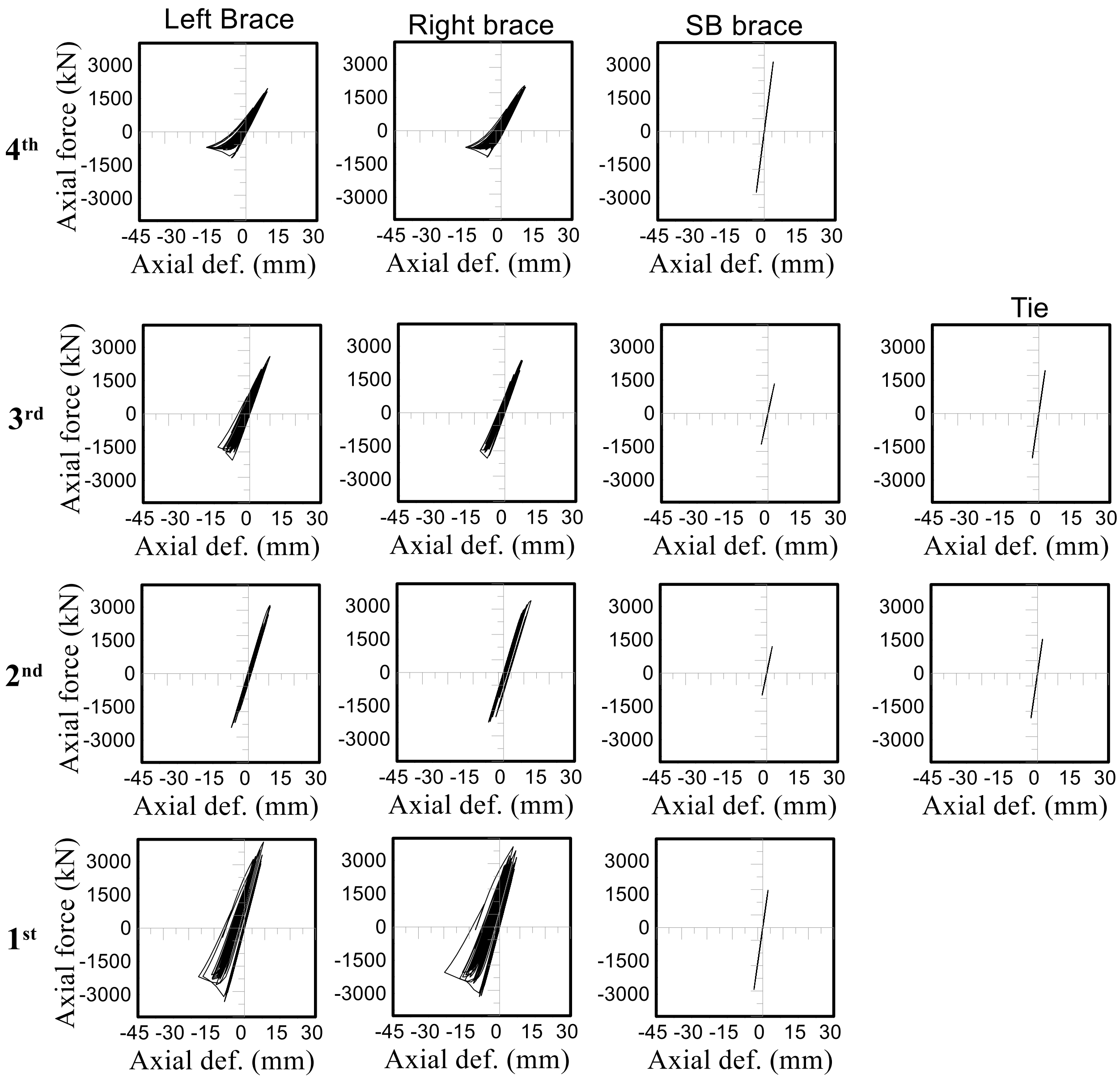

Fig. 4.23. Hysteresis loops of left side SBF-DS braces and SB members under GM #S3 FKS010 scaled at design level

Figs. 4.22 and 4.23 indicate larger inelastic demand in braces located at the top and bottom floor of SBFs. However, some input energy is also dissipated by the 3rd and 2nd floor braces. Under all considered GMs scaled at design level demand, all members of SB truss behave elastically. When compared to the MD-CBF building (see Fig. 3.17), at DL demand, the response of ductile braces of SBFs is noticeably reduced.

4.5 Summary

The design of SB truss members is challenging and the design procedure has evolved during the last decade. The members of SB truss are expected to respond elastically, while sustaining the yielding of ductile members. The Modified Modal Pushover Analysis (MMPA), introduced by Chopra et al. (2004), calculates the seismic demands from higher modes while assuming the structural system elastic. This was done by analyzing the response *of the first mode when is inelastic and the response of higher modes when the system is elastic.* Then, the peak response was computed by employing the SRSS modal combination rule to which the gravity load was added. They have also assumed that the coupling of elastic modes upon the initiation of inelastic behaviour is negligible and the combination of inelastic response using the elastic modes is allowed. To make the MPA or MMPA method attractive for practitioners, Wiebe et al (2015) proposed considering the prescribed lateral forces from building codes to calculate the first mode response and the elastic higher mode response from the MPA but using a truncated elastic response spectrum. It was assumed that the higher modes are uncoupled or weakly coupled. Then, Simpson (2018) noted that the SB behaviour is similar to that of a "beam-like bending behaviour… and the strongback could be modeled as a simply-supported beam of equivalent lateral stiffness." Moreover, it resulted that the SB exhibited significant stiffness and strength in the second and higher modes even after yielding of ductile members, while the 2^{nd} mode is more like bending response.

Herein, two SB configurations were considered: a) adjacent exterior and the system was labelled SBF-E and b) reversed exterior, labelled SBF-DS. It was also observed that the second mode shape of the 4-storey building analysed was like bending-type rather than shear.

The summary of findings resulted from this chapter are:

1. The forces triggered into the exterior SB members can be derived through horizontal equilibrium under the ductile brace member forces which represent the inelastic contribution. The elastic contribution is due to higher modes effect. For an exterior SB truss, the tie members do not support the ductile braces and both top and bottom floor braces and ties form the truss tensile or compressive chord. The column that support the truss is continuous and represents the other truss's chord.
2. In this chapter, to size the SB members, two design methods were presented. One method discussed bellow is more elaborated while the other is based on the bending-type behaviour of second vibration mode and the consideration of analysing the SB s a simple supported beam which is pinned at the base and supported by a roller at the top. This simplified model provides suitable member sizes for preliminary design of SB truss.
3. For the more elaborated design method, the modal analysis by means of response spectrum on the 3D ETABS model is employed. From modal analysis resulted that the first mode and the third and higher modes are in shear, while the second mode is in bending. To compute the higher modes contribution and more specifically that of second and third modes, the elastic response spectrum was truncated between the second and first mode period, as well as between the third and second mode period. The larger axial forces triggered in SB members were associated with the second mode contribution and these forces decrease from top to lower floor; however, at bottom floor, the force associated with the first mode is the largest. The forces in the first mode are limited by the global mechanism, while forces in the higher modes by the ground motion intensity.
4. When the SB truss is very stiff, it responds mainly in the first mode. Hence, stronger truss members withstand large seismic intensity demand, increase floor accelerations and storey

shear forces. Interaction between the SB truss and primary system is the highest at the top floor where the relative stiffness of SB's brace with respect to ductile braces is the largest.

5. The SBF is able to mitigate the storey mechanism and provide uniform distribution of ISD along the building height, while the RISD is very low when comparing to the reparability threshold of 0.5%h_s. However, the floor acceleration and storey shear increase due to the higher mode contribution.
6. The behaviour of SBF-E versus that of SBF-DS is slightly different. The sizes of reversed SB truss members are larger than those of adjacent exterior truss. The back-to-back trusses, labeled herein diamond shape, behave in bending and shear. When comparing the MD-CBF response with that of SBF-DS, in case of SBF-DS, the storey shear shows lower demand at upper floors and larger demand at bottom floor which is explained by the large section used at the bottom brace of diamond shape truss. Meanwhile, when the SBF-DS is employed, both left and right inelastic braces dissipate similar amount of hysteretic energy. Conversely, for the SBF-E building, the most loaded are the inelastic braces adjacent to SB
7. At design level demand (2%/50 years), the strongback behaves elastically under both crustal and subduction ground motion suites. At design level demand, the nonlinear response of SBF in terms of ISD and RISD is not affected by the long duration ground motions. However, under subduction ground motions, larger floor acceleration was observed in comparison with the FA demanded by crustal ground motions.

CHAPTER 5. INCREMENTAL DYNAMICS ANALYSIS

5.1 Incremental dynamic analysis

To identify the failure mode of the 4-storey SBF building, the Incremental Dynamic Analysis (IDA) was employed and the results were compared with those obtained for the 4-storey MD-CBF building. In this analysis only the SBF-E building is investigated.

5.1.1 The IDA response of MD-CBF building

The 4-storey MD-CBF building presented in Chapter 3 is investigated from yielding to failure. Herein, the near-collapse limit state (NC) is defined when the first brace experienced fracture caused by the low-cycle fatigue and the adjacent brace is on the verge of failure. It is noted that after the first brace fails, for a small increase of intensity measure (IM), the building experiences a significant increase in peak interstorey drift. According to Vamvatskos and Cornell's (2002), the near-collapse point is determined by identifying the point on the IDA curve at which the slope is equal to or less than 20% of the elastic slope for a given increase in IM during an individual ground motion. In this study, the spectral acceleration at the 1st mode period S(T1) was selected as the IM and the peak interstorey drift among floors as the Engineering demand parameter (EDP).

5.1.1.1 IDA curves of 4-storey MD-CBF building under crustal ground motions

The IDA curves computed for each one of the seven selected crustal GMs listed in Table 3.20 of Chapter 3 are presented in Fig. 5.1. Each point on the IDA curves was determined for an incremental increase of S(T1) by 0.1g. The horizontal dashed line in Fig. 5.1 represents the design spectral acceleration at the first mode period of building, which is S(T1) = 1.1g, where T1= 0.554 s. It is noted that the design spectral acceleration is associated with 2% in 50 years probability of exceedance (2475 years return period). The solid black circle indicates the yield point of the first brace, while the void circles pinpoint the NC LS, defined for the IM that triggered the first brace failure caused by low-cycle fatigue. The 50th percentile (median) IDA curve is represented by the red solid line. Analysing the median IDA curve in Fig. 5.1, is concluded that at NC LS the building is able to withstand a spectral acceleration demand of $S(T1)_{NC}$ = 2.5g while exhibiting an interstorey drift of 2.35%h_s.

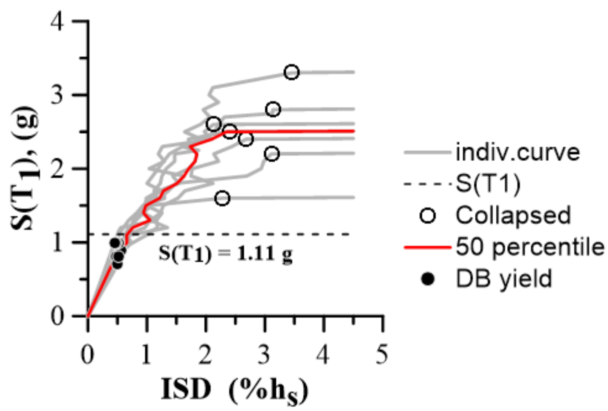

Fig. 5.1. IDA curves of 4-storey MD-CBF building under crustal ground motions

To identify the failure mode, the nonlinear responses of a 4-storey MD-CBF building under crustal ground motions at the near-collapse limit state are carried out. These responses plotted in Fig. 5.2 are expressed by interstorey drift (ISD), residual interstorey drift (RISD), floor acceleration (FA), and shear force. The peak of mean ISD and RISD with values of approximately 2.6%h_s and 0.47%h_s, respectively, occurred at the third floor. Meanwhile, the peak of mean FA of 1.35g occurred at the second floor, while the mean of base shear was almost 4800 kN. It is noted that the failure of 1st brace is associated with an ISD varying between 2%h_s and 3%h_s. Notably, the damage was concentrated at the third floor for almost all GMs, except for GM #C6, where the peak ISD and RISD were observed at the bottom floor, while the first brace failure occurred at the 2nd floor.

Fig. 5.3 presents the hysteresis loops of braces at NC LS associated with $S(T_1)_{N\text{-}C}$ = 2.4g, illustrating the seismic response under the #C6 record. In this case, the upper floor braces experienced low damage, while the two-storey failure mechanism occurred at the bottom floors.

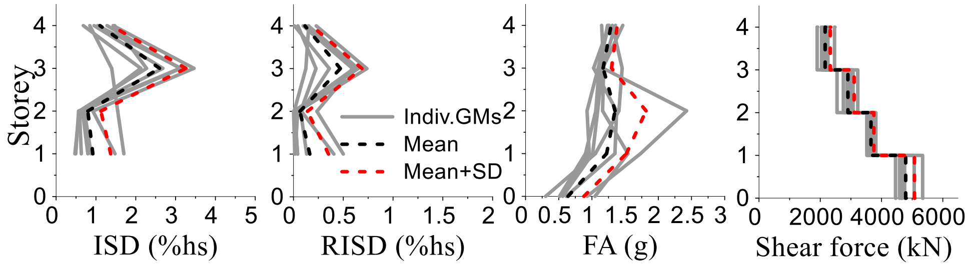

Fig. 5.2. Nonlinear response of 4-storey MD-CBF building subjected to crustal ground motions at near collapsed limit state expressed in terms of: a) ISD, b) RISD, c) FA and d) Shear force.

The 1st brace failure occurred at 2nd floor right brace. It is interesting noting that all right braces behave almost elastically.

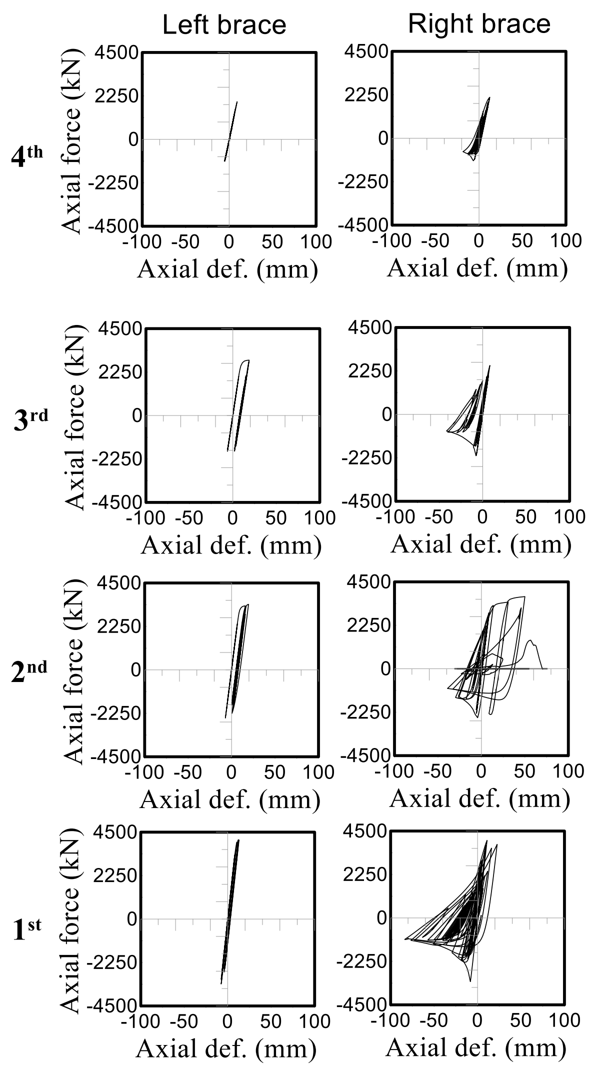

Fig. 5.3. Hysteretic response of HSS braces of 4-storey MD-CBF building at NC LS under #C6 739-250 record scaled at $S(T_1)_{N\text{-}C} = 2.4g$

5.1.1.2 IDA of 4-storey MD-CBF building under subduction ground motions

Figure 5.4 presents the IDA curves computed for the 4-storey MD-CBF building under subduction ground motions listed in Chapter 3. As aforementioned, the design spectral acceleration at the 1st mode period (T1) is S(T1) = 1.1g. On each IDA curve of Fig. 5.4, the first brace yielding is denoted by a black solid circle and the NC LS is marked by a void black circle. The median IDA or 50th percentile IDA is represented by solid red line. From the median IDA results that the collapse point is associated with $S(T_1)_{NC}$ = 1.9g and 2.05%h_s ISD. As resulted, under subduction records, the MD-CBF building reached the NC LS at 76% of $S(T1)_{NC}$ recorded for crustal records.

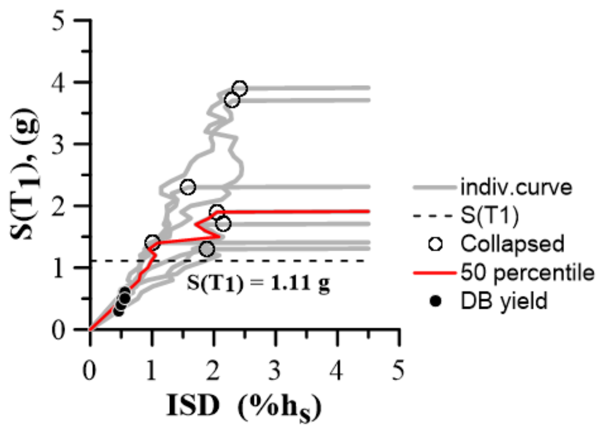

Fig. 5.4. IDA curves of 4-storey MD-CBF building under subduction ground motions

Figure 5.5 presents the nonlinear responses of a 4-storey MD-CBF building under subduction ground motions scaled at the NC LS. These responses are expressed in terms of ISD, RISD, FA, and shear force. From Fig. 5.5 resulted that the peak of mean ISD = 1.72%h_s occurred at top floor, the peak of mean RISD = 0.29%h_s occurred at 3rd floor, the peak FA of around 2.0g occurred at 1st and 2nd floor, while the mean base shear is 4712 kN. Under subduction ground motions, the damage is mostly concentrated at upper two floors. Ground motion #S3 is selected to illustrate the response of MD-CBF building at NC LS; hence, the hysteresis response of ductile braces at NC LS are plotted in Fig. 5.6. As illustrated, the behavior of the ductile braces under #S3 subduction ground motion is different from that observed under the crustal ground motion #C3. Thus, damage is concentrated in both left and right braces of top floors due to the high excitation of higher modes.

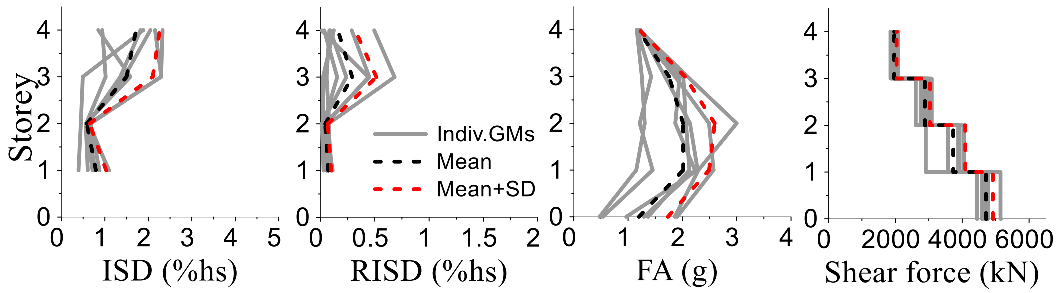

Fig. 5.5. Nonlinear response of 4-storey MD-CBF building subjected to subduction ground motions at NC LS expressed in terms of: a) ISD, b) RISD, c) FA and d) Shear force.

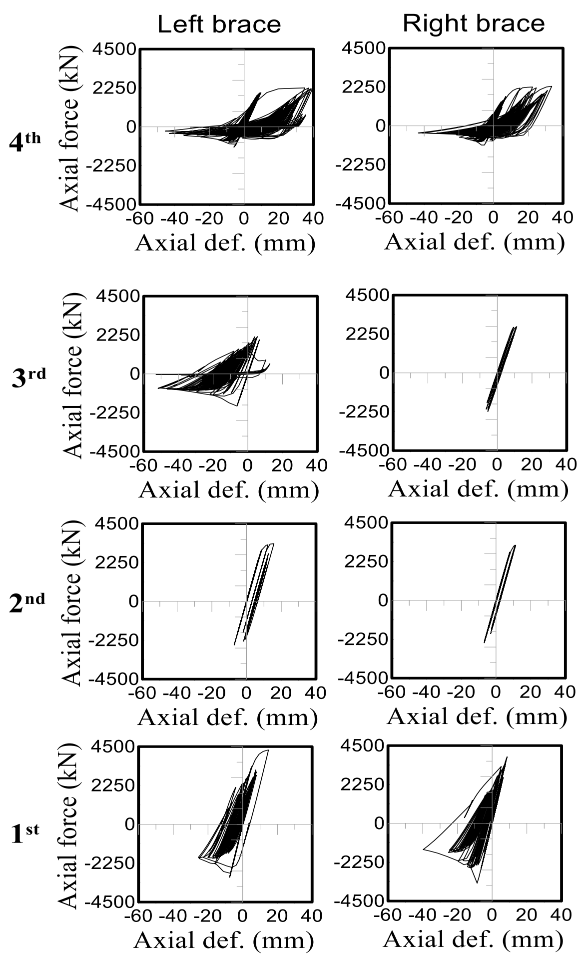

Fig. 5.6. Hysteretic response of HSS braces of 4-storey MD-CBF building at NC LS under #S3 FKS010 record scaled at $S(T_1)_{N-C} = 1.7g$

The left side braces of 3rd and 4th floors exhibited failure caused by low cycle fatigue. As depicted in Fig. 3.11, in the short period range, the spectral ordinates of scaled subduction GMs are 3-5 times larger than the design spectrum.

In comparison with the response of MD-CBF under crustal GMs, the subduction records demand about two times larger FA, while exhibiting lower ISD at the NC LS. Under crustal GMs, all but one IDA curve showed weaving behaviour. However, under subduction GMs, five out of seven IDAs show softening behaviour.

5.1.2 The IDA response of SBF-E building

The IDA curves were computed for the 4-storey SBF-E building under both crustal and subduction ground motion sets. The analysis reveals that the SB is able to behave elastically even after one or two ductile braces experienced fracture due to low-cycle fatigue.

5.1.2.1 IDA of SBF-E building under crustal ground motions

The same 7 crustal GMs are employed to carry out nonlinear dynamic analysis of 4-storey SBF-E building. The IDA curves are plotted in Fig. 5.7. As depicted, the IDAs show waving behaviour. Moreover, the failure of first ductile brace occurred at high demand when comparing to the MD-CBF building. In general, the 1st and 2nd ductile braces fractured subsequently followed by yielding of SB brace or tie. Under 5 out of 7 GMs, the bottom brace of SB yielded before the tie.

The nonlinear responses of a 4-storey SBF-E building under crustal ground motions at NC LS are presented in terms of ISD, RISD, FA, and SF in Fig. 5.8. It is noted that these responses are presented in the same figure although the failure occurred at different intensity demand.

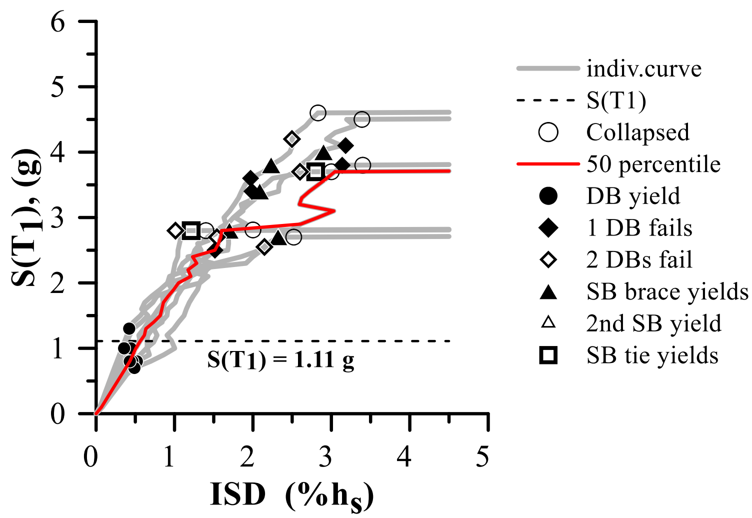

Fig. 5.7. IDA curves of 4-storey SBF-E building under crustal ground motions

The general tendency shows the first mode response, where damage is concentrated at bottom floors. At NC LS, the peak of mean ISD is 2.5%h_s, while that of RISD is below 0.5%, which is within the reparability threshold. Unlike the MD-CBF model, the SBF-E shows damage triggered at the 2nd and 1st floors instead of upper floors. More details are presented in Section 5.2.

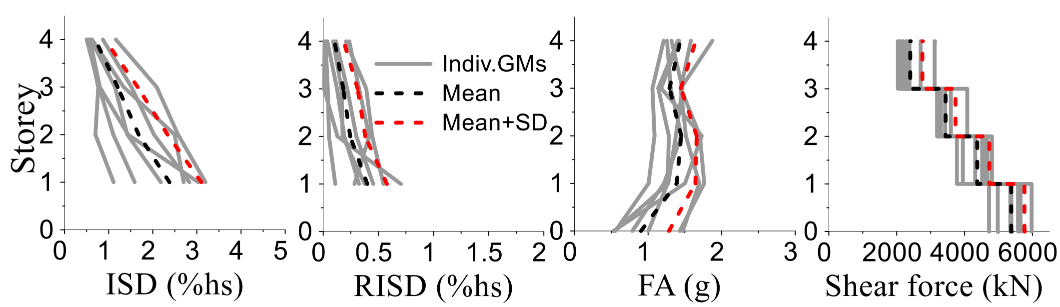

Fig. 5.8. Nonlinear response of 4-storey SBF-E building subjected to crustal ground motions at NC LS expressed in terms of: a) ISD, b) RISD, c) FA, and d) Shear force

5.1.2.2 IDA of SBF-E building under subduction ground motions

The same 7 subduction GMs are employed to perform nonlinear dynamic analysis of 4-storey SBF-E building. The IDA curves of 4-storey SBF-E building resulted under the same subduction GMs are presented in Fig. 5.9. Similar to responses under crustal GMs, the fracture of ductile braces occurred at higher intensity demand when comparing to the intensity value recorded for MD-CBF at NC LS. The nonlinear responses of 4-storey SBF-E building under subduction GMs scaled at NC LS demand are presented in Fig. 5.10, although the failure under each record occurred at different intensities.

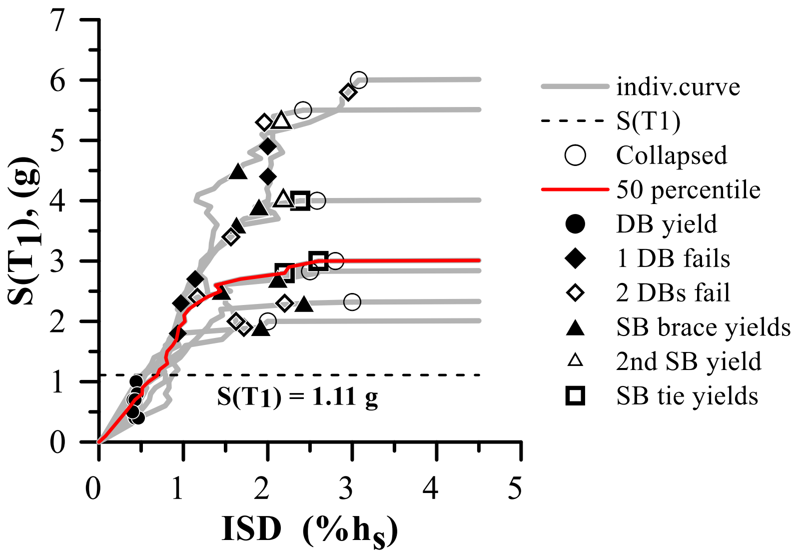

Fig. 5.9. IDA curves of 4-storey SBF-E building under subduction ground motions

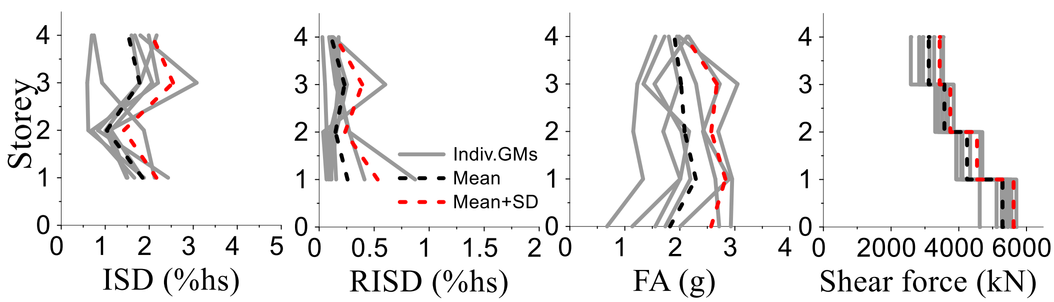

Fig. 5.10. Nonlinear response of 4-storey SBF-E building subjected to subduction ground motions at NS LS expressed in terms of: a) ISD, b) RISD, c) FA and d) Shear force.

Comparing Fig. 5.10 with Fig. 5.8 it results that failure of 4-storey SBF-E building subjected to subduction ground motions occurred at smaller ISD and RISD, but the building experienced large FA. The peak of mean ISD and RISD of SBF-E building occurred at 3rd floor and is about 2.0%h_s and 0.2%h_s, respectively. However, the peak of mean FA is about 2.0 g and occurs at 1st floor.

5.2 Comparison of 4-st. SBF-E behaviour against the 4-st. MD-CBF building

This section presents a comparison from yielding to failure of nonlinear responses of 4-storey SBF-E building against the nonlinear behaviour of 4-storey MD-CBF building.

5.2.1 Comparison of SBF-E vs. MD-CBF buildings under crustal ground motions

Fig. 5.11 shows a comparison of IDA curves computed for the 4-storey SBF-E building against the IDA curves of MD-CBF building subjected to crustal ground motion. The blue dashed line represents the IDA curve for the MD-CBF building, while the black line represents the IDA curves for the SBF-E building. Moreover, the black dash line shows the intensity demand at design level. The yielding of the first ductile brace (DB yield) is marked by solid black circles, while the failure of the 1st and 2nd ductile braces is denoted by black diamond shape and void diamond shape, respectively. The black crosses indicate the occurrence of 0.5%h_s RISD. The black and void triangles represent the yielding of the first and second brace of SB truss, respectively, the void square shows the yielding of SB's tie, while the void circles indicate the collapse point.

As depicted, under #C3, #C4, and #C7 GMs the failure of ductile braces occurred at bottom floors and was followed almost simultaneously by the yielding of ground floor brace of SB. An example of hysteresis loops of ductile braces and SB members under #C3 is illustrated in Fig. 5.12. It is noted that the IDA under #C3 is representative for the median IDA. Under #C2, #C5, and #C6, the failure of ductile right braces of bottom two floors occurs simultaneously with yielding of SB's tie of 2nd floor (#C2) as illustrated in Fig. 5.13. Under #C5 and #C6 records, the fracture of right ductile brace of bottom floor and yielding of SB' brace at the same floor occurred almost simultaneously as per Fig. 5.14. However, under the #C1 GM, the ground floor brace of SB truss yielded before the failure of ductile brace.

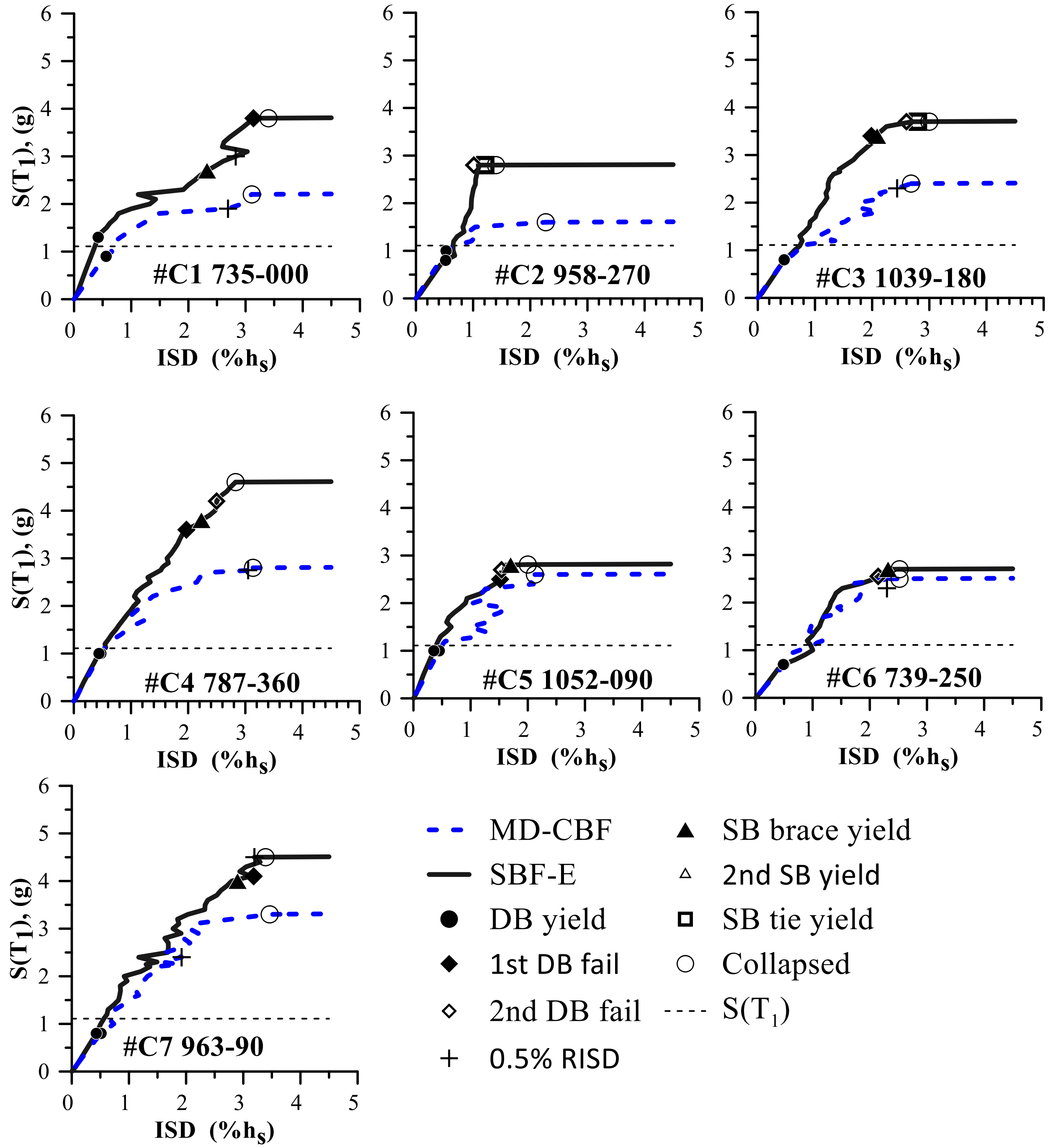

Fig. 5.11. IDA curves of 4-storey SBF-E vs. IDAs of MD-CBF computed under each crustal GM

Table 5.1 presents the intensity demand S(T1) that corresponds to different limit states defined on the IDA curve of 4-storey MD-CBF and SBF-E under crustal GMs.

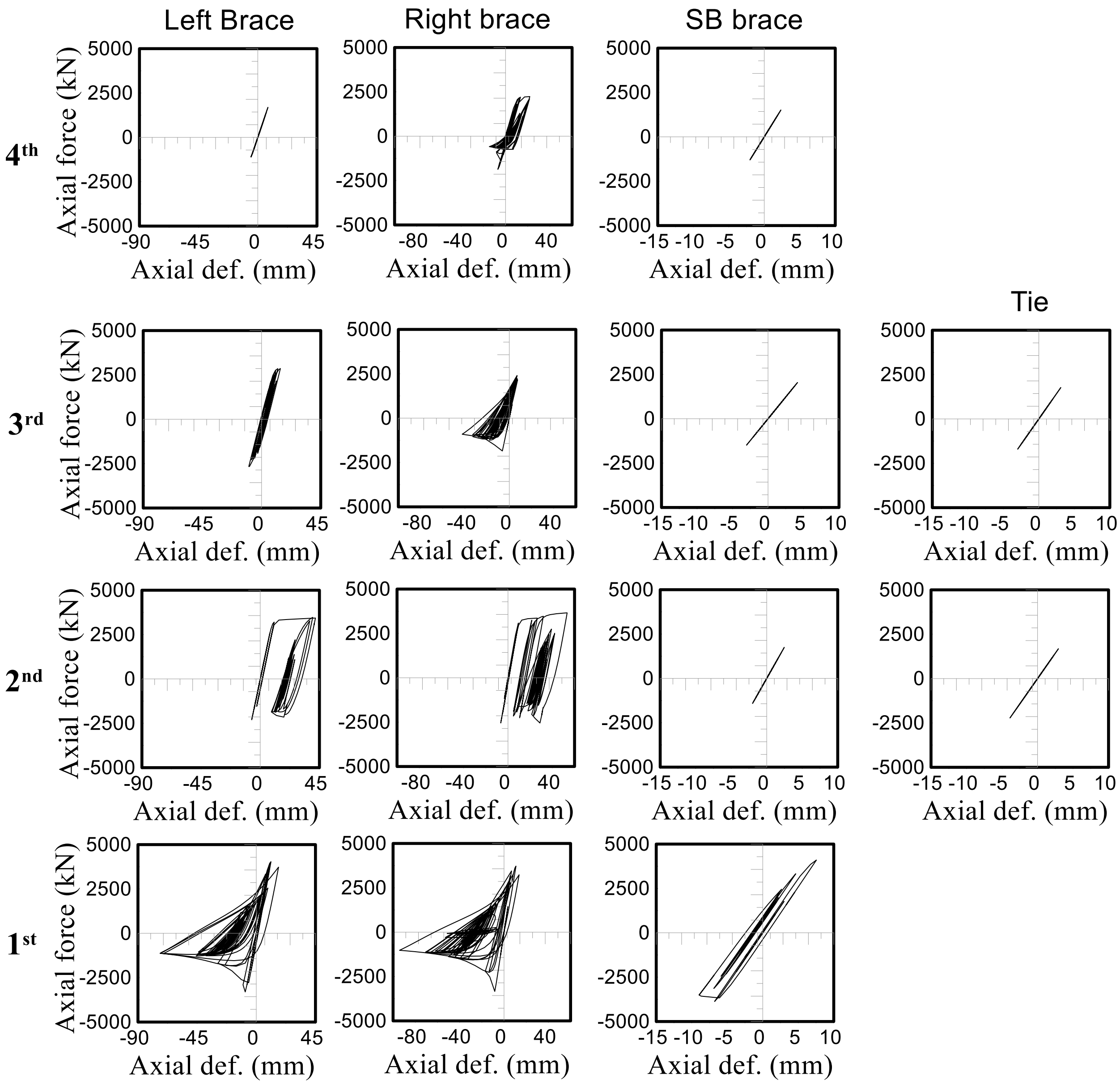

Fig. 5.12. Hysteresis loops of ductile braces and SB members of 4-storey SBF-E building under crustal #C3 scaled at S(T1) =3.4g that was captured before the occurrence of ductile braces fracture at bottom floor where the SB brace has already experienced yielding (SB-Y LS)

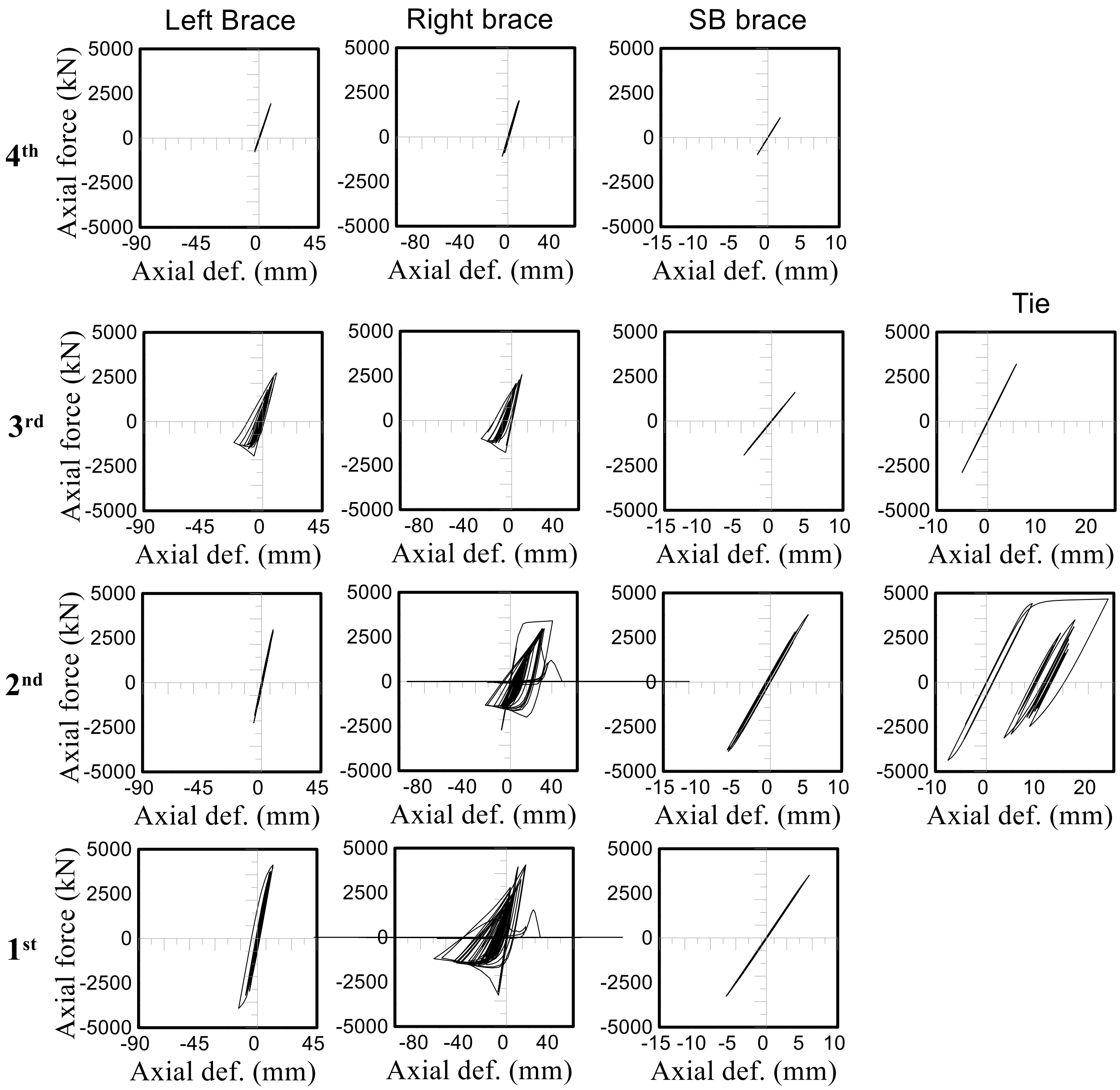

Fig. 5.13. Hysteresis loops of ductile braces and SB members of 4-storey SBF-E building under crustal #C2 scaled at S(T1) =2.8g (NC LS) that induced failure of ductile right brace of bottom two floors and yielding of SB tie

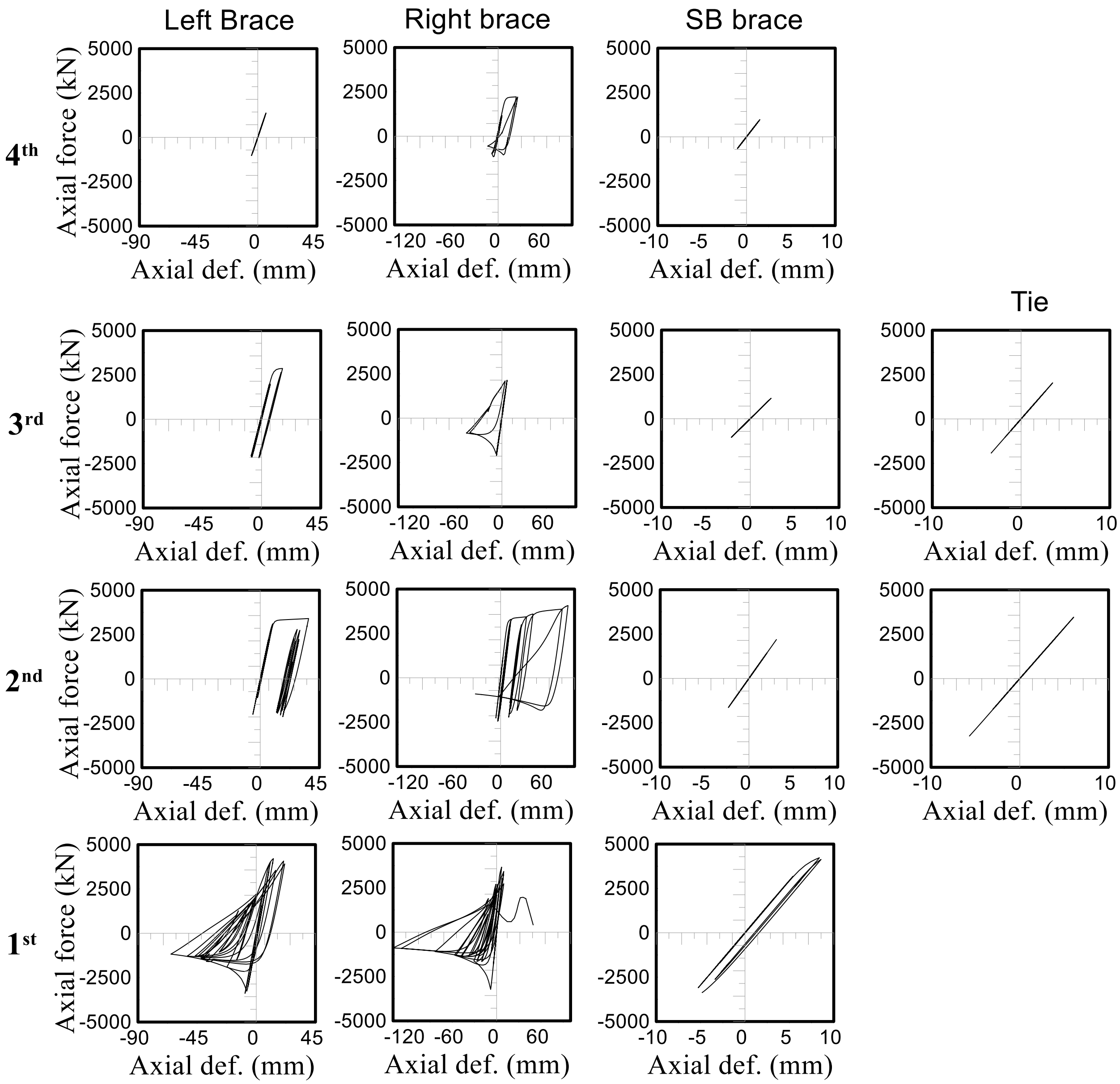

Fig. 5.14. Hysteresis loops of ductile braces and SB members of 4-storey SBF-E building under crustal #C6 scaled at S(T1) =2.7g that induced failure of ductile brace of bottom floor and yielding of SB brace of bottom floor

On each IDA, the following limit states were defined: Design LS, Reparability LS when RISD =0.5%hs, Brace Failure, BF LS, (e.g. failure of first ductile brace), Progress of braces failure, PBF LS, (e.g. failure of 2nd ductile brace), SB member yielding, SB-Y LS (e.g. yielding of 1st brace or tie) and the near collapse limit state (NC LS).

Table 5.1 Intensity demand $S(T_1)$ triggering various limit states mapped on IDA curves of 4-storey SBF-E building *vs.* 4-storey MD-CBF building under crustal GMs

GM	Type	D LS	Reparability LS	BF LS	PBF LS	SB-Y LS	NC LS
#C1	MD-CBF	1.05	1.90	2.20	-	-	2.20
	SBF-E	1.05	3.00	3.80	-	2.70	3.80
#C2	MD-CBF	1.12	-	1.60	-	-	1.60
	SBF-E	1.12	-	2.80	2.80	2.80	2.80
#C3	MD-CBF	1.09	2.30	2.40	-	-	2.40
	SBF-E	1.09	-	3.40	3.70	3.40	3.70
#C4	MD-CBF	1.13	2.75	2.80	-	-	2.80
	SBF-E	1.13	-	3.60	4.20	3.80	4.60
#C5	MD-CBF	1.16	-	2.60	-	-	2.60
	SBF-E	1.16	-	2.60	2.70	2.80	2.80
#C6	MD-CBF	1.16	2.40	2.40	-	-	2.40
	SBF-E	1.16	-	2.55	2.55	2.70	2.70
#C7	MD-CBF	1.12	2.40	3.30	-	-	3.30
	SBF-E	1.12	4.50	4.10	-	4.10	4.50

From Table 5.1 results that the SBF-E building withstands in average fifty percent larger S(T1) intensity at NC LS when comparing to MD-CBF building.

Table 5.2 records the S(T1) demand that triggered the failure of first ductile brace of MD-CBF and SBF-E buildings and the associated peak ISD. Based on the analysis of the 4-storey SBF-E building to crustal GMs, is concluded that the first ductile brace's failure is linked to peak ISD lower than 2%h_s, with two exceptions as GM #C2 and GM #C5.

Table 5.2 Intensity demand ($S(T_1)$) vs. damage (%ISD) associated with failure of 1st ductile brace of considered buildings under crustal GMs

Type	#C1		#C2		#C3		#C4		#C5		#C6		#C7	
	S(T1)	ISD	S(T1)	ISD	S(T1)	ISD	S(T1)	ISD	S(T1)	ISD	S(T1)	ISD	S(T1)	ISD
MD-CBF	2.2	3.1	1.6	2.3	2.4	2.7	2.8	3.1	2.6	2.1	2.4	2.4	3.3	3.5
SBF-E	3.8	3.1	2.8	1.0	3.4	2.0	3.6	2.0	2.6	1.6	2.55	2.1	4.1	3.1

Figure 5.15 presents the distribution of ISD, RISD, FA and shear force along the building height recorded under the intensity demand when the 4-storey MD-CBF experienced brace fracture (see Table 5.2).

The findings demonstrate that at the intensity that triggered the first brace fracture in the MD-CBF building, the SBF-E building shows uniform distribution of ISD with a small tendency of increase at bottom floor. The peak ISD is below 2.0%h_s, while the peak RISD is less than 0.3%h_s. The FA shows also a uniform distribution with a slight tendency of increase at top floor. The storey shear is slightly increase at upper floors and shows a relatively large increase at bottom floor under #C1 and #C5 GMs. To summarize, the ISD and RISD is substantially lower for SBF-E than for MD-CBF, the floor acceleration for both SBF-E and MD-CBF is similar, while the storey shear force in SBF-E is slightly larger than that observed for the MD-CBF.

The hysteresis loops of braces of 4-storey MD-CBF under the #C6 739-250 GM scaled at intensity S(T1) = 2.4g that triggered the NC LS are plotted in Fig. 5.3. As depicted, it was the 2nd storey right brace that exhibited fracture while re-loaded in tension; then, the bottom storey right brace experienced very large shortening in compression being in verge of failure. Thus, damage was concentrated mainly in the right side braces and more specifically at bottom two floors, while the left side braces responded almost elastically.

Figure 5.16 shows that under the same intensity demand (S(T1) = 2.4g) the SBF-E is able to engage both the tension and compression braces (e.g. right and left side braces), while the SB members behave elastically. Thus, the SBF-E mitigates damage concentration and lowers the RISD as shown in Fig. 5.16. At the same intensity demand, the FA is almost the same.

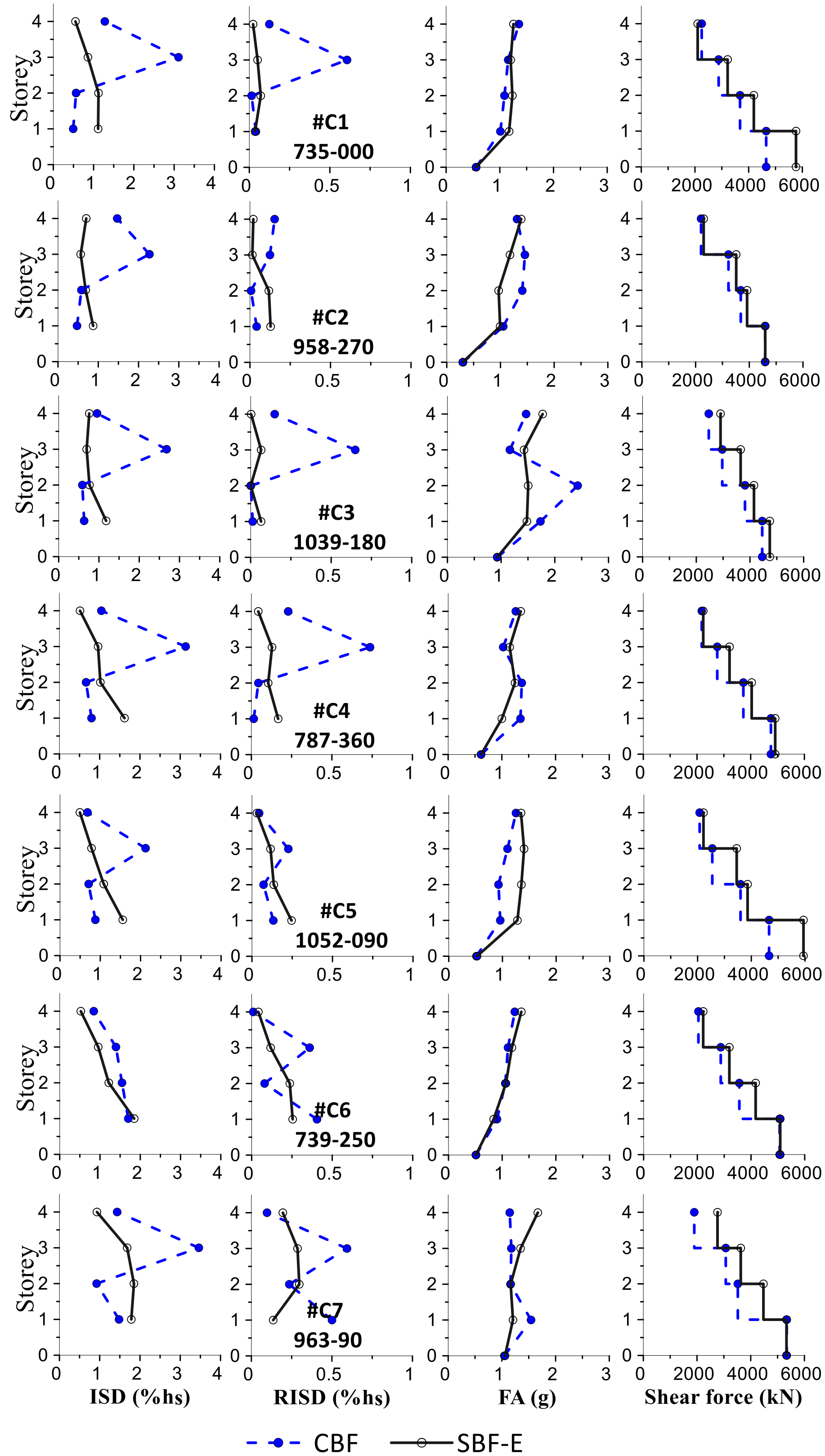

Fig. 5.15. Nonlinear response of 4-st. SBF-E against the 4-s. MD-CBF building subjected to crustal GMs scaled at the intensity at which the 1st brace of 4-st. MD-CBF experienced fracture

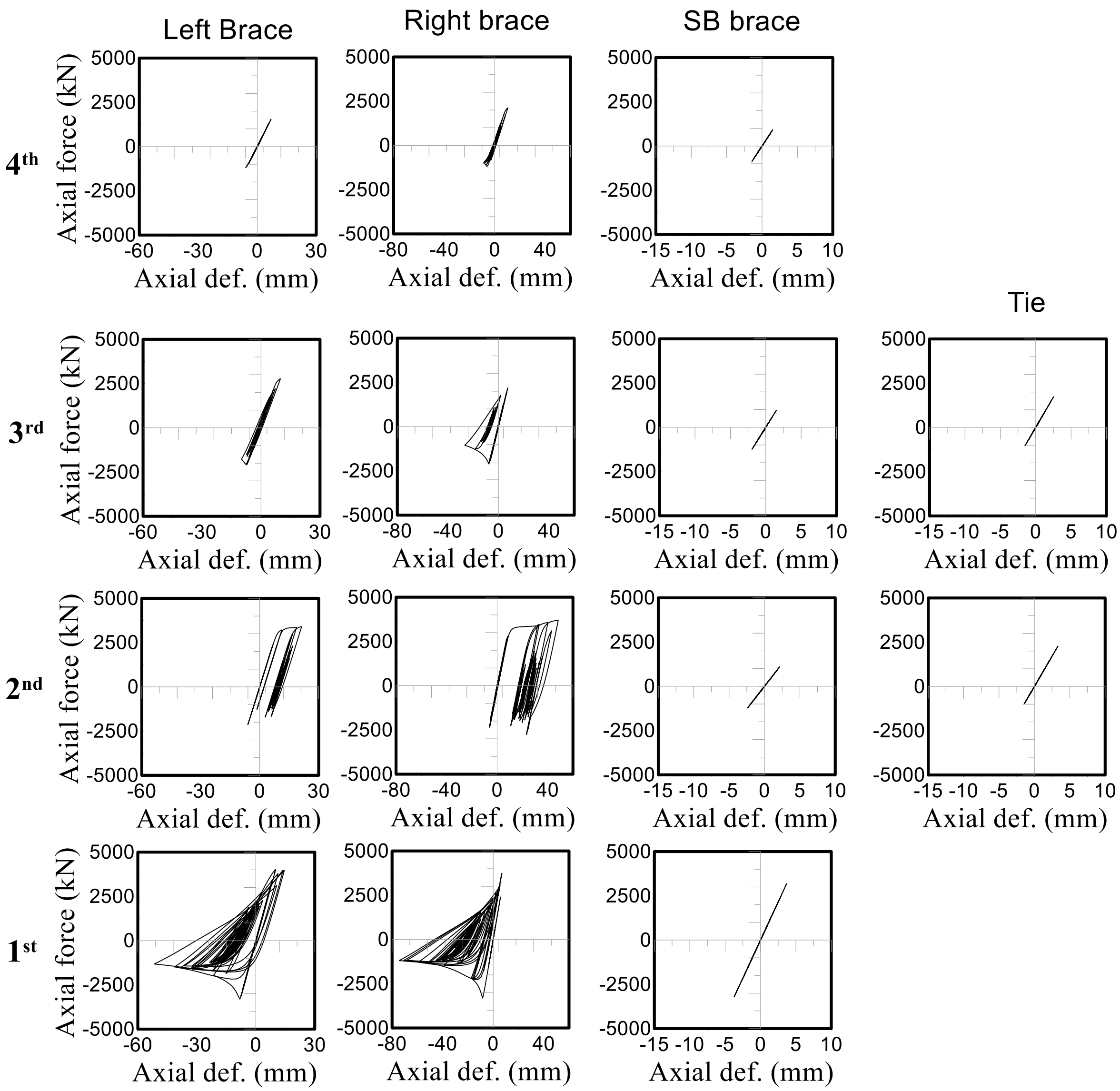

Fig. 5.16. Hysteresis loops of ductile braces and SB members of 4-storey SBF-E building under crustal GM #C6 739-250 scaled at S(T1) =2.4g

Figure 5.17 presents the distribution of ISD, RISD, FA and shear force along the building height recorded under the intensity demand of crustal ground motions that triggered the NC LS in the 4-storey SBF-E building. The S(T1) intensity that triggered the NC LS under each crustal GM is listed in Table 5.2.

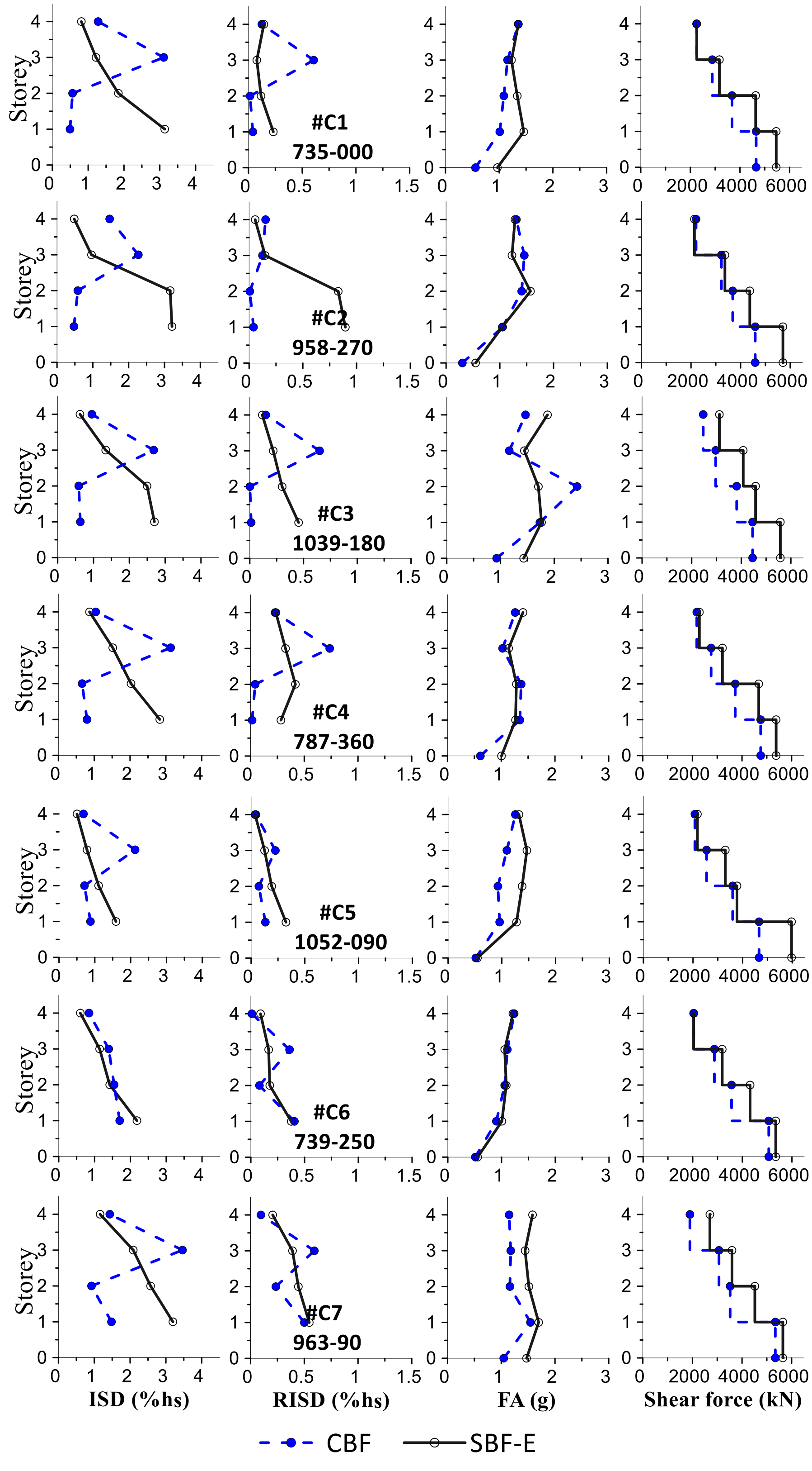

Fig. 5.17. Nonlinear response of 4-storey SBF-E building under each crustal GM scaled at NC limit state vs. the response of 4-storey MD-CBF building at NC LS

To summarize, at NC-LS, the ISD distribution is almost linear and increases from top to bottom. The shape of ISD distribution is influenced by the characteristics of crustal GMs, which mean period varies between 0.41 s for #C2 to 0.67 s for #C4. However, the #C6 record has the larger mean period of 0.9 s. It is worth mentioning that the first mode period of SBF-E building is 0.52 s which is close to the mean period of #C7 GM (t_m = 0.53 s). These ground motions characteristics are presented in Chapter 3. Damage increases downwards with peak ISD about 3% at bottom floor. The RISD is still below 0.5%hs, while the FA shows a uniform distribution with a peak around 1.5 g. The larger base shear occurred under the #C3 and #C5 GMs.

Referring to the response of 4-storey SBF-E building under crustal ground motion #C6 739-250 scaled at the SB-Y limit state, Fig. 5.18 shows that after the fracture of first ductile brace, all members of the SB but one behave elastically. The yielding of SB's bottom brace was initiated and then developed as per Fig. 5.14. When scaled at NC LS the building response under #C2 and #C3 GM shows similar failure mode; hence, the bottom and 2nd floor ductile braces on the SB side exhibited fracture that triggered yielding of the 2nd floor SB's tie, as shown in Fig. 5.13 and Fig. 5.19, respectively.

The type of failure mode exhibited by the 4-storey SBF-E building under crustal GMs is illustrated in Fig.5.20.Thus, the typical failure mode was captured under the #C3 GM shown in Fig. 5.19.

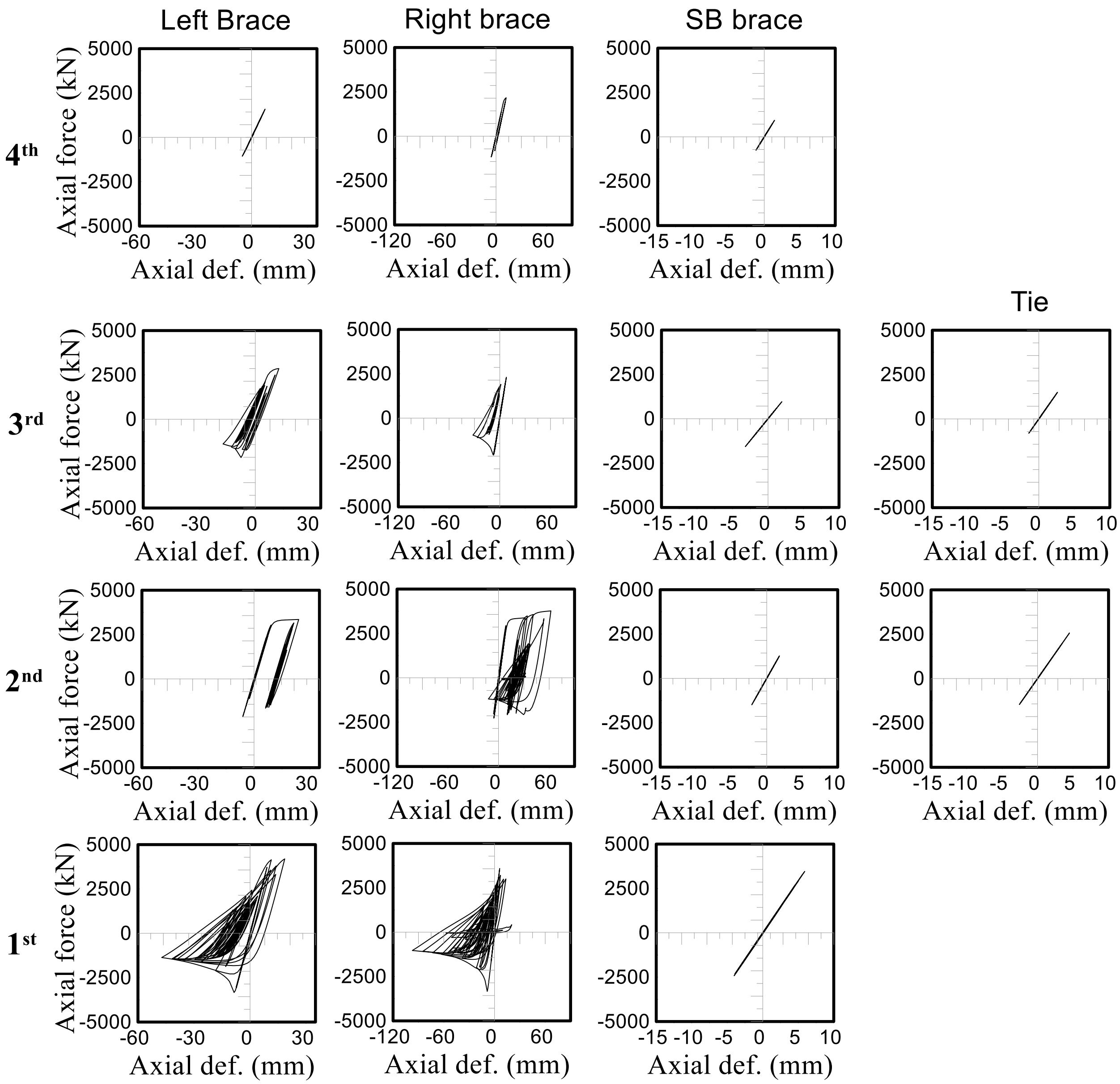

Fig. 5.18. Hysteresis loops of ductile braces and SB members of 4-storey SBF-E building under crustal GM #C6 739-250 scaled at SB-Y limit state (S(T1) = 2.55g), where yielding of bottom brace of SB was initiated

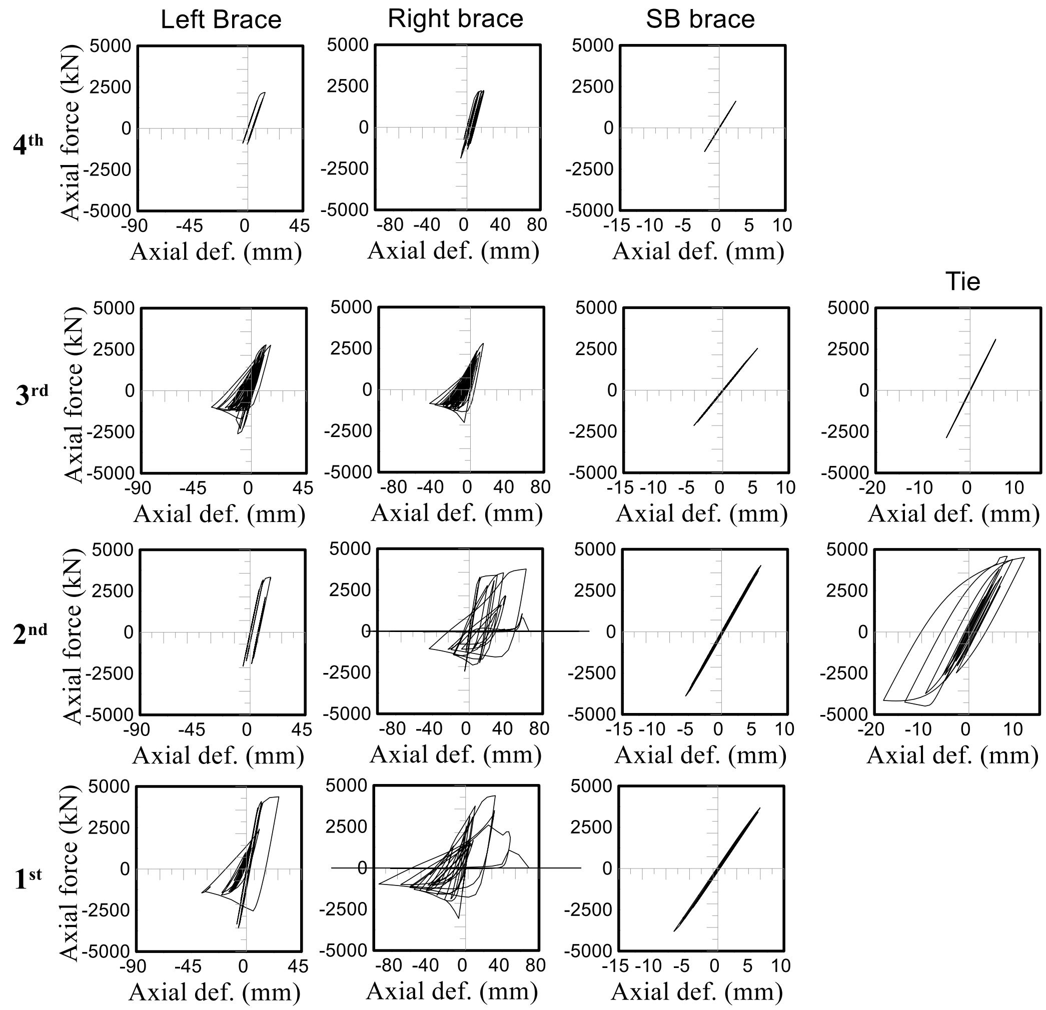

Fig. 5.19. Hysteresis loops of ductile braces and SB members of 4-storey SBF-E building under crustal GM #C3 1039-180 scaled at NC LS limit state (S(T1) = 3.7g), where two bottom ductile braces fail and the tie of 2nd floor exhibited yielding

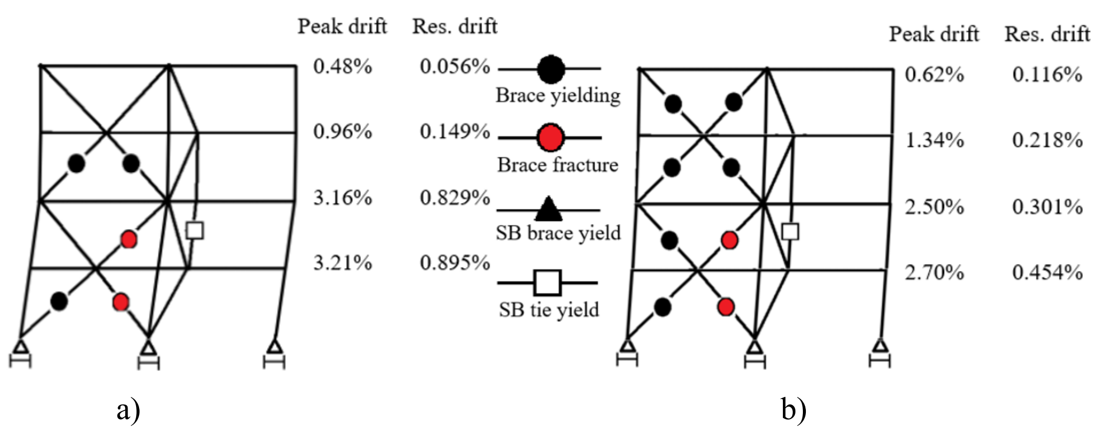

Fig. 5.20. Failure mode of 4-storey SBF-E building under crustal GM a) #C2 958-270 scaled at NC LS limit state (S(T1) =2.8g); and b) #C3 1039-180 scaled at NC LS limit state (S(T1) =3.7g)

5.2.2 Comparison of 4-storey SBF-E vs. MD-CBF building under subduction GMs

This section discusses the comparison of the responses of a 4-storey SBF-E building against the 4-storey MD-CBF building under subduction GMs.

Figure 5.21 shows each IDA curve of SBF-E building vs. that of MD-CBF building under each one of the seven subduction GMs selected. The same symbols shown in Fig. 5.11 are used. All IDA curves of 4-storey SBF-E building, but two exhibit weaving behavior. The two records that imposed softening behaviour are #S1 and #S3. The SBF-E building exhibited the NC LS at higher demand than the MD-CBF building.

Thus, under #S5 and #S7 GMs there are two ductile braces that exhibited fracture while the SB members still behave elastically. Figure 5.22 shows the braces hysteresis under the #S5 GM scaled at S(T1) = 2.0g. Under the #S2 record, the 3rd floor brace of SB yields before the failure of first ductile brace that occurred at 3rd floor (see Fig. 5.23 where the plots are under #S2 scaled at 4.8g which is SB-Y LS). In the case of SBF-E response under #S3, #S4, and #S6 records, the failure of 1st ductile brace occurred at 3rd floor almost simultaneously with yielding of first SB brace located at 3rd floor as well. This behaviour resulted under #S4 GM scaled at S(T1) = 2.5g (SB-Y LS) is depicted in Fig. 5.24.

Table 5.3 presents the intensity demands S(T1) on the IDA curve that defines several limit states as presented above. Hence, the SBF-E building withstand stronger seismic demand than the MD-CBF and more specifically, the SBF-E building withstands 60% more S(T1) intensity at NC LS when comparing to MD-CBF building. Thus, the SBF-E system is more beneficial for buildings in subduction-prone regions. Then, Table 5.4 presents the spectral acceleration S(T1) and the associated ISD recorded when the first ductile brace exhibited fracture.

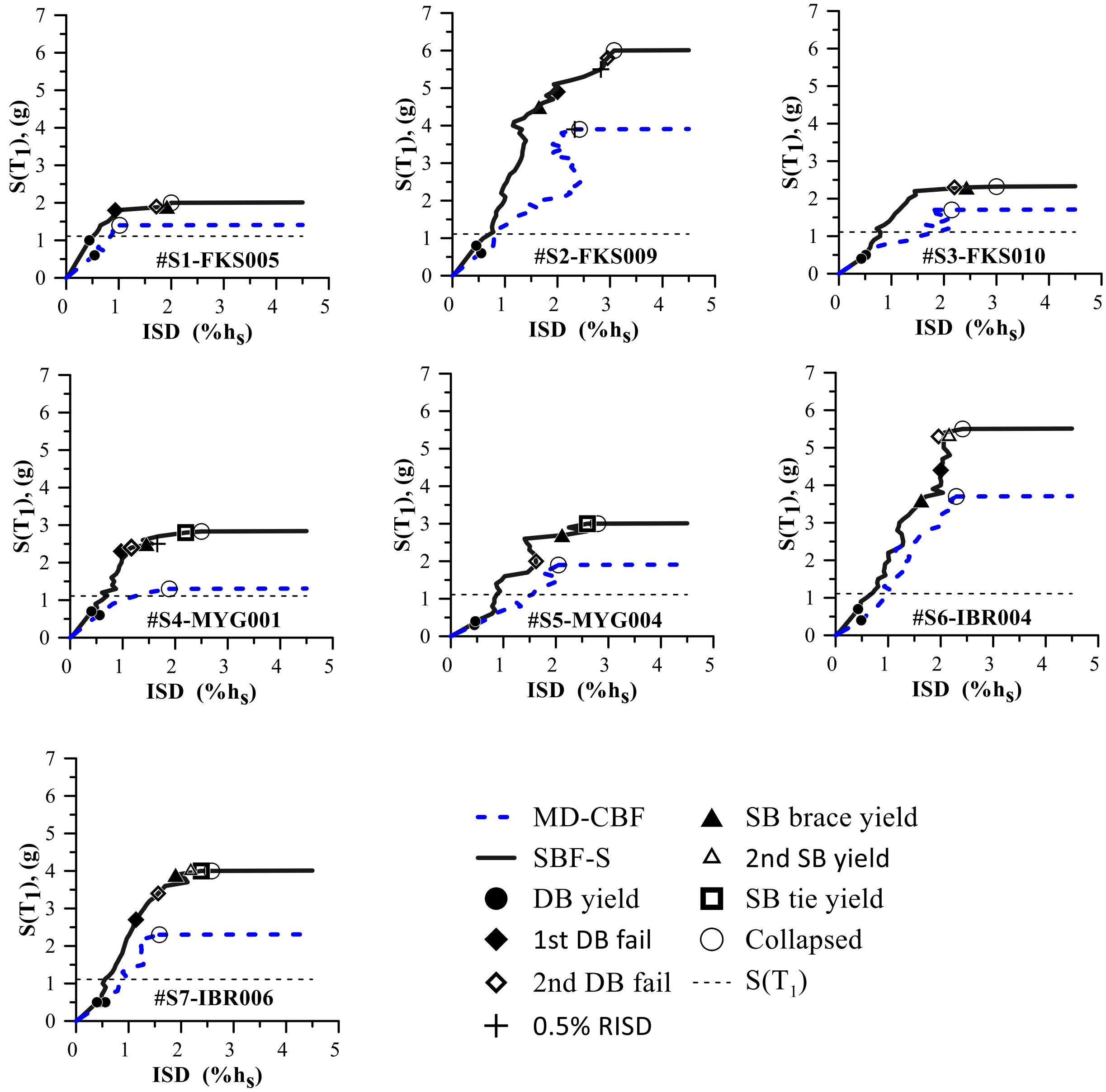

Fig. 5.21. IDA curves of 4-storey SBF-E vs. 4-storey MD-CBF building under each subduction ground motion

Table 5.3 Intensity demand $S(T_1)$ triggering various limit states mapped on IDA curves of 4-storey SBF-E building vs 4-storey MD-CBF building under subduction GMs

GM	Type	D LS	Reparability LS	BF LS	PBS LS	SB-Y LS	NC LS
#S1	MD-CBF	1.12	-	1.40	-	-	1.40
	SBF-E	1.12	-	1.80	1.90	1.90	2.00
#S2	MD-CBF	1.17	3.90	3.90	-	-	3.90
	SBF-E	1.17	5.50	4.90	5.80	4.50	6.00
#S3	MD-CBF	1.11	-	1.70	-	-	1.70
	SBF-E	1.11	-	2.30	2.30	2.30	2.30
#S4	MD-CBF	1.12	-	1.30	-	-	1.30
	SBF-E	1.12	2.50	2.30	2.40	2.50	2.80
#S5	MD-CBF	1.12	-	1.90	-	-	1.90
	SBF-E	1.12	-	2.00	2.00	2.70	3.00
#S6	MD-CBF	1.14	-	3.70	-	-	3.70
	SBF-E	1.14	-	4.40	5.30	3.60	5.50
#S7	MD-CBF	1.13	-	2.30	-	-	2.30
	SBF-E	1.13	-	2.70	3.40	3.90	4.00

Table 5.4 Intensity demand S(T1) vs. damage (%ISD) associated with failure of 1st ductile brace of studied buildings under subduction ground motions

Type	#C1		#C2		#C3		#C4		#C5		#C6		#C7	
	S(T1)	ISD	S(T1)	ISD	S(T1)	ISD	S(T1)	ISD	S(T1)	ISD	S(T1)	ISD	S(T1)	ISD
MD-CBF	1.4	1.0	3.9	2.4	1.7	2.1	1.3	1.9	1.9	2.0	3.7	2.3	2.3	1.6
SBF-S	1.8	0.9	4.9	1.9	2.3	2.2	2.3	1.0	2.0	1.6	4.4	2.0	2.7	1.1

From Table 5.4 results that the peak ISD associated with the failure of the first ductile brace is less than 2.5%h_s for both the 4-storey SBF-E and MD-CBF buildings. In general, the SBF-E building experienced lower peak ISD when comparing to that recorded for the MD-CBF building.

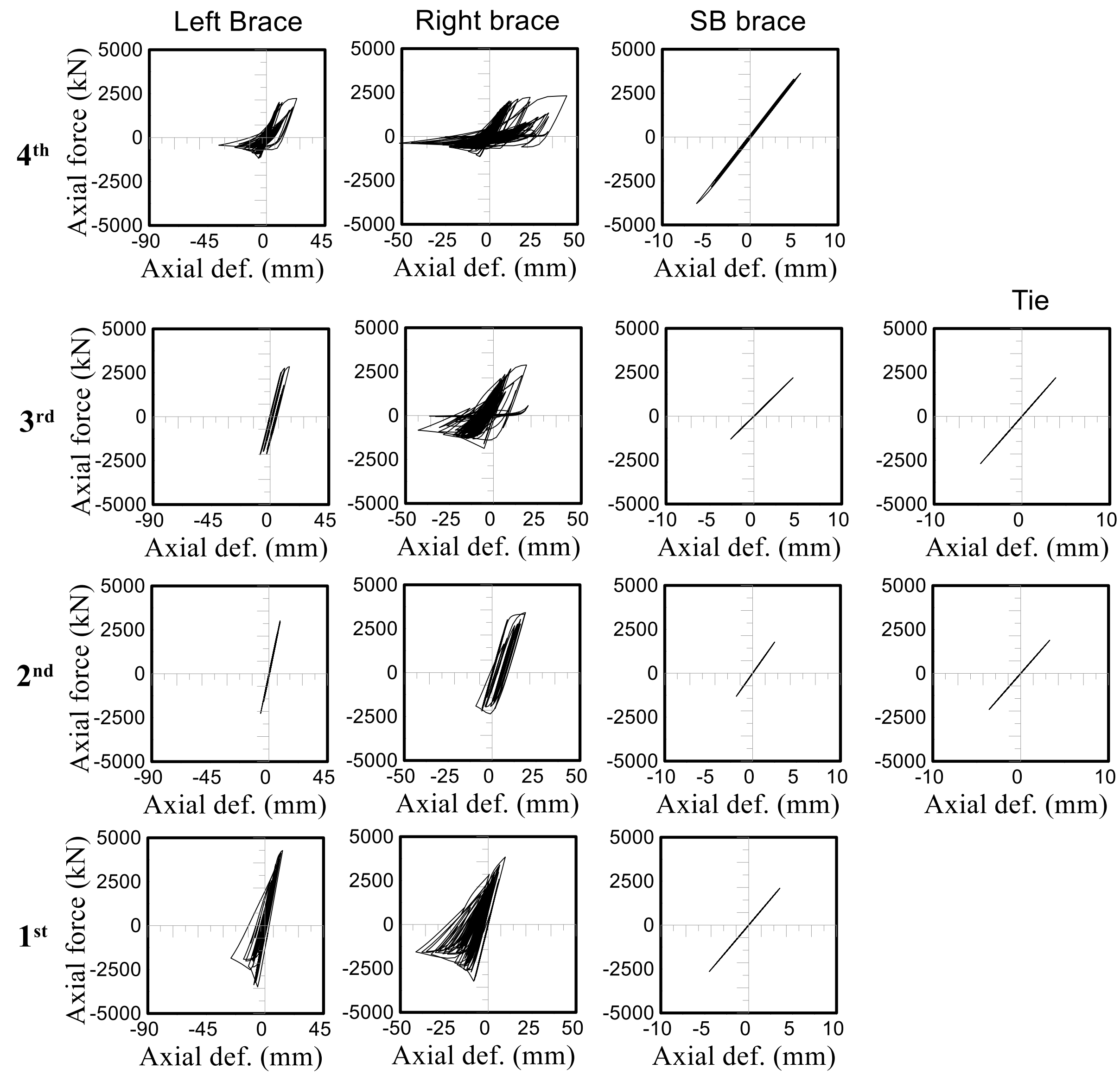

Fig. 5.22. Hysteresis loops of ductile braces and SB members of 4-storey SBF-E building under crustal GM #S5 scaled at S(T1) =2.0g that induced ductile braces failure at 3rd floor and yielding of SB brace at top floor (SB-Y LS)

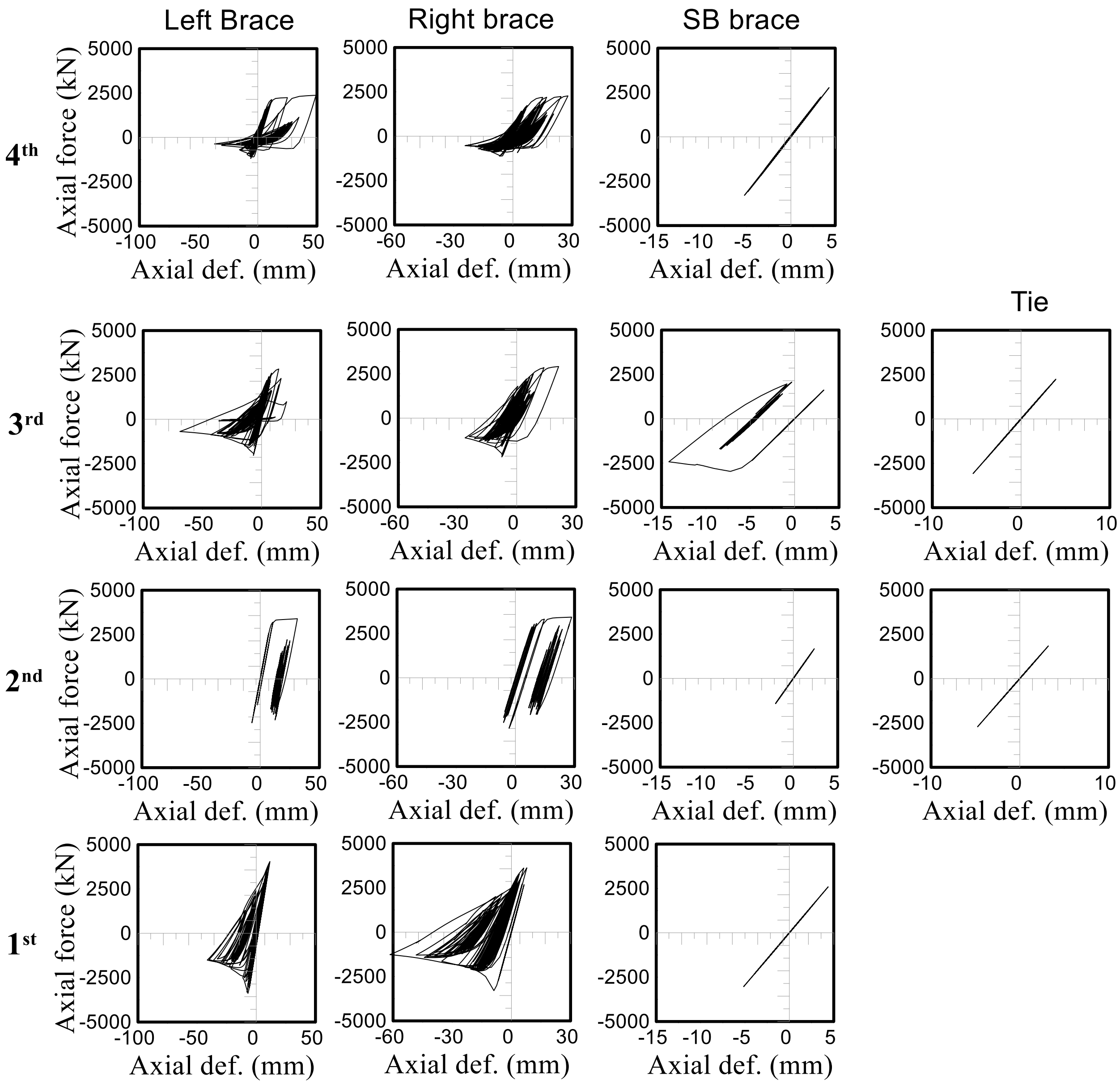

Fig. 5.23. Hysteresis loops of ductile braces and SB members of 4-storey SBF-E building under crustal GM #S2 scaled at S(T1) =4.8g that induced yielding of SB brace before failure of ductile brace (SB-Y LS)

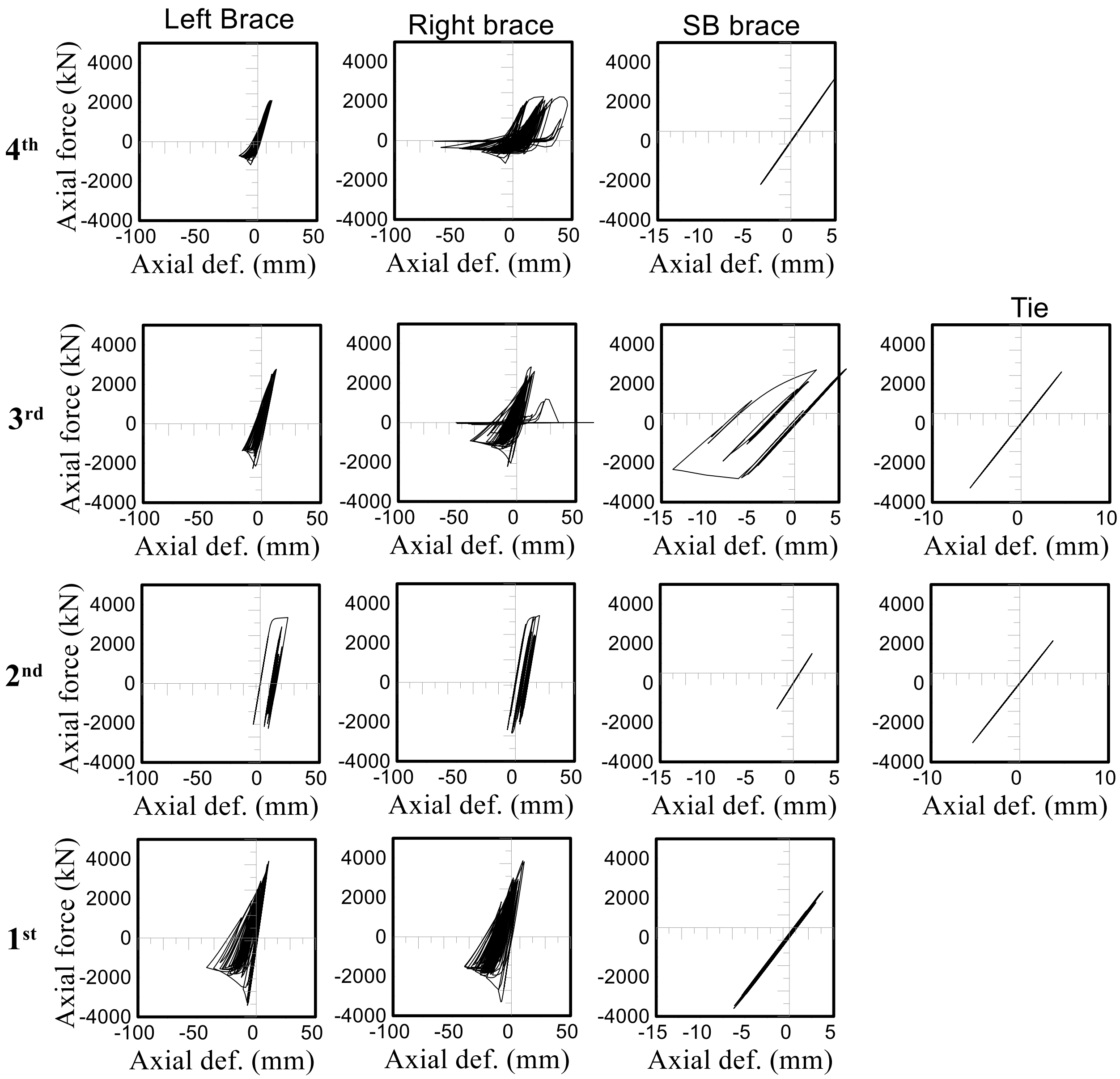

Fig. 5.24. Hysteresis loops of ductile braces and SB members of 4-st. SBF-E building under crustal GM #S4 scaled at S(T1) =2.5g that induced ductile braces failure and yielding of SB brace (SB-Y LS)

Figure 5.25 presents the distribution of ISD, RISD, FA and shear force along the building height recorded under the intensity demand when the 4-storey MD-CBF experienced brace fracture. The S(T1) intensity that triggered brace fracture of MD-CBF under each subduction GM is listed in Table 5.4. From Fig. 5.25 results that the 4-storey SBF-E effectively limit the ISD of each floor within 1.5%h_s and RISD within 0.25%h_s, while FA of about 2.0g is uniformly distributed along the building height. In general, the floor acceleration results for both SBF-E and MD-CBF are similar, while the storey shear force in SBF-E is slightly larger at all floors.

The hysteresis loops of braces of 4-storey MD-CBF building recorded under the subduction ground motion #S3 FKS010 scaled at the NC LS, corresponding to S(T1) = 1.7g, is shown in Fig. 5.6. As depicted, the upper left braces reached high damage while the 3rd floor left brace experienced fracture. For comparison purposes, Fig. 5.26 presents the hysteresis loops of all ductile braces and SB members of 4-storey SBF-E building under the same #S3 FKS010 record, scaled to S(T1) = 1.7g which is the intensity that triggered the failure of the first brace of the 4-storey MD-CBF building. Figure 5.26 shows an uniform distribution of damage along the building height, while almost all ductile braces dissipate the input energy and all SB truss members behave elastically.

The nonlinear responses of studied buildings excited by all seven subduction GMs scaled at NC LS are presented in terms of ISD, RISD, FA, and storey shear in Fig. 5.27. Analysing the ISD distribution is concluded that the upper floors are excited by the higher modes. This is explain by the short mean period of subduction ground motions which is similar to 2nd mode period of SBF-E building. At NC-LS, under some subduction records the peak FA reached 3.0g, while the storey shear increased especially at upper floors when comparing with the MD-CBF building responses.

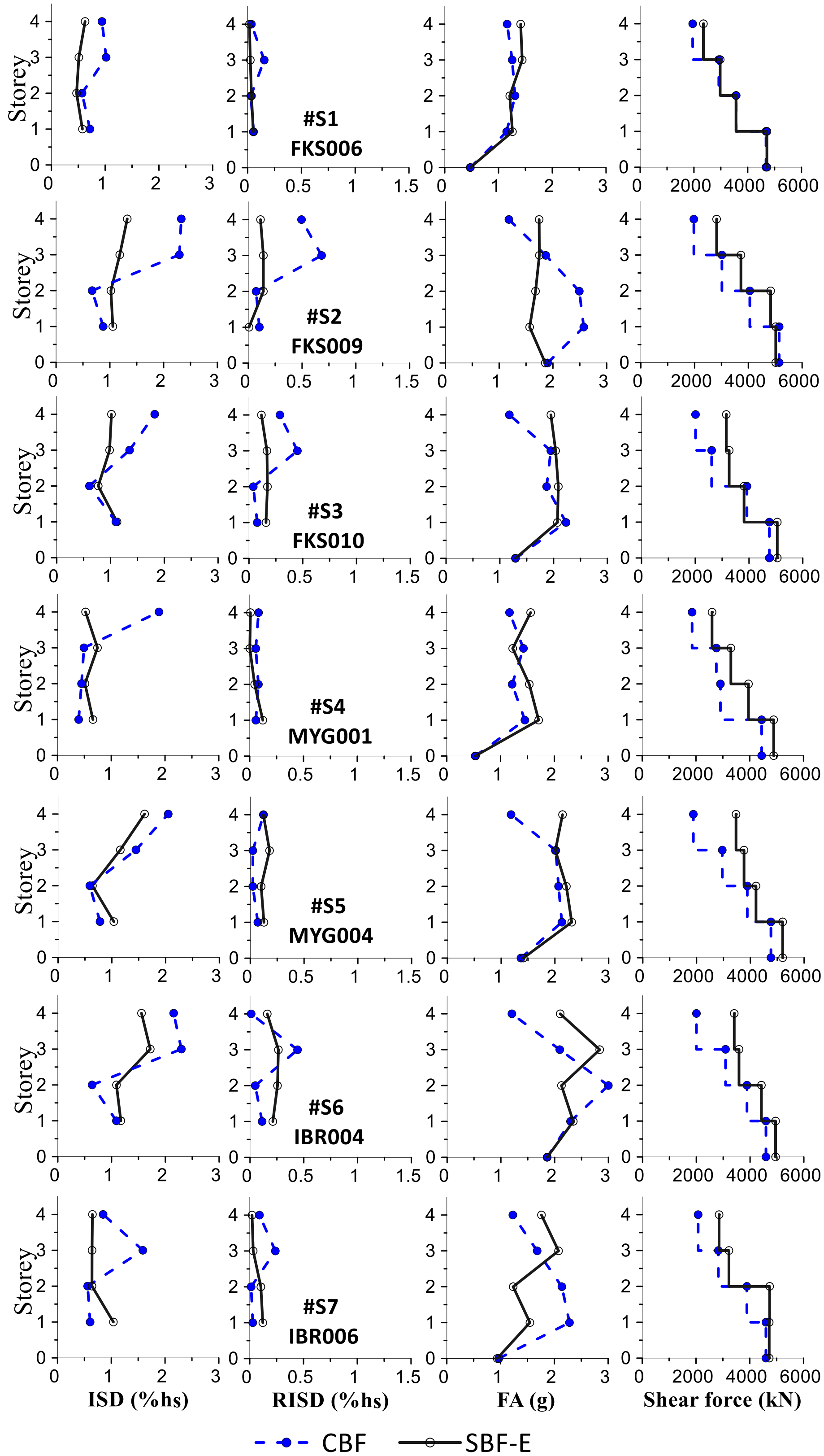

Fig. 5.25. Nonlinear response of 4-storey SBF *vs*. 4-storey MD-CBF building subjected to subduction GMs scaled to the intensity implying fracture of 1st brace of 4-storey MD-CBF

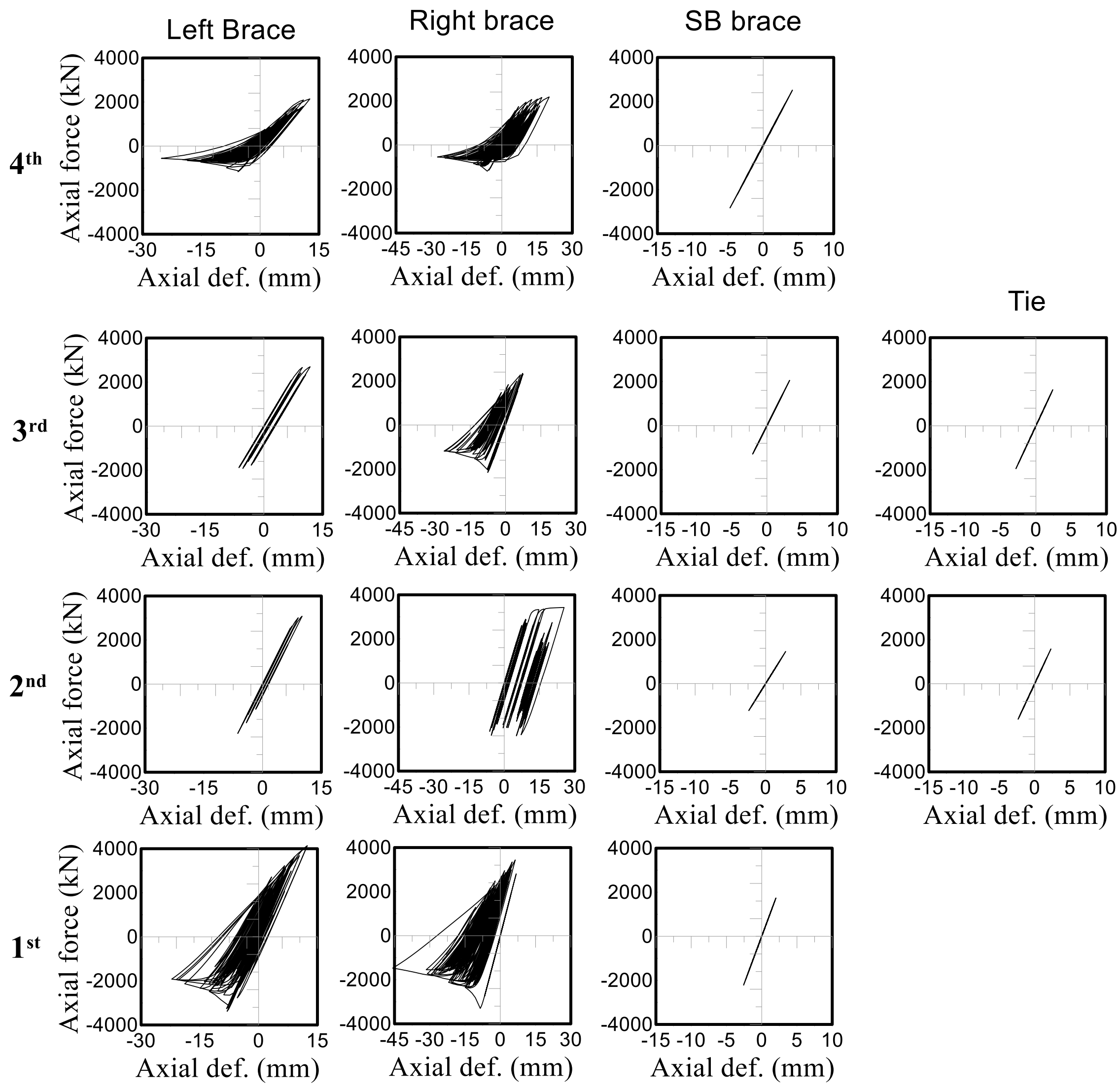

Fig. 5.26. Hysteresis loops of ductile braces and SB members of 4-storey SBF-E building under GM #S3 FKS010 scaled at NC limit state of MD-CBF ($S(T1)_{NC}$ =1.7g)

Figure 5.28 and Fig. 5.29 show the hysteresis loops of ductile braces and members of SB of 4-storey SBF-E building under subduction ground motion #S3 FKS010 and #S5 MYG004 scaled at NC LS, respectively. From Fig. 5.29 resulted that all ductile braces on the SB side reached fracture caused by low-cycle fatigue, while the 3rd floor SB brace and tie exhibited slight yielding. Other typical case of failure mode was observed under the #S3 GM as plotted in Fig. 5.28 that shows that at least three ductile braces reached failure caused by low cycle fatigue, the SB members but one which is the bottom floor brace respond elastically.

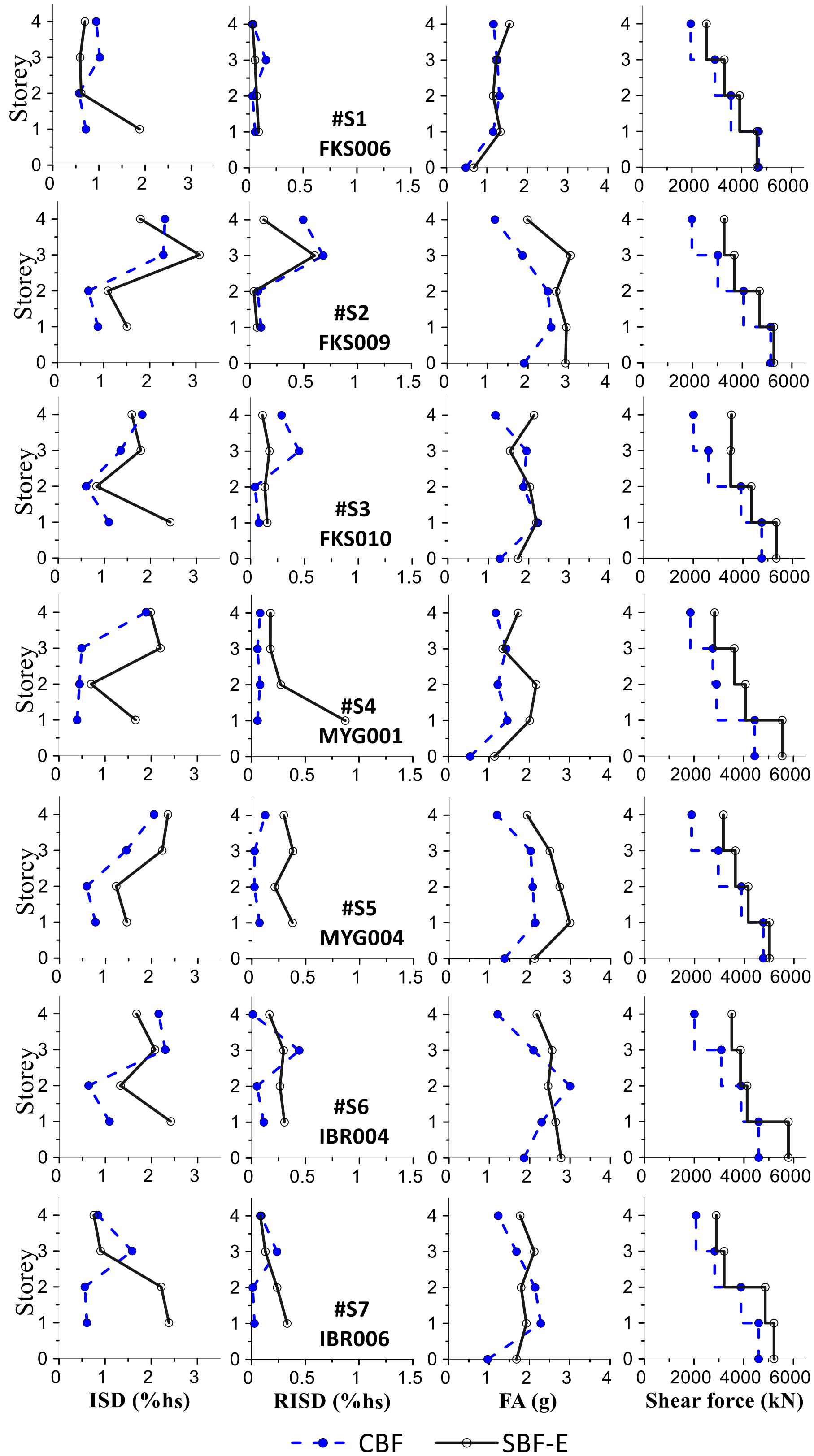

Fig. 5.27. Nonlinear response of 4-storey SBF-E buildings vs. 4-storey MD-CBF subjected to subduction GMs at NC LS

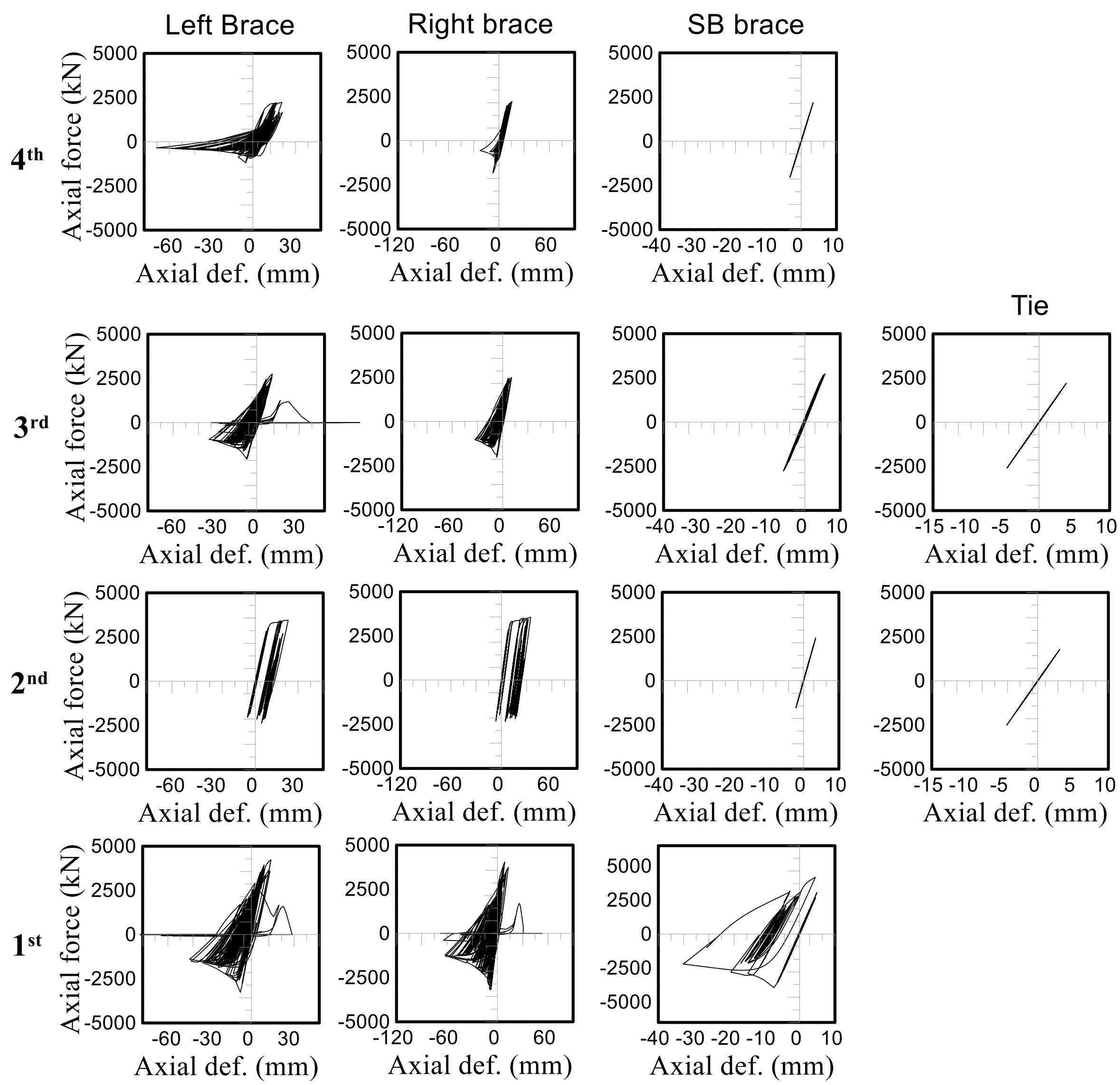

Fig. 5.28. Hysteresis loops of ductile braces and SB members of 4-storey SBF-E building under GM #S3 FKS010 scaled at $S(T1)_{NC}$ =2.3g (NC LS)

The two identified failure modes under subduction GMs are illustrated in Fig.5.30. Thus, (1) either the left or right brace of 3rd floor exhibited fracture followed by yielding or 3rd floor brace of SB and failure of both ductile brace of bottom floor (e.g. #S4, #S6), or both ductile braces of bottom floor exhibited fracture followed by yielding of bottom brace of SB and failure of 3rd floor left or right ductile brace (#S3); and (2) all ductile braces on the side adjacent to SB failed caused by low cycle fatigue and either the 3rd floor or bottom floor brace of SB exhibits yielding (e.g. #S5 & #S7).

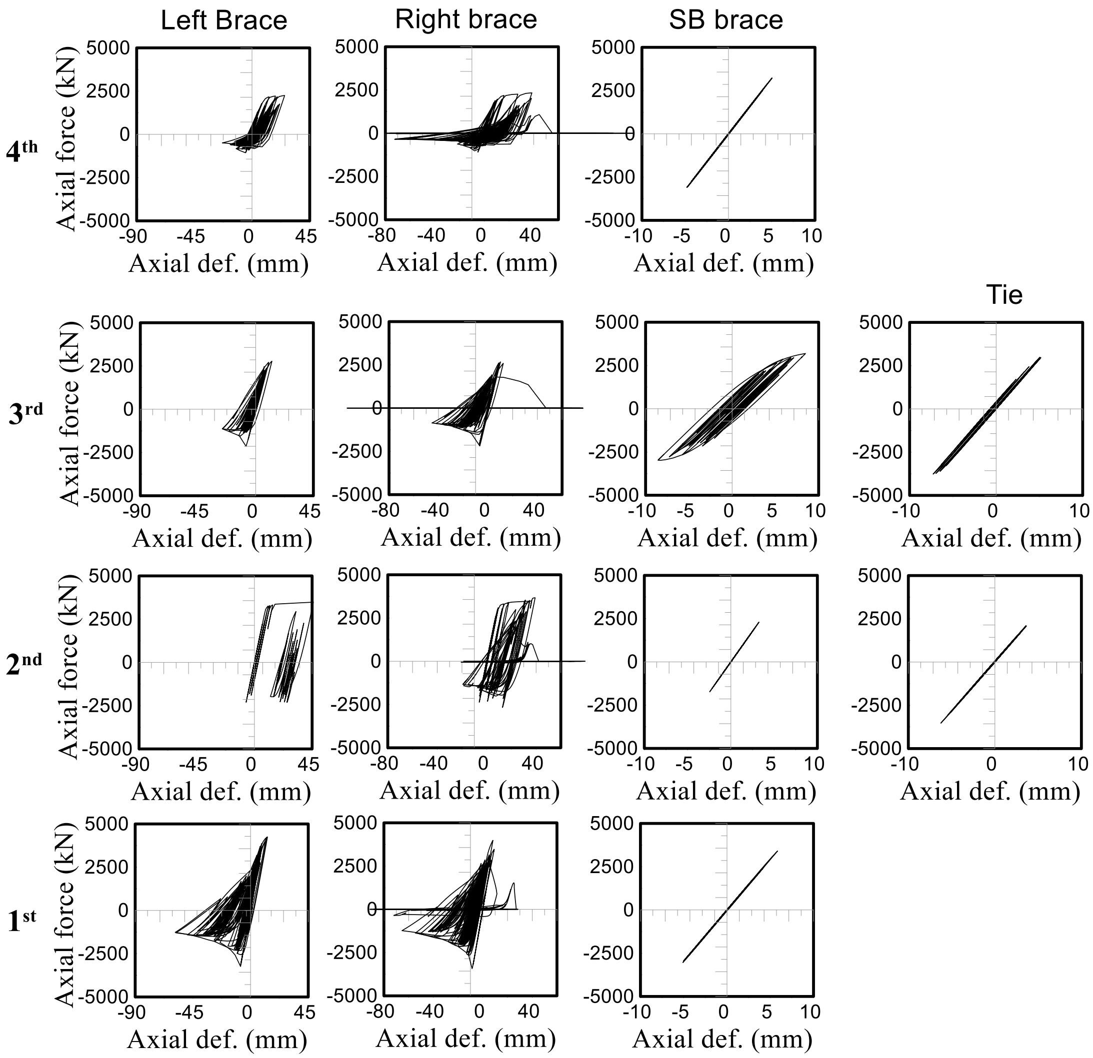

Fig. 5.29. Hysteresis loops of ductile braces and SB members of 4-storey SBF-E building under GM #S5 MYG004 scaled at S(T1) NC =3.0g (NC LS)

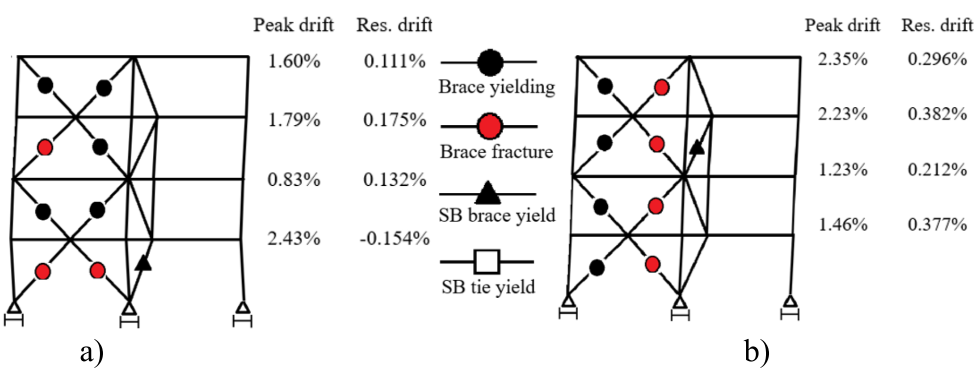

Fig. 5.30. Two types of failure mode of 4-storey SBF-E building under subduction GM a) #S3 FKS010 scaled at NC LS (S(T1) = 2.3g); b) #S5 MYG004 scaled at NC LS (S(T1) = 3.0g)

5.3 Assessment of collapse safety

To verify the collapse safety of studied buildings, the methodology provided in FEMA P-695 (FEMA, 2009) is applied. The collapsed margin ratio, CMR, is defined as the ratio between the median collapse intensity, $\hat{S}_{CT}$, resulted from the median IDA curve resulted under the set of selected GM and the spectral acceleration intensity at the first mode period, S(T1), associated to 2%/ 50 years design level. Table 5.5 provides the $\hat{S}_{CT}$, the S(T1), and the CMR for both 4-storey MD-CBF building and the 4-storey SBF-E building under both sets of crustal and subduction GMs.

Table 5.5. Collapse Margin Ratio, Adjusted Collapse Margin Ratio, and Collapse Safety Criteria

Building	Ground motion	$S(T1)_{DL}$	$\hat{S}_{CT}$	CMR	ACMR	ACMR/ $ACMR_{10\%}$	Pass or Fail
4-st. MD-CBF	Crustal GMs	1.11	2.45	2.23	2.42	1.27	Pass
	Subduction GMs	1.11	1.90	1.73	1.88	0.99	Borderline
4-st. SBF-E	Crustal GMs	1.11	3.60	3.23	3.50	1.84	Pass
	Subduction GMs	1.11	2.95	2.68	2.90	1.53	Pass

According to FEMA (2009), the collapse margin ratio, CMR, should be amplified by the spectral shape factor, SSF, to account for the effects of spectral shape. This is accounted for in order to consider the frequency content or spectral shape of the ground motion record set. The product of SSF and CMR is labelled the adjusted collapse margin ratio, ACMR, and is given in Eq. (5.1).

$$ACMR = SSF\ X\ CMR \tag{5.1}$$

The spectral shape factors, SSF, is a function of the fundamental period, T1, and the period-based ductility, μ_T. The SSF can be obtained from Table 7-1 of FEMA P695. The T1 of 4-storey SBF-E is 0.52s and that of 4-storey MD-CBF is 0.55 s, which leads to SSF = 1.082 and 1.085, respectively. The ACMR value is provided in Table 5.5.

The total system collapse uncertainty, β_{TOT}, is a function of record-to-record (RTR) uncertainty, β_{RTR}, design requirements-related (DR) uncertainty, β_{DR}, test data-related (TD) uncertainty, β_{TD}, and modelling (MDL) uncertainty, β_{MDL}. The expression of β_{TOT} is given by Eq. (5.2).

$$\beta_{TOT} = \sqrt{\beta_{RTR}^2 + \beta_{DR}^2 + \beta_{TD}^2 + \beta_{MDL}^2} \tag{5.2}$$

According to tables provided in Tables of DEMA P695, the following assumptions were considered in other to quantify the uncertainty parameters of Eq. (5.2).

1. The quality rating of design requirements was considered as (A) Superior and the associated uncertainty is $\beta_{DR} = 0.1$;
2. The quality rating of test data from an Experimental Investigation program was assumed as (B) Good and the associated uncertainty is $\beta_{TD} = 0.2$;
3. The quality rating of Index archetype models took the value of (B) Good, with $\beta_{MDL} = 0.2$.

Considering $\beta_{RTR} = 0.4$ and the values provided above it results $\beta_{TOT} = 0.5$.

The collapse margin safety criteria provided in FEMA P695 (2009) was given in Eq. (2.1) and the parameter $ACMR_{10\%} = 1.9$ resulted from Table 7-3 using data from the case studies presented. The ratio $ACMR/ACMR_{10\%}$ is provided in Table 5.5. From Table 5.5 the findings are:

a) Both 4-storey MD-CBF and SBF-E buildings pass the collapse safety criteria when subjected to crustal GMs; hence, the 4-storey SBF-E building provides about 50% larger collapse margin safety than the 4-storey MD-CBF building;
b) Under the subduction ground motions, the 4-storey SBF-E passes the collapse safety criteria, while the 4-storey MD-CBF is borderline. Thus, the MD-CBF system is not recommended in subduction zone prone regions.

5.4 Summary

To assess the effect of ground motion types and higher modes on the nonlinear response of SBF with adjacent exterior strongback (SBF-E), the Incremental Dynamic Analysis (IDA) was employed and the response is expressed in terms of ISD, RISD, FA, and storey shear. Due to the location of case study in the proximity of Cascadia subduction fault, both types of crustal and subduction ground motions were considered. The selected crustal ground motions are records from Northridge and Loma Prieta earthquake events. The shear wave velocity corresponds to Site Class C and the mean period of crustal records is between 0.41 s to 0.67 s which is around the first mode period of 4-storey SBF-E building (T1 = 0.52 s). The mean period of subduction records is between 0.15 s and 0.25 s; hence, these records excite the 2nd vibration mode. Analysing the nonlinear responses of SBF-E versus the MD-CBF building, the main findings are:

1. When the 4-storey SBF-E building was subjected to crustal GMs scaled to NC LS it was found that the ISD distribution follows the first mode response. Although the both left and right braces dissipate the input energy at all floors, the bottom floor ductile braces are the most loaded and reached fracture caused by low-cycle fatigue while the bottom brace of SB starts dissipating the input energy. When comparing the NC LS response of 4-storey MD-CBF building against that of SBF-E building, it was found that the SBF-E undergoes in average fifty percent larger S(T1) intensity. Hence, under all crustal records but one, #C2, scaled at NC LS, the SB members experienced yielding of bottom floor brace. In the case of #C2 excitation, the tie member exhibited yielding. It is noted that the mean period of crustal records is between 0.41 s to 0.67 s which is around the first mode period of 4-storey SBF-E building, T_1=0.52s. To sustain larger seismic demand after two ductile

braces experienced failure, is recommended to increase the size of bottom floor brace of SB.

2. Under all subduction records scaled to NC LS, in average, the ISD distribution follows the second mode response. Both the left and right ductile braces dissipate the input energy at all floors. In general, there are two types of failure mode: (1) either the left or right brace of 3rd floor failed first followed by yielding or 3rd floor brace of SB and failure of both ductile brace of bottom floor (e.g. #S4, #S6), or both ductile braces of bottom floor fracture first followed by yielding of bottom brace of SB and failure of 3rd floor left or right ductile brace (#S3); and (2) all ductile braces on the side adjacent to SB truss failed caused by low cycle fatigue and either the 3rd floor or bottom floor brace of SB exhibited yielding (e.g. #S5 and #S7). These types of failure modes are explained by the short period excitation of subduction records that have the mean period around 0.15-0.25 s; hence, they excite mostly the 2nd mode. When comparing the nonlinear response at NC LS, the 4-storey SBF-E building withstands 60% more S(T1) intensity than the MD-CBF building. This shows that the SBF-E is recommended in subduction zone prone regions.
3. From analyses resulted that both 4-storey MD-CBF and SBF-E buildings pass the collapse safety criteria when subjected to crustal ground motions. However, when these buildings are subjected to subduction ground motions, the 4-storey MD-CBF exhibits borderline response and the system is not recommended in subduction zone prone regions. Moreover, under both ground motion sets, the 4-storey SBF-E building provides about 50% larger collapse margin safety than the 4-storey MD-CBF building.

CHAPTER 6. Conclusions and Future Work

6.1 Summary and Conclusions

To mitigate the concentration of damage under seismic excitations the Strongback Braced Frame (SBF) is proposed. The SBF is composed of a primary ductile system and an elastic vertical truss (strongback) that is able to re-center the system and prevent the occurrence of dynamic instability. Although this system is not new, a comprehensive method used to size the strongback truss (SB) members is lacking. It is worth mentioning that higher-mode forces are not limited by the yield mechanism of ductile system and these forces are amplified by the large inertial effects relative to the first-mode response. Current studies conducted on SBF are for low-rise buildings where the strongback truss is integrated into the half side of ductile braced frame. In consequence, this leads to large ductile brace sizes. Thus, installing the SB exterior to ductile system is beneficial.

In this research work, the SBF is derived from Moderately Ductile Concentrically Braced Frame (MD-CBF) with split-X braces and the same ductility-related (R_d) and overstrength-related (R_0) force reduction factors as indicated in the NBC 2015 for the MD-CBF are used. To extend the knowledge in the field, the SB is placed in two configurations: adjacent exterior (SBF-E), and reversed exterior (SBF-DS).

The main objectives are: i) to simplify the design method for SBF to be used by practitioners, ii) to analyse the effects of ground motions characteristics and higher modes on the nonlinear seismic response of low-rise buildings braced by SBFs with exterior SB and iii) to discuss the seismic performance of SBF against that of traditional MD-CBF.

The design of SB truss members is challenging and the design procedure has recently evolved. In summary, the Modified Modal Pushover Analysis (MMPA) introduced by Chopra et al. (2004), calculates the seismic demands from higher modes while assuming the structural system elastic. This was done by analyzing the response *of the first mode when is inelastic and the response of higher modes when the system is elastic.* Then, the peak response was computed by employing the SRSS modal combination rule to which the gravity load was added. They have also assumed that the coupling of elastic modes upon the initiation of inelastic behaviour is negligible and the combination of inelastic response using the elastic modes is allowed. To make the MPA or MMPA method attractive for practitioners, Wiebe et al (2015) considered the prescribed lateral forces from building codes for calculating the first mode response and the elastic higher mode response using the MPA method and a truncated elastic response spectrum. It was assumed that the higher modes are uncoupled or weakly coupled. Recently, Simpson (2018) noted that the SB behaviour is similar to that of a "beam-like bending behaviour… and the strongback truss could be modeled as a simply-supported beam of equivalent lateral stiffness." Moreover, it was highlighted that the SB exhibited significant stiffness and strength in the second and higher modes even after yielding of ductile members, while the second vibration mode is like bending type.

Considering the above remarks, this research work brings new developments into the design method for SBFs. Herein, the case study is a 4-storey SBF office building located on Site Class C in Victoria, B.C. Two sets of ground motions were considered in analysis: i) short-duration crustal ground motions, and ii) long-duration subduction ground motions characterised by Trifunac duration > 60 s. Detailed numerical models were developed in OpenSees and the nonlinear responses of case study were expressed in terms of interstorey drift (ISD), residual interstorey drift (RISD), floor acceleration (FA) and storey shear. To identify the types of failure mechanism, the incremental dynamic analysis was employed, and the IDA curves were developed considering both sets of crustal and subduction GMs. The collapse margin safety was assessed under both sets of crustal and subduction GMs and compared against the benchmark 4-storey MD-CBF building.

The findings reported below are limited to low-rise building, while the ductile brace members are buckling braces. In addition, for an exterior SB truss, the tie members do not support the ductile braces and both top and bottom floor braces and ties of SB form the tensile or compressive chord. The column that support the truss is continuous and represents the other chord..

1. For designing the SB members, a five-step design method and a simplified design method are presented.

2. Referring to the five-step design method, the forces triggered into the exterior SB members are due to the first mode contribution (yielding of ductile braces), r_{1_pl}, the higher modes contribution, r_{HM}, and the associated gravity load, r_g. The r_{1_pl} can be derived through the horizontal equilibrium under the ductile brace member forces which represent the inelastic contribution. The elastic contribution is due to the higher modes effect. This contribution (r_{HM}) is calculated using modal analysis by means of elastic response spectrum. For computation of 2nd and 3rd mode responses, the elastic response spectrum was truncated between the second and first mode period, as well as between the third and second mode period. The forces resulted from higher modes are combined using the SRSS combination rule. The larger axial forces triggered in SB members were associated with the second mode contribution and these forces decrease from top to lower floor; however, at bottom floor, the force associated with the first mode is the largest. It is noted that the forces in the first mode are limited by the global mechanism, while forces in the higher modes by the ground motion intensity. In the case of adjacent exterior SB, the bending moments

triggered in SB column include the first and higher mode contributions in addition to axial forces.

3. The simplified design method resulted from the observation of 2nd mode shape plotted from modal analysis. It was found that the 2nd mode shape is bending-type and the SB truss can be analysed as a simply supported beam which is pinned at the base and supported by a roller at the top, whereas the length of the truss is the building's height. The truss was loaded with point loads resulted from the horizontal equilibrium under the ductile brace member forces which represent the inelastic contribution. The simplified model provides suitable member sizes for SB's braces and ties.

4. When the SB truss is very stiff, it responds mainly in the first mode. Hence, stronger truss members withstand large seismic intensity demand, increase floor accelerations and storey shear forces. Interaction between the SB truss and primary system is the highest at the top floor where the relative stiffness of SB's brace with respect to ductile braces is the largest.

5. The SBF is able to mitigate the storey mechanism and provide uniform distribution of ISD along the building height, while the RISD is very low when comparing to the reparability threshold of 0.5%h_s. However, the floor acceleration and storey shear increase due to higher mode contribution.

6. The behaviour of SBF-E versus that of SBF-DS is slightly different. The sizes of reversed SB truss members are larger than those of adjacent exterior truss. When comparing the MD-CBF response with that of SBF-DS, in case of SBF-DS, the storey shear shows lower demand at upper floors and larger demand at bottom floor which is explained by the large section used at the bottom brace of diamond shape truss. Meanwhile, when the SBF-DS is

employed, both left and right inelastic braces dissipate similar amount of hysteretic energy. Conversely, for the SBF-E building, the most loaded are the inelastic braces adjacent to SB

7. At design level demand (2%/50 years), the SB members behave elastically under both crustal and subduction ground motion suites. The distribution and magnitude of ISDs and RISDs of SBF are not affected by the long duration ground motions because some ductile braces are still in the elastic range while the others experienced buckling in compression but not yielding in tension. However, under subduction ground motions, larger floor acceleration was observed in comparison with FA demanded by crustal ground motions.

8. When the 4-storey SBF-E was subjected to crustal ground motions scaled to near collapse limit state (NC LS), in general, the bottom and 2nd floor right braces (adjacent to SB) are the most loaded and reached fracture caused by low-cycle fatigue while the bottom brace of SB starts dissipating the input energy. This behaviour is associated with a dominant first mode due to the matching of first mode period of building with that of the mean period of crustal GMs. When comparing the NC LS response of 4-storey MD-CBF building against that of SBF-E building, it was found that the SBF-E withstands in average fifty percent larger S(T1) intensity. Hence, under all crustal records but one, #C2, scaled at NC LS, the SB members experienced yielding of bottom floor brace. In the case of #C2 excitation, the tie member exhibited yielding. If larger seismic demand intensity is expected, is recommended to increase the size of bottom floor brace of SB.

9. Under all subduction records scaled to NC LS, in average, the ISD distribution follows the second mode response. Both the left and right braces dissipate the input energy at all floors. In general, there are two types of failure mode: (1) either the left or right brace of 3rd floor failed first followed by yielding or 3rd floor brace of SB and failure of both ductile brace

of bottom floor, or both ductile braces of bottom floor exhibited fracture followed by yielding of bottom brace of SB and failure of 3rd floor left or right ductile brace; and (2) all ductile braces on the side adjacent to SB truss exhibited fracture caused by low cycle fatigue and either the 3rd floor or bottom floor brace of SB yields. These types of failure modes are explained by the short period excitation of subduction records that have the mean period around 0.15-0.25 s. When comparing the nonlinear response at NC LS, the 4-storey SBF-E building withstands 60% larger S(T1) intensity than the MD-CBF building. This shows that the SBF-E is recommended in subduction zone prone regions.

10. From analyses resulted that both 4-storey MD-CBF and SBF-E buildings pass the collapse safety criteria when subjected to crustal ground motions. However, when these buildings are subjected to subduction ground motions, the 4-storey MD-CBF exhibits borderline performance and the system is not recommended in subduction zone prone regions. Moreover, under both ground motion sets, the 4-storey SBF-E building provides about 50% larger collapse margin safety than the 4-storey MD-CBF building.

6.2 Future Work

From this research work resulted that further investigations are needed and future research is required. The recommendations are listed below.

- Analyse the SBF buildings with reversed SB truss which does not form a symmetrical pivoting truss.

- Conduct comparative analysis when various types of ductile braces are considered for the primary system. The employment of buckling restrained braces and/or friction-sliding braces bring the advantage of large base shear coefficients R_dR_0.
- Assess the height limit for SBF buildings.
- To overpass the drawback of higher modes contribution encountered in high-rise building, the modular SBF system shall be developed, as well as a design method.
- The evaluation of economic loss expressed in terms of repair cost and repair time, as well as, the resilience of SBF building under natural events shall be investigated in further studies.

REFERENCES

Aguero, A., Izvernari, C., and Tremblay, R. (2006). "Modelling of the Seismic Response of Concentrically Braced Steel Frames Using the OpenSees Analysis Environment". International Journal of Advanced Steel Construction, Vol. 2-3, pp. 242-274.

Bertero, V. (1977) "Strength and Deformation Capacities of Buildings under Extreme Environments." Structural Engineering and Structural Mechanics, 53, 29-79.

Bosco, M., Rossi, P.P. (2009). "Seismic performance of eccentrically steel braced frames", Eng. Struct. 31, 664–679.

Bosco, M., Marino, E.M. and Rossi, P.P. (2012). "Behavior Factor of Dual Concentrically Braced Systems Designed by Eurocode 8". The 15th World Conference on Earthquake Eng., 2012, Lisbon.

Canadian Standards Association (CSA). (2019). "Design of Steel Structures". S16.1-14 Standard, CSA, Mississauga, ON

Chen, L., Tremblay, R., and Tirca, L. (2019a). "Practical seismic design procedure for steel braced frames with segmental elastic spines". J. of construct. steel research 153, 395-415.

Chen, L., Tremblay, R., & Tirca, L. (2019b). "Modular tied eccentrically braced frames for improved seismic response of tall buildings". J. of construct. steel research, 155, 370–384.

Chen, L. (2022). "Design and Assessment of Steel Buildings with Strongback Braced Frames and Exterior Strongback System." MASc thesis, Concordia University, Montreal.

FEMA (2009). "Quantification of Building Seismic Performance Factors". Report No. FEMA-P695, SAC Joint Venture, Federal Emergency Management Agency, Washington, DC.

Froozanfar, M., Moradi, S., Kianoush, R., Speicher, M. S., & di Sarno, L. (2024). “Review of self-centering rocking systems for earthquake-resistant building structures: State of the art.” In Journal of Building Engineering (Vol. 84). Elsevier Ltd.

Giugliano, M.T., Longo, A., Montuori, R., and Piluso,V. (2010). “Failure Mode and Drift Control of MRF-CBF Dual Systems”. The Open Construct. and Building Technology J., 2010, 4, 121-133.

Hsiao, P-C, Lehman, D.E., and Roeder, C.W. (2012). “Improved analytical model for special concentrically braced frames.” Journal of Constructional Steel Research, Vol. 73, pp. 80-94.

Hsiao, P.C., Lehman, D., and Roeder, C. (2013). “A Model to Simulate Special Concentrically Braced Frames Beyond Brace Fracture”, Journal of Earthquake Engineering and Structural Dynamics, Vol. 42, pp. 182-200.

Hajjar, J. F., Hurriyet Sesen, A., Jampole, E., Wetherbee, A., & Hurriyet, A. (2013). “A synopsis of sustainable structural systems with rocking, self-centering, and articulated energy-dissipating fuses”. Department of Civil and Environmental Engineering Reports.

Ji, X., Kato, M., Wang, T., Hitaka, T., & Nakashima, M. (2009). “Effect of gravity columns on mitigation of drift concentration for braced frames”. J. Constr. Steel Res., 65(12), 2148-2156.

Khatib, I.F., Mahin, S.A. and Pister, K.S., (1988) “Seismic Behavior of Concentrically Braced Frames”, UCB/EERC-88/01 Report, Earthquake Engineering Research Center, University of California, Berkeley, CA.

Kiggins, S. and Uang, C.M., (2006) “Reducing residual drift of buckling-restrained braced frames as a dual system”, Engineering Structures, Vol.28, pp.1525-1532

Lamarche, C., and Tremblay, R., (2008). “Accounting for Residual Stresses in the Seismic Stability of Nonlinear Beam-Column Elements with Cross-Section Fiber Discretization”.

Lignos, D. and Karamanci, E. (2013), “Predictive Equations for Modelling Cyclic Buckling and Fracture of Steel Braces”, 10th International Conference on Urban Earthquake Engineering, March 1-2, 2013, Tokyo Institute of Technology, Tokyo, Japan.

Lai, J., & Mahin, S. (2015). “Strong-back System: A Way to Reduce Damage Concentration in Steel Braced Frames”. J. Struc. Eng., 141(9): 04014223.

Longo, A., Montuori R., Piluso,V. (2014). “Theory of plastic mechanism control for MRF–CBF dual systems and its validation”. Bull Earthquake Eng (2014) 12:2745–2775.

Longo, A., Montuori R., Piluso,V. (2016). “Moment frames – concentrically braced frames dual systems: analysis of different design criteria”, Structure and Infrastructure Eng., 12:1, 122-141.

Menegotto, M., and Pinto, P.E. (1973). “Method of analysis of cyclically loaded RC plane frames including changes in geometry and non-elastic behavior of elements under normal force and bending”. Preliminary Report IABSE, vol 13.

Martini, K., N. Amin, P.L. Lee, and D. Bonowitz. (1990). "The Potential Role of Non-Linear Analysis in the Seismic Design of Steel Structures." Proceedings of th e4th U.S. National Conference on Earthquake Engineering. EERI. 67–76.

McKenna, F., and Fenves, G. L. (2004). “Open system for earthquake engineering simulation (OpenSees)”.⟨http://www.opensees.berkeley.edu/index.html⟩(Mar. 5, 2015).

MacRae, G.A., Kimura, Y., Roeder, C., (2004) “Effect of Column Stiffness on Braced Frame Seismic Behavior”, Journal of Structural Engineering, Vol. 130, No. 3, pp.381-391.

Merzouq, S., Tremblay, R. (2006). “Seismic Design of Dual Concentrically Braced Steel Frames for Stable Seismic Performance for Multi-Story Buildings”. Proceedings of the 8th U.S. National Conference on Earthquake Engineering. San Francisco, CA.

McCormick J, Aburano H, Ikenaga M, Nakashima M. (2008). “Permissible residual deformation levels for building structures considering both safety and human elements.” 14thWCEE, Beijing, China, Paper ID 05 06-0071.

Millichamp, D. (2021). “Collapse Safety Assessment of Steel Multi-storey Buildings with Friction Sliding Braced Frames and Backup Moment Resisting Frames as a Dual System”, MASc thesis, Concordia University, Montreal, Canada.

Popov, E.P., and Black, R.G. (1981). “Steel struts under severe cyclic loadings”. ASCE Journal of the Structural Engineering Division, 107: 1857 – 1881.

Popov, E. P., J. M. Ricles, and K. Kasai. (1992). "Methodology for Optimum EBF Link Design." Earthquake Engineering, Tenth World Conference. EERI. 3983-3988.

Pollino, M., Slovenec, D., Qu, B., & Mosqueda, G. (2017). “Seismic Rehabilitation of Concentrically Braced Frames Using Stiff Rocking Cores.” J. of Structural Engineering, 143(9).

Palermo, M., Laghi, V., Gasparini, G., & Trombetti, T. (2018). Coupled Response of Frame Structures Connected to a Strongback. Journal of Structural Engineering, 144(9).

Rossi, P.P. (2007) “A design procedure for tied braced frames”, Earthq. Eng. Struct. Dyn. 36, 2227–2248.

Razavi, M. and Sheidaii, M.R. (2012), “Seismic performance of cable zipper-braced frames”, Journal of Constructional Steel Research, Vol. 74, pp. 49-57.

Rutenberg, A. (2013). “Seismic shear forces on RC walls: review and bibliography”. Bulletin of Earthquake Engineering, 11(5), 1727-1751.

Rahimi, R., Banan, M.R. and Banan, M.R. (2016), “Lateral cyclic behavior of zipper braced frames-considering connection details”, Int. Journal of Steel Structures, Vol. 16 No. 1, pp. 11-21

Shaback, B. and Brown, T. (2003), "Behaviour of Square Hollow Structural Steel Braces with end Connections under Reversed Cyclic Axial Loading", Canadian J. of Civil Engineering, Vol. 30, No. 4, pp. 745-753.

Salawdeh, S., and Goggins, J., (2013), "Numerical Simulation for Steel Brace Members Incorporating a Fatigue Model", Engineering Structures, Vol. 46, pp. 332-349.

Sepahvand, M. F., Akbari, J., & Kusunoki, K. (2019). "Plastic design of moment resisting frames using mechanism control." Journal of Constructional Steel Research, 153, 275–285.

Steele, T., Wiebe, L. (2016) "Dynamic and equivalent static procedures for capacity design of controlled rocking steel braced frames". Earthquake Engng.Struct. Dyn., 2349–2369.

Simpson, B. G. (2018). Design Development for Steel Strongback Braced Frames to Mitigate Concentrations of Damage. UC Berkeley. ProQuest ID: Simpson_berkeley_0028E_18230. Merritt ID: ark:/13030/m5518w8n. Retrieved from https://escholarship.org/uc/item/5kb2x4wv .

Simpson, B., & Mahin, S. (2018b). "Experimental and Numerical Investigation of Strongback Braced Frame System to Mitigate Weak Story Behavior". ASCE, J. Struct. Eng., 144(2).

Simpson, B. (2020). "Higher-mode force response in multi-story strongback-braced frames." Earthquake Eng. Struct. Dyn.49 (14): 1406–1427.

Trifunac, M.D. and Brady, A.G. (1975) "On the correlation of seismic intensity scales with the peaks of recorded strong ground motion". Bulletin of the Seismological Society of America, 65, 139-162.

Tesfamariam, S., and Goda K. (2015), "Loss estimation for non-ductile reinforced concrete building in Victoria, British Columbia, Canada: effects of mega-thrust Mw9-class subduction earthquakes and aftershocks", Earthq. Eng. Struct. Dyn.

Tremblay, R., Filiatrault, A., Timler, P., and Bruneau, M., (1995) “Performance of steel structures during the 1994 Northridge earthquake”. Canadian Journal of Civil Engineering. 22(2): 338-360.

Tremblay, R., & Robert, N. (2001). “Seismic performance of low- and medium-rise chevron braced steel frames”. Canadian Journal of Civil Engineering, 28(4), 699–714. https://doi.org/10.1139/cjce-28-4-699

Tremblay, R. (2002), “Inelastic Seismic Response of Steel Bracing Members”, Journal of Constructional Steel Research, Vol. 58, pp. 665-701.

Tremblay, R. (2003). Achieving a stable inelastic seismic response for multi-story concentrically braced frames. AISC J. Struct. Eng., 40(2), 111-129.

Tremblay, R. (2008). “Influence of Brace Slenderness on the Fracture Life of Rectangular Tubular Steel Bracing Members Subjected to Seismic Inelastic Loading”. Proc. 2008 ASCE Structures Congress, Vancouver, BC.

Tremblay, R., and Tirca, L., (2003). “Behaviour and design of multi-storey zipper concentrically braced steel frames for the mitigation of soft-storey response.”

Tremblay, R., and Poncet, L. (2007). Improving the Seismic Stability of Concentrically Braced Steel Frames. Engineering Journal, AISC, 44(2): 103-116.

Tremblay, R., L. Chen, and L. Tirca. (2014). "Enhancing the Seismic Prerformance of Multi-storey Buildings with a Modular Tied Braced Frame System with Added Energy Dissipating Devices." International Journal of High-Rise Buildings 3(1): 21-33.

Tirca, L., and Tremblay, R., (2004) “Influence of Building Height and Ground Motion Type on the Seismic Behavior of Zipper Concentrically Braced Steel Frames”, the 13th World Conference on Earthquake Engineering, August 1-6, Vancouver, B.C., Canada, Paper No. 2894.

Tirca, L., and Chen, L., (2012). “The Influence of Lateral Load Patterns on the Seismic Design of Zipper Braced Frames.” Engineering Structures Journal. Vol. 40, 2012, pp. 536-555.

Tirca, L., and Chen, L. (2014). “Numerical simulation of inelastic cyclic response of HSS braces upon fracture”, J. Adv. Steel Constr. 10 (4) 442–462.

Tirca, L., Chen, L., and Tremblay, R. (2015). “Assessing collapse safety of CBF buildings subjected to crustal and subduction earthquakes”. Journal of Constructional Steel Research, Volume 115, December 2015, Pages 47-61.

Takeuchi, T., X. Chen, and R. Matsui. (2015). "Seismic performance of controlled spine frames with energy dissipating members." J. Constructional Steel Research 114: 51–65.

Uriz, P. (2005), “Towards Earthquake Resistant Design of Concentrically Braced Steel Buildings”, Ph.D. Dissertation, University of California, Berkeley.

Uriz, P. and Mahin, S. (2008), “Toward Earthquake Resistant Design of Concentrically Braced Steel Frame Structures”, PEER Report 2008/08.

VVG Blakeley, R., Cooney, R., & Megget, L. (1975). Seismic shear loading at flexural capacity in cantilever wall structures.

Vamvatsikos, D., and Cornell, C.A (2002). “Incremental Dynamic Analysis”. Earthquake Engineering Struct. Dyn. 2002; 31:491–514.

Whittaker, A., Uang, C., & Bertero, V. (1990). An Experimental Study of the Behavior of Dual Steel Systems. Berkeley, CA: Earthquake Engineering Research Center.

Wijesundara, K.K., Nascimbene, R. and Rassati, G. (2018), “Evaluation of the seismic performance of suspend zipper column concentrically braced steel frames”, Journal of Constructional Steel Research, Vol. 150, pp. 452-461.

Wang, Y. (2018). “Seismic performance of steel buildings with braced dual configuration and traditional frame systems through nonlinear collapse simulations”. MASc thesis, Concordia University, Montreal, Canada.

Xie, Q. (2008). “Dual System Design of Steel Frames Incorporating Buckling-Restrained Braces”. The 14th World Conference on Earthquake Engineering, October 12-17, 2008, Beijing, China.

Yang, T.Y., Mahin, S. (2005), “Limiting Net Section Fracture in Slotted Tube Braces”, Steel Tips, Structural Steel Education Council, Orinda, Ca.

Yang, C.S., Leon, R. T., and DesRoches, R. (2008a). “Design and behavior of zipper-braced frames”. Engineering Structures, 30(4), 1092–1100.

Yang, C.S., Leon, R.T. and DesRoches, R., (2008) “Pushover Response of a Braced Frame with Suspended Zipper Struts”, Journal of Structural Engineering, Vol.134, No.10, pp.1619-1626.

Yang, C.S., DesRoches, R., and Leon, R.T., (2010) “Design and Analysis of Braced Frames with Shape Memory Alloy and Energy-Absorbing Hybrid Devices”, Engineering Structures, Vol. 32, pp.498-507.

Yu, H., Guo, Y., Zhang, Y. and Wang, X. (2016), “Design and seismic response of modified suspended zipper braced frames”, Journal of Constructional Steel Research, Vol. 120, pp. 8-24.

Ziemian, R. (2010). “Guide to Stability Design Criteria for Metal Structures”. J. Wiley & Sons.

APPENDIX A

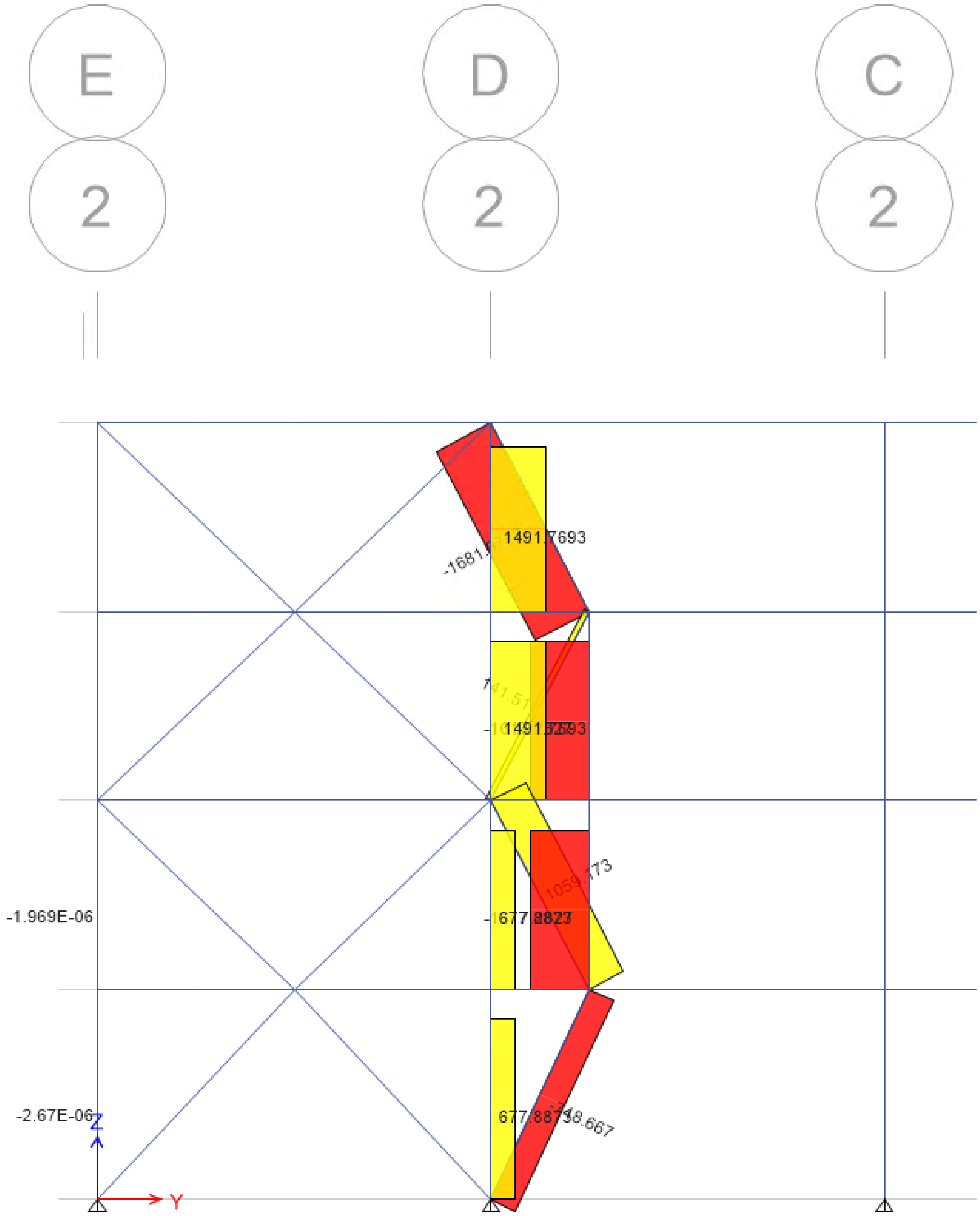

Fig. 1. Axial forces associated with the 2nd higher mode in the 3D-ETABS model of SBF-E

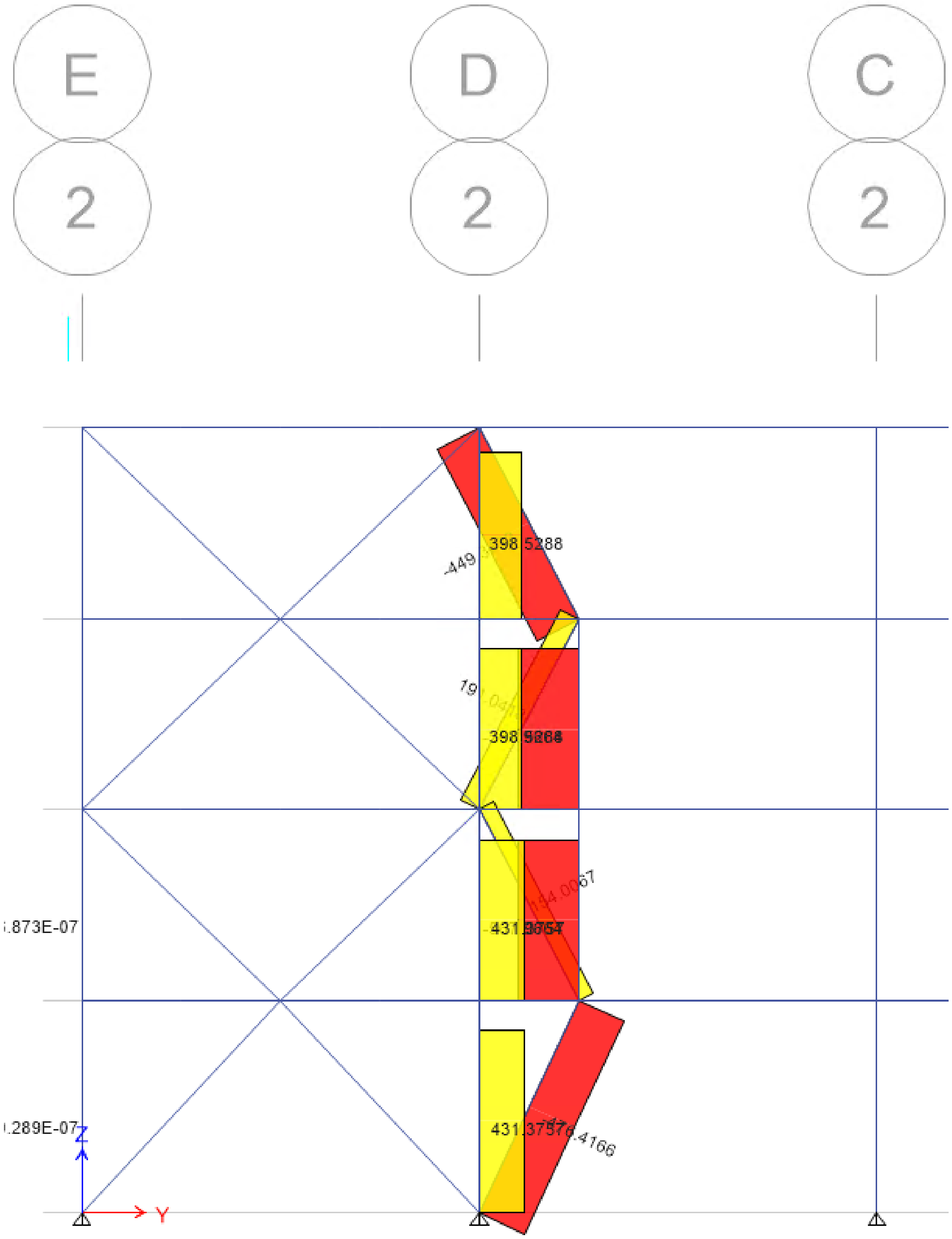

Fig. 2. Axial forces associated with the 3rd higher mode in the 3D-ETABS model of SBF-E

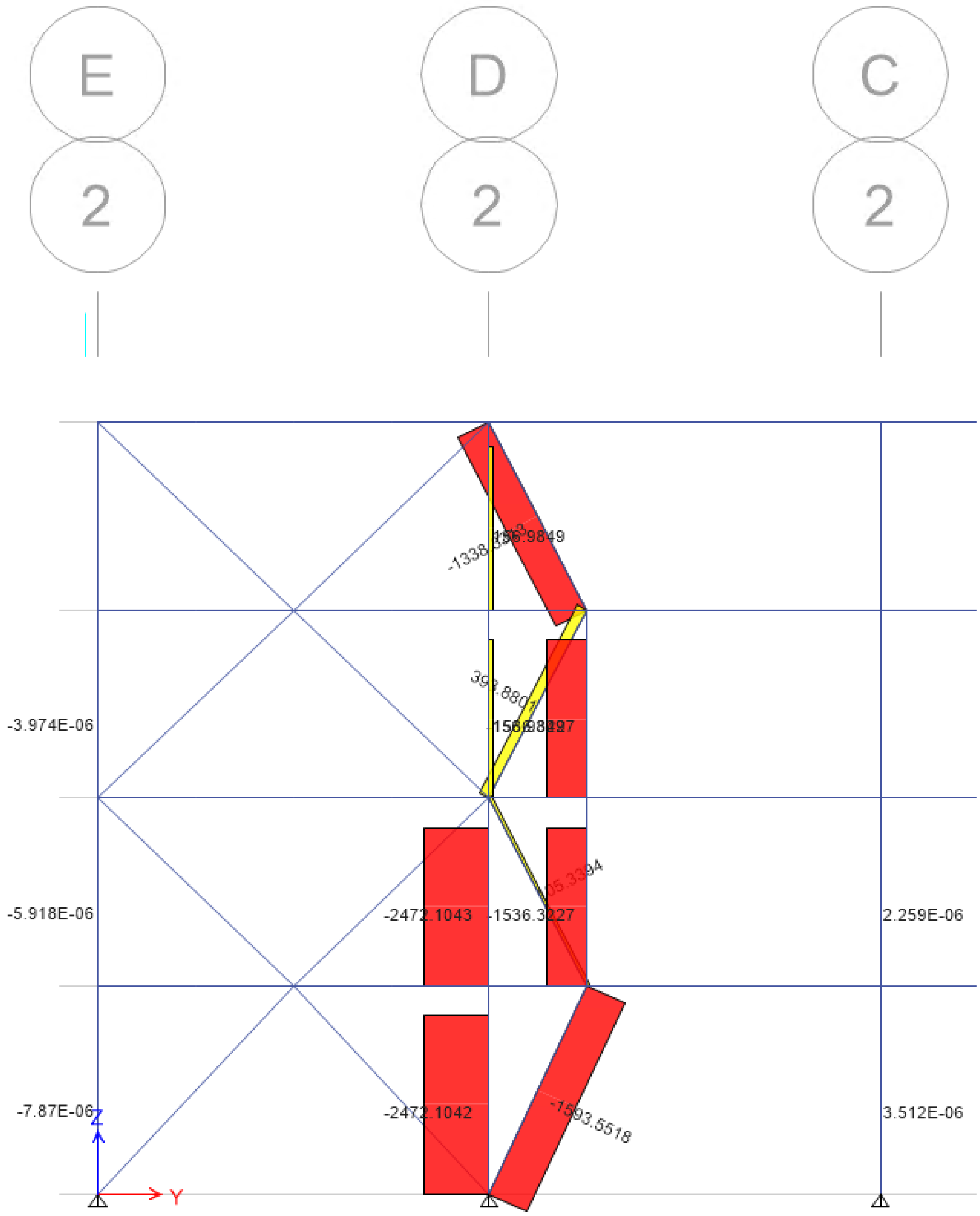

Fig. 3. Axial forces associated with the 1st mode in the 3D-ETABS model of SBF-E

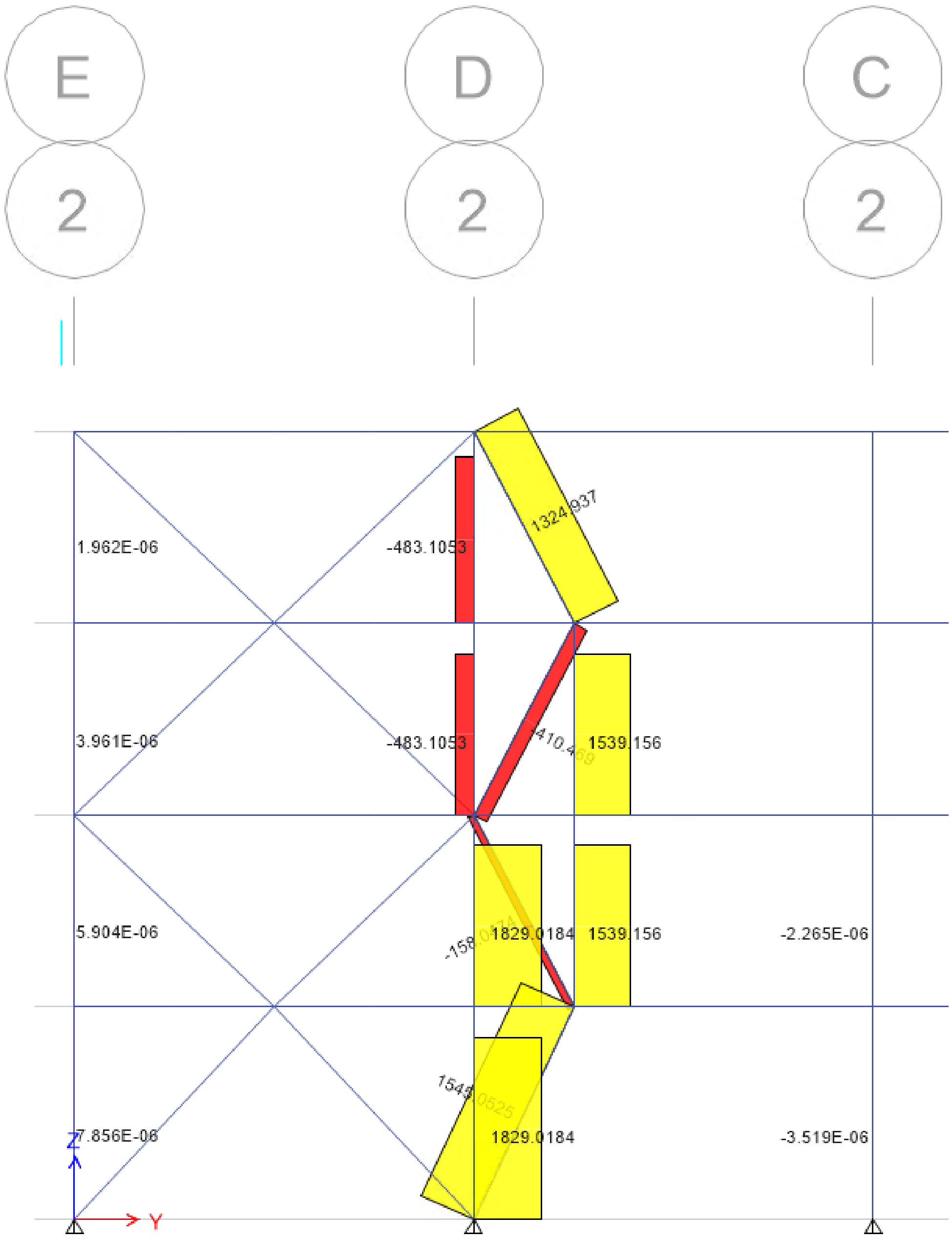

Fig. 4. Axial forces associated with the 1st mode in the 3D-ETABS model of SBF-E (reversed loading direction)

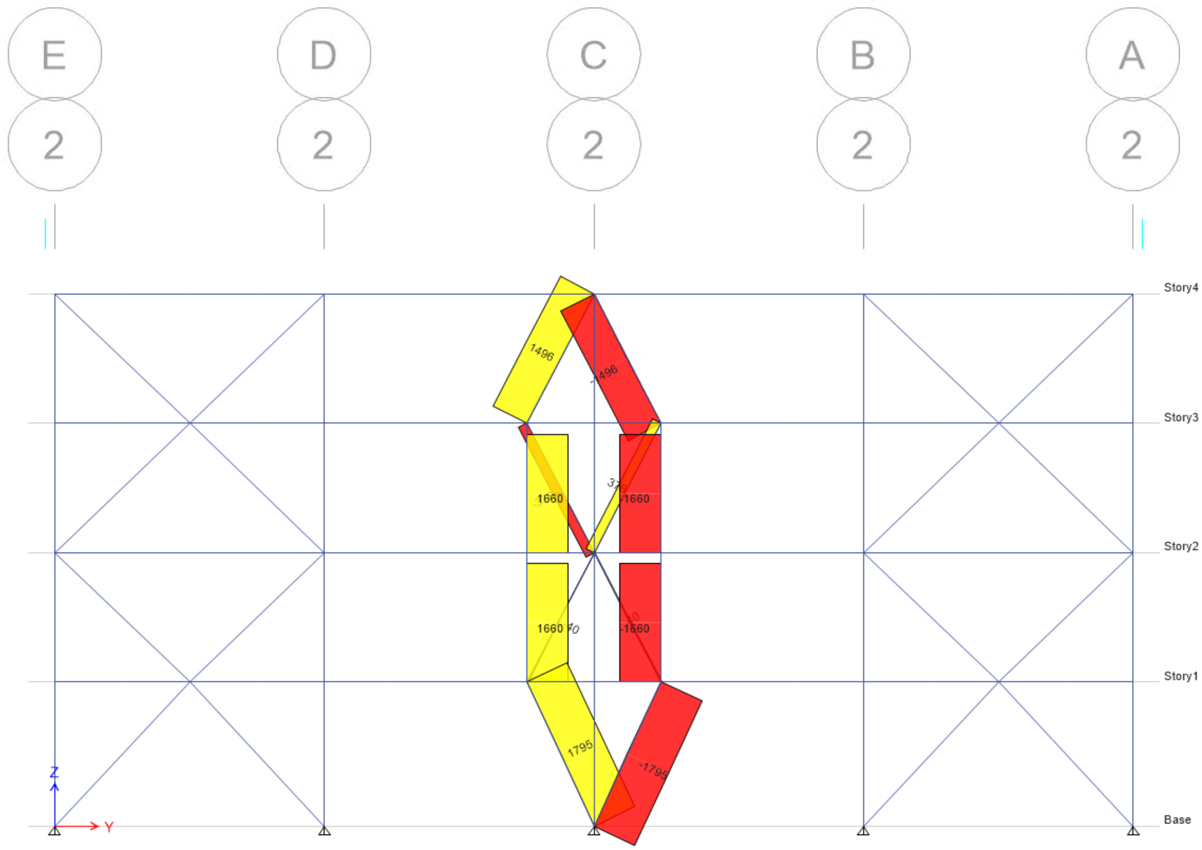

Fig. 5. Axial forces associated with the 1st mode in the 3D-ETABS model of SBF-DS

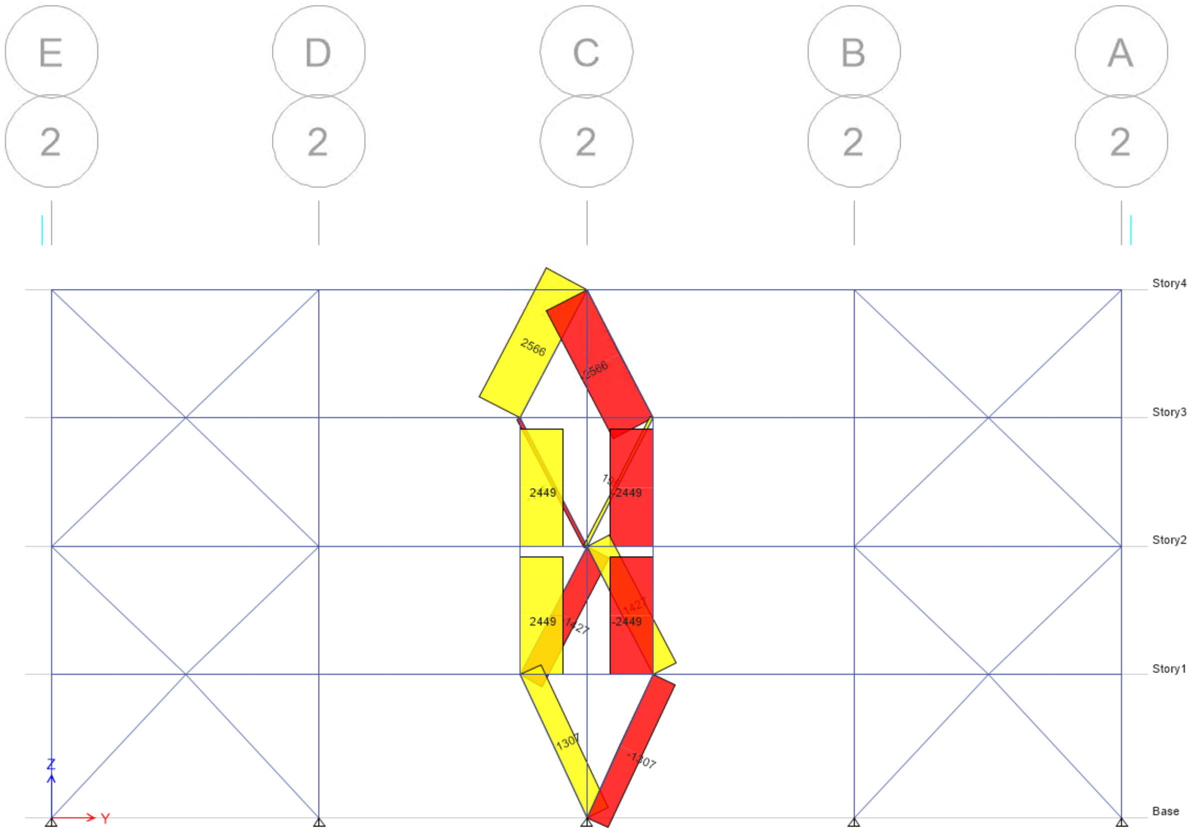

Fig. 6. Axial forces associated with the 2nd mode in the 3D-ETABS model of SBF-DS

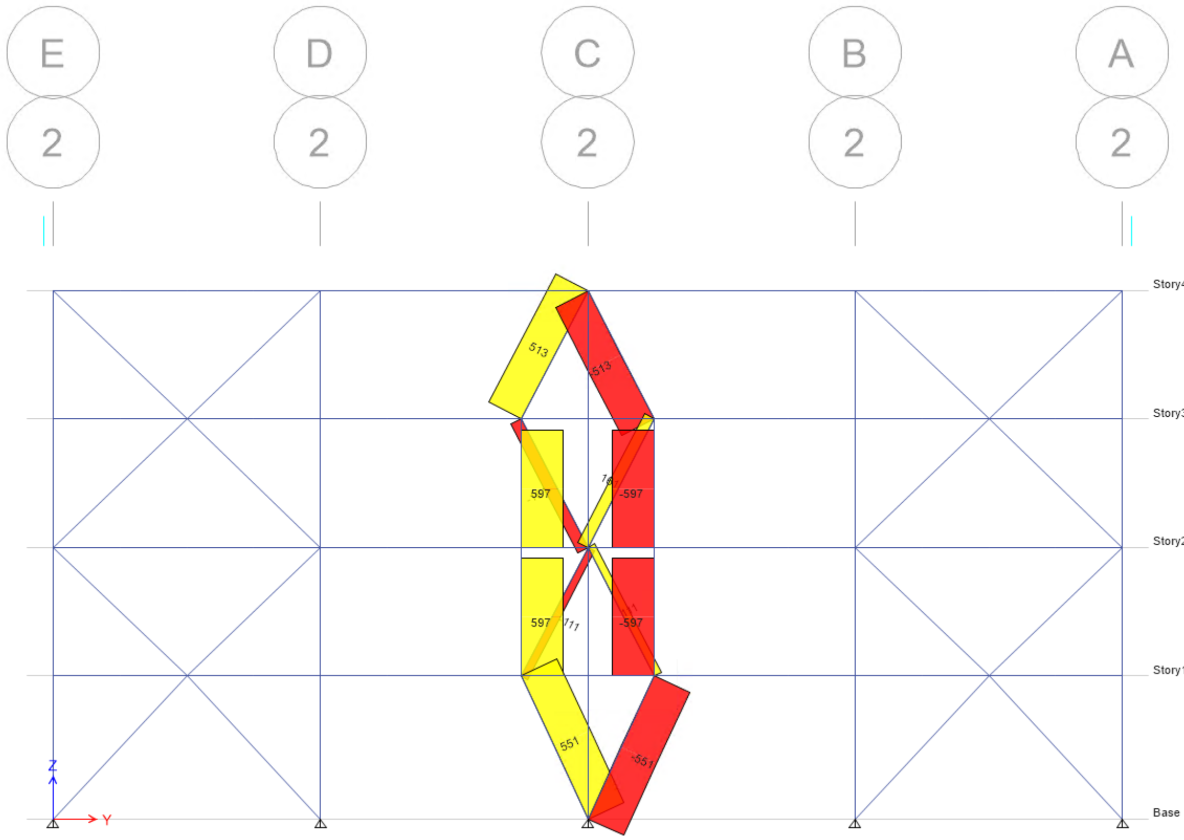

Fig. 7. Axial forces associated with the 3rd mode in the 3D-ETABS model of SBF-DS